EXPLORING PAVEMENT TEXTURE AND SURFACE SKID RESISTANCE USING SOFT COMPUTING TECHNIQUES

By

GUANGWEI YANG

Bachelor of Civil Engineering
Zhengzhou University
Zhengzhou, China
2008

Master of Civil Engineering
Southwest Jiaotong University
Chengdu, China
2011

Submitted to the Faculty of the
Graduate College of the
Oklahoma State University
in partial fulfillment of
the requirements for
the Degree of
DOCTOR OF PHILOSOPHY
December, 2017

EXPLORING PAVEMENT TEXTURE AND SURFACE SKID RESISTANCE USING SOFT COMPUTING TECHNIQUES

Dissertation Approved:

Dissertation Adviser Dr. Qiang (Joshua) Li

Committee Member Dr. Kelvin C.P. Wang

Committee Member Dr. Stephen A. Cross

Outside Committee Member Dr. Keith A. Teague

ACKNOWLEDGEMENTS

Firstly, I would like to express my sincere gratitude to my advisor Dr. Qiang (Joshua) Li and Dr. Kelvin C.P. Wang for the continuous support of my Ph.D. study and related research, for their patience, motivation, and immense knowledge. I would not started my research and achieved those successful results without their help and guidance in all the time of research and writing of this dissertation. Thanks for bring me to the conferences or seminars to learn from those outstanding experts and colleagues. I could not have imagined having a better advisor and mentor for my Ph.D. study.

Besides my advisor, I would like to thank the rest of my dissertation committee members: Dr. Stephen A. Cross and Dr. Keith A. Teague, for their insightful comments and encouragement, but also for the hard question which incented me to widen my research from various perspectives.

I am grateful to my beautiful and beloved wife, Mengyu Yin, who has provided me an enormous support in all the aspects of my life in last five years. She gave birth to my handsome son and adorable daughter who bring precious happiness and memory to our family. She did excellent job in taking care of everybody in the family and her Ph.D. study also. I am so grateful and proud of having her as the sunshine in my life.

With a special thanks going to my parents and parents-in-law: they provided a lot support to my young family for no reason and execution, just like they did in past thirty years taking care of me and my wife. I would not have a happiness family and finish my Ph.D. study without their help. Also, I want to point out my siblings: that's a special support to me for taking care of my parent in China when I am studying in the U.S.

Last but not the least, I would like to thank Justin, Jason Zhan, Allen Zhang, Ace Yue, Yang Liu, and Dr. Chen in general. It was a great memory to travel dozens of states collecting field data with Justin in multiple trips: I learned a lot from those experiences. It was fantastic to have the opportunity to work majority of my research with your help, and thanks for all the fun we have had in the last four and half years.

Name: GUANGWEI YANG

Date of Degree: DECEMBER, 2017

Title of Study: EXPLORING PAVEMENT TEXTURE AND SURFACE SKID RESISTANCE USING SOFT COMPUTING TECHNIQUES

Major Field: Civil Engineering

Abstract: Pavement skid resistance and texture characteristics are important aspects of road safety. Traditional pavement friction measurement from limited contact with pavement is influenced by multiple factors such as temperature, water depth, and testing speed. Friction prediction from texture data has a potential to save resources and reduce inconsistence of friction measurement due to the existence of water and rubber in friction data collection. This dissertation investigates the application of pavement 2-dimensional /3-dimensional (2D/3D) texture data for friction evaluation from different perspectives.

3D texture data with ultra-high resolution 3D laser scanner and friction data with Dynamic Friction Tester are collected on the Long Term Pavement Performance (LTPP) Specific Pavement Study 10 (SPS-10) site in Oklahoma. 2D macro-texture data with High Speed Profiler and friction data with Grip Tester are measured on 49 High Friction Surface Treatment (HFST) sites scattered in 12 states in the United States.

Firstly, novel 3D parameters, rather than traditional texture indicators, are calculated for 3D texture data to identify the most important and appropriate texture parameters for skid resistance evaluation. Pavement friction models including the identified 3D texture parameters are developed with fairly good accuracy.

Secondly, the wavelet and deep learning methodologies are employed to better use 2D macro-texture data. Discrete wavelet transform is implemented to decompose 2D macro-texture data, which are collected on six HFST sites in Oklahoma, into multiple wavelengths. The Total Energy and Relative Energy are calculated as indicators to represent macro-texture characteristics at various wavelengths. A robust non-contact friction prediction model incorporating energy indicators is proposed with good accuracy. In addition, FrictionNet, a Convolutional Neural Network based model, is developed to pairwise relationship between pavement texture and friction using 2D macro-texture profile as a whole. 49 HFST sites distributed in the 12 states are surveyed including various types of lead-in and lead-out pavement sections. The FrictionNet achieves high accuracy for training, validation, and testing in friction prediction.

In summary, novel 3D texture parameters for 3D texture data are identified, and new computing technologies are implemented to better use 2D macro-texture data with respect to pavement friction evaluation. The results demonstrate the potential of using non-contact texture measurements for pavement friction evaluation.

TABLE OF CONTENTS

LIST OF TABLES

LIST OF FIGURES

CHAPTER I INTRODUCTION

1.1 Background

Pavement skid resistance properties play a significant role in road safety. It has long been recognized that adequate friction between the vehicle tire and pavement is a critical factor in reducing crashes and improving roadway safety. Some studies have reported that up to 13.5% of fatal crashes and 25% of all crashes happen during wet weather condition (Kuemmel et al., 2000). Therefore, it is important that Departments of Transportation (DOTs) monitor the friction of their pavement networks frequently and systematically to minimize friction-related vehicle crashes by ensuring that pavements provide adequate friction properties throughout their lives. A proactive friction management program can help identify areas that have elevated friction-related crash rates, investigate road segments with friction deficiencies, and prioritize use of resources to reduce friction-related vehicle crashes in a cost-effective manner (AASHTO, 2008; Flintsch & McGhee, 2009).

There are many devices currently used for measuring pavement friction, which can be categorized into three groups based on the friction measurement principles: (1) side-force friction testers (e.g. Mu-meter, ASTM E670-09); (2) slip-speed testers, including devices with 100% slip (e.g., Locked-wheel trailers ASTM E274-06), fixed slip tester (e.g. Grip Tester and Dynatest Highway

Friction tester, E2340/E2340M-11R15), and variable slip tester (e.g., Roar ASTM E1859/E1859M-11R15); and (3) small slider testers (e.g. Dynamic Friction Tester, ASTM E1911-09a; and British Pendulum Tester, ASTM E0303-93R13). Full-scale friction measurement devices apply the first two principles, while the small testers are generally operated in a static manner. Dragging a testing tire/rubber pad across a road/specimen has been the most common approach in measuring the skid resistance of a road during the past decades (Flintsch et al., 2012).

Pavement texture is a critical factor to maintain desired pavement skid resistance under traffic polish, and it is recognized as another safety factor contributing to crash ratios (Hall et al., 2009; Roe et al., 1991; Roe et al., 1998). Pavement texture is defined as the deviations of pavement surface from a true planar surface, and normally two types of surface texture affect wet pavement friction: micro-texture (wavelengths of 1 μm to 0.5 mm) and macro-texture (wavelengths of 0.5 mm to 50 mm) (Henry, 2000). Pavement micro-texture is mainly dependent on aggregate shape, angularity and texture, while macro-texture is a function of asphalt mix properties, compaction method, aggregate gradation, or groove treatment in some surfaces. Of fundamental importance on both wet and dry roads, especially important at low speeds, is the micro-texture, while macro-texture is critical to skid resistance on wet pavement for high speed (Flintsch et al., 2012).

Pavement micro-texture is normally collected in laboratory statically through high resolution devices based on imaging analysis (Ergun et al., 2005; Dunford, 2012; Nataadmadja et al., 2012; Ueckermann et al., 2015). Pavement macro-texture can be measured via sand patch test, Circular Track Meter, or High Speed Profiler in terms of Mean Texture Depth (MTD) and Mean Profile Depth (MPD) in field (ASTM E965-15; ASTM E2157-15; Flintsch et al., 2012). It is widely accepted that minimal MPD or MTD should be maintained for various pavement surfaces with desired surface skid resistance for roadway safety over their lives (Henry, 2000; Dupont & Bauduin, 2005; Ahammed & Tighe, 2010).

1.2 Problem Statement

Existing friction measurements universally require the contacting of testing rubbers/tires and pavement surface. Many factors, such as pavement temperature, water film depth, testing speed, and tire conditions, impact the consistency of friction measurement. The currently available friction testing devices require wetting pavement surface and consuming testing tires during data collection. Due to the limitation of water tank volume used in friction measurement, current skid resistance survey is generally performed at the project level on a needed basis. In addition, existing friction measurement methods rely on physical contact between testing tires/sliders and pavement, which cover only a small portion of pavement surface. Because of potential traffic wandering during time series friction data collection, the friction data could be measured along different paths resulting in inconsistent measurements.

Additionally, due to the viscoelastic properties of friction testing tires, friction values could vary even for measurements on the same pavement section but at different pavement temperature. Temperature correction is needed to quantify the temperature variation in friction measurement (Jayawickrama & Thomas, 1998; Sang et al., 2008; Bijsterveld & Val, 2016). However, acquiring such adjustment factors could be challenging because the temperature variation is limited within a short period of time while traffic polishing on pavement is insignificant.

Besides, acquired friction number decreases with the increase of testing speed (Sang et al., 2008). It is challenging to maintain the standard testing speed 64 km/h (40 MPH) in the field in many occasions, such as high volume roads with higher traffic speed or sharp curves. Accordingly, speed adjustment is necessary for comparing data collected at different speeds over different sites. In addition, friction measurements via traditional devices are also depending on contact pressure, water film depth, and the level of wearing of the testing tire.

Various studies have found the correlation between pavement friction and pavement texture. Various parameters, such as traffic level, aggregate characteristics, and pavement texture, were included to develop pavement friction prediction models (Ergun et al., 2005; Ahammed & Tighe, 2008; Ahammed & Tighe, 2012; Rezaei & Masad, 2013; Ueckermann et al., 2015). Other studies measured 3-dimensional (3D) pavement macro-texture data in the field via high-speed laser scanners using a wide range of texture indicators and evaluated their relationships with pavement friction performance (Liu & Shalaby, 2015; Li et al., 2016). Several other research activities correlated pavement texture with friction performance using advanced data analysis methodologies including "Hilbert-Huang transform", fractal analysis, power spectral analysis, and wavelet analysis (Hartikainen et al., 2014; Rado & Kane, 2014; Villani et al., 2014; Zelelew et al., 2014; Kane et al., 2015). A comprehensive evaluation of field performance for several high friction surface treatment (HFST) sites was conducted and no direct relationship was found between mean profile depth (MPD) and friction performance (Izeppi et al., 2010). There has been limited research to investigate the relationship between pavement friction and micro-texture based on 2-dimensional (2D) pavement profiles or 3D images with resolution up to 0.015 mm (Bitelli et al., 2012; Serigos, 2013; Kanafi et al., 2015; Li, 2016). However, they relied on traditional texture parameters to characterize micro-texture property and failed to identify proper texture parameters to predict pavement friction performance. Despite extensive studies conducted in the past decades, the relationship between pavement texture and surface skid resistance has not been fully understood.

With the development of non-contact 3D measurement technologies and the vast improvement in the computing and processing power of computers in the past decades, it is feasible and desirable to describe road surface texture in both macro- and micro-scale under 3D at high resolution. These 3D based indices and parameters not only promise a quantum leap in describing road surface texture characteristics, but also could provide in-depth understanding of the relationship between texture and friction for the purpose of replacing existing friction measurement methodologies. If such a

relationship between pavement friction and texture is proved to be rigorous, it may be feasible to apply non-contact pavement texture measurements for skid resistance analysis.

On the other hand, pavement 2D macro-texture data has been collected extensively without contact at highway speed by transportation agencies. However, the analysis of pavement 2D macro-texture profile is usually limited to the calculation of traditional parameter MPD which is outdated and irrelevant to friction characteristics. To better use 2D macro-texture profile data, it is feasible to extract information or directly use rich profile data as a whole for friction prediction with advanced soft computing technologies.

1.3 Research Objectives

The objective of this work is to explore the potential relationship between pavement texture and surface skid resistance using soft computing techniques. An Ultra-high resolution 3D laser scanner named LS-40 and a Dynamic Friction Tester are used to collect high resolution 3D texture data and friction data on the Long Term Pavement Performance (LTPP) Specific Pavement Study 10 (SPS-10) site in Oklahoma. An AMES High Speed Profiler and a Grip Tester are employed to measure high speed macro-texture profile and friction data on 49 High Friction Surface Treatment (HFST) sites located in 12 states in United States.

Specifically, the research aims to address the following sub-objectives:.

- To better characterize pavement 3D texture attributes. Five categories of novel 3D areal parameters, including height parameters, function related parameters, hybrid parameters, spatial parameters, and feature parameters, are explored using the high resolution 3D texture data for friction evaluation. The most influential 3D macro- and micro-texture parameters which exhibit good correlation with friction data will be identified.

- To study the high speed texture profiles for better skid resistance characterization. Discrete wavelet transform is implemented to decompose pavement 2D macro-texture data into multi-scales. Two types of energy indicators, Total Energy (TE) and Relative Energy (RE), are calculated from the decomposed texture profiles to represent the characteristics of macro-texture at various wavelengths and investigate their suitability for pavement friction prediction.
- To develop deep learning based friction perdition model using high speed texture profiles. A Convolutional Neural Network (CNN) friction prediction model is developed using high speed pavement texture data as a whole for friction prediction. 49 high friction surface treatment (HFST) sites located in 12 states are tested with different surface types, including HFST, traditional flexible & rigid pavements with and without grooving, bridge deck. 80%, 10%, and 10% of the prepared data sets are randomly selected for model training, validation, and testing.

1.4 Organization of Dissertation

The following chapters are included in this dissertation to achieve the research objectives:

- Chapter 2 – performs comprehensive literature review on pavement texture and measurement, pavement skid resistance and measurement, and relationship between pavement texture and skid resistance.
- Chapter 3 – explores novel 3D texture parameters to characterize pavement 3D texture attributes. The core material volume and the peak density are identified as the most influential macro- and micro-texture parameters. A non-contact pavement friction prediction model with fairly good accuracy is therefore developed based on the selected 3D texture parameters.

- Chapter 4 – decomposes 2D macro-texture profiles into multi-scale via discrete wavelet methodology. Contribution of macro-texture at different wavelengths to friction performance is evaluated via energy indicators. A non-contact friction prediction model with good accuracy is proposed incorporating the 2D macro-texture energy indicators.
- Chapter 5 – introduces FrictionNet as a non-contact friction prediction model which identifies the pairwise relationship of a whole 2D macro-texture profile and friction data. Variety of pavement types are considered, and the model achieves high accuracy in predicting friction number.
- Chapter 6 – summarizes the conclusions in this dissertation and the recommended future works.

CHAPTER II LITERATURE REVIEW

2.1 Pavement Texture and Measurement

2.1.1 Pavement Texture

Pavement texture is defined as the deviations of the pavement surface from a true planar surface (Hall et al., 2009). Two types of surface texture affect wet pavement friction: micro-texture (wavelengths of 1μm to 0.5mm) and macro-texture (wavelengths of 0.5mm to 50mm) (Henry, 2000). As Figure 2.1 shows, micro-texture is the degree of roughness imparted by individual aggregate particles, whereas macro-texture is the degree of roughness imparted by the deviating among particles. Micro-texture is generally provided by the relative roughness of the aggregate particles in asphalt pavement, and by the fine aggregate in concrete surface. Macro-texture is generally provided by proper aggregate gradation in asphalt pavement, and by a supplemental treatment such as tinning, broom, diamond grinding, or grooving for concrete surface.

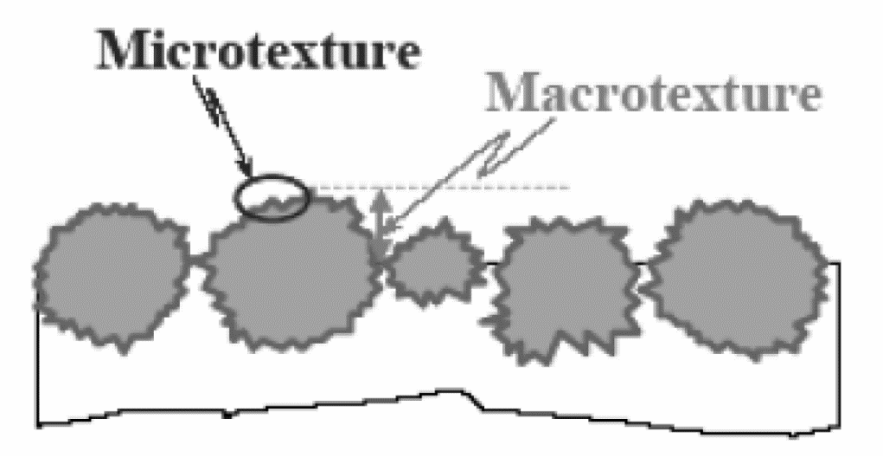

Figure 2.1 Micro-texture and Macro-texture (Flintsch et al., 2003)

Currently there is no national wide specification on pavement texture within the U.S. while some countries provide following requirement to maintain proper performance of pavement texture. Great Britain attempted to provide a MTD of 1.5 mm (0.06 in.) for new asphalt pavements, and Minnesota required a MTD greater than 0.8 mm (0.03 in.) on new concrete surfaces (Henry, 2000). Current British specification also requested a minimum 0.65 mm (0.026 in.) sand patch MTD for transversely textured new concrete surfaces while 1.0 mm (0.039 in.) laser-based MTD to meet the skid resistance requirement (Ahammed & Tighe, 2010). France had established specifications from $\geqslant$ 0.40 mm (0.016 in,) to $\geqslant$ 0.70 mm (0.028 in.) glass beads MTD on urban and suburban roads depending on speed, longitudinal grade, and number of lanes per direction; as rural (interurban) roads, the desired glass beads MTD varied from $\geqslant$ 0.60 mm (0.024 in.) to $\geqslant$ 0.80 mm (0.031 in.) depending on speed, longitudinal slope, curve radius, and number of lanes per direction (Dupont & Bauduin, 2005). China specified texture depth (TD) greater than 0.55 mm (0.022 in.) on asphalt interstate pavements, and TD varies from 0.77 mm (0.03 in.) to 1.1 mm (0.043 in.) on interstate concrete pavements. Larson et al. (2008) had recommended a minimum macro-texture for Ohio, which is the same as the French specification for intervention at network level, but a 1.0 mm (0.039 in.) as an investigatory (desirable) value for network as well as project levels. Threshold of texture depth on trunk roads to maintain good skid resistance for high speeds

at different levels were summarized as following: > 1.1 mm (0.043 in.) as ‘Sound’, 0.8 mm (0.031 in.) – 1.1 mm (0.043 in.) as ‘Some Deterioration’, 0.4 mm (0.016 in.) – 0.8 mm (0.031 in.) as ‘Warning Level of Concern’ and < 0.4 mm (0.016 in.) as ‘Severe Deterioration Requiring Urgent Investigation and Possible Remedial Action’ (Viner et al., 2006).

Researches on relating pavement texture to crash ratio, pavement texture variation, and texture maintenance level have been conducted. Roe et al. (1991) applied high-speed texture meter to assess texture depth, and claimed that coarse macro-texture related less accident than fine texture, and accident risk started to increase when texture depth was less than 0.7 mm (0.028 in.). Sensor-measured texture depth was also identified a critical point of the effect of texture depth on loss of friction: below 0.7 mm (0.028 in.), less friction was observed due to the lower texture depth (Roe et al., 1998). Kanafi et al. (2015) monitored variation of pavement texture and observed macro-texture reduction and micro-texture increase during summer time. Early rapid reduction followed by an increase and subsequent gradual decline of macro-texture change of asphalt concrete samples in lab was observed by close range photogrammetry with proprietary photogrammetric software (Millar et al., 2009). Wavelet analysis was applied to interpret macro-texture collected by CT meter to determine the wavelength ranges and energy content that affect the macro-texture properties of asphalt pavements (Zelelew et al., 2013; Zelelew et al., 2014).

2.1.2 Texture Measurement

(a) Sand Patch Method

(b) Outflow Meter Device

Figure 2.2 Traditional Macro-texture Measurement

ASTM has two standards relating to traditional pavement macro-texture measurement: E965-15 "Standard Test Method for Measuring Pavement Macro-texture Depth Using a Volumetric Technique" and E2380/E2380M-15 "Standard Test Method for Measuring Pavement Texture Drainage Using an Outflow Meter" (Figure 2.2). In E965, Mean Texture Depth (MTD) is calculated by dividing sample volume to the area covered by the material and reported as texture indicator. In E2380, the outflow meter time is recorded to indicate pavement drainage information and MTD is estimated to represent texture information. Therefore sand patch test only captures pavement texture information, whereas the test by outflow meter relates the texture

to the drainage capacity and provides an indication of pavement hydroplaning potential under wet conditions. The Grease Smear Method is applied to evaluate airport pavement macro-texture by FAA, and texture depth requirement for runway is also documented in AC 150/5320-12C (FAA, 1997). Doty (1974) compared sand patch and outflow meter methods and concluded poor to fair repeatability of sand patch test. Pidwerbesky et al. (2006) applied fast Fourier transform to analyze the texture image collected on chip seal pavement and verified the potential to replace sand patch test by digital image process. Sarsam and Ali (2015) compared sand patch test and close range photogrammetric approaches, and high correlation between these two devices indicated that photogrammetric approach could produce permanent documentation of texture condition with lower cost and comparable accuracy.

Figure2.3 Circular Track Meter

ASTM E2157-15 “Standard Test Method for Measuring Pavement Macro-texture Properties Using the Circular Track Meter” introduces a laser based static device to collect pavement macro-texture profile (Figure 2.3). The CT meter is designed to measure the same circular track that is measured by the Dynamic Friction Tester. The computer software can process the data to report

either the Mean Profile Depth (MPD) in accordance with Practice ASTM E1845 or the RMS or both for collected texture profile. Prowell and Hanson (2005) applied CT meter to collect macro-texture profiles on different asphalt sections and concluded CT meter produced comparable result with the ASTM E965 sand patch test. Watson et al. (2011) collected texture data on different locations by CT meter and demonstrated greater texture number existed in warmer months than the cooler months.

(a) LS-40 Scanner

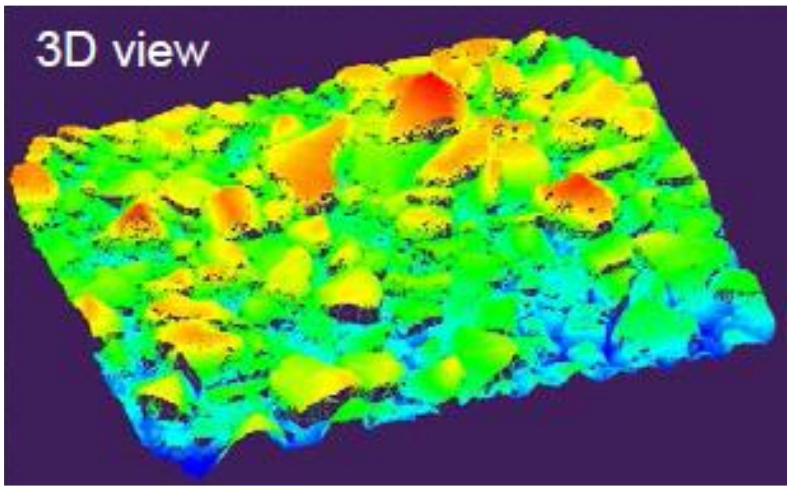

(b) 3D Pavement Surface View

Figure 2.4 LS-40 Portable 3D Surface Analyzer

A 3D surface measurement and analysis device, named LS-40 Portable 3D Surface Analyzer (Figure 2.4), scans a 4.5” by 4” areas and produces a high resolution (0.01mm) digital surface structure with an intensity image and a surface depth related range image. LS-40 provides the data to calculate mean profile depth (MPD) by processing thousands of profiles over the entire scanned surface according to ASTM E1845 specifications, with optional processing modules of measuring other surface features, such as aggregate form factor, angularity calculation based on multiple contour measurements, and micro-texture indicators, such as Slope Variance (SV) and Root Mean Square (RMS). LS-40 can be not only used in the laboratory, but also be placed on a localized pavement surface area in the field to collect 2048 times 2448 cloud points at ultra-high resolution of 0.01mm (0.0004 inches). Liu and Shalaby (2015) applied photometric stereo device to collect and reconstruct pavement 3D surface, calculated simulated mean texture depth, root-mean-square roughness, skewness and kurtosis to relate texture to noise and friction performance.

Figure 2.5 RoboTex (Moravec 2013)

RoboTex is a line laser-based pavement texture profiler proposed by Transtec Group with capability of producing 3D texture images continuously (Figure 2.5). It measures in three dimensions with sub-millimeter accuracy and produce standard texture metrics such as MPD.

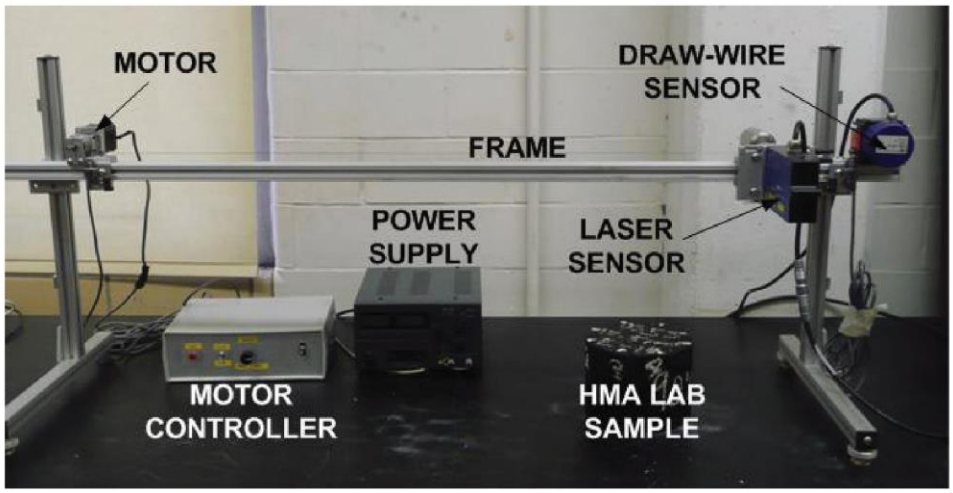

Figure 2.6 Stationary Laser Profilometer (Miller et al. 2012)

Stationary Laser Profilometer (SLP) is another line laser-based stationary pavement texture profiler with high repeatability (Figure 2.6). SLP could capture the micro-texture and macro-texture spectrum of asphalt mixtures and generate corresponding parameter to characterize pavement texture properties (Miller et al., 2012; Chen et al., 2015).

Figure 2.7 High Speed Profiler

There are also many High Speed Profilers (Figure 2.7) that collecting pavement texture profile and calculating MPD in network evaluation. McGhee et al. (2003) conducted validation experiment of high-speed texture measuring equipment, and the result demonstrated extremely

well correlation with the static referencing device. Flintsch et al. (2012) pointed out a device that measures friction and macro-texture concurrently was needed to determine both low-speed and high-speed friction performance from a single measurement pass. Moreover, measurement of pavement micro-texture is still limited by laser's accuracy and more research should incorporate micro-texture to predict pavement skid resistance.

2.2 Pavement Skid Resistance and Measurement

2.2.1 Pavement Skid Resistance

Hall et al. (2009) concluded pavement friction was the force that resists the relative motion between a vehicle tire and a pavement surface. Pavement friction is the result of a complex interplay between two principal frictional force components—adhesion and hysteresis (Figure 2.8). Adhesion is the friction that results from the small-scale bonding/interlocking of the vehicle tire rubber and the pavement surface as they come into contact with each other. It is a function of the interface shear strength and contact area. The hysteresis component of frictional forces results from the energy loss due to bulk deformation of the vehicle tire. That loss leaves a net frictional force which can help to stop the forward motion. Najafi et al. (2015) revealed pavement friction coefficient was a critical factor influencing the crash ratios on both wet and dry condition for urban roads.

Friction numbers less than 38 should be reported to the transportation divisions in North Carolina for possible surface treatment or resurfacing of the pavement (Corley-Lay, 1998). Friction number 30 (20) tested with ribbed (smooth) tire according to ASTM E 274 is defined as threshold for further investigation and remedial action in California, Michigan and New York (Virginia) (McGovern et al., 2011). The Mu values, collected via Scandinavian Airport and Road Systems AB (SARSYS) Friction Tester (SFT), below 0.6 require planning maintenance, and of 0.5 are the minimum acceptable value according to Federal Aviation Administration's criteria (Watkins et al., 2010).

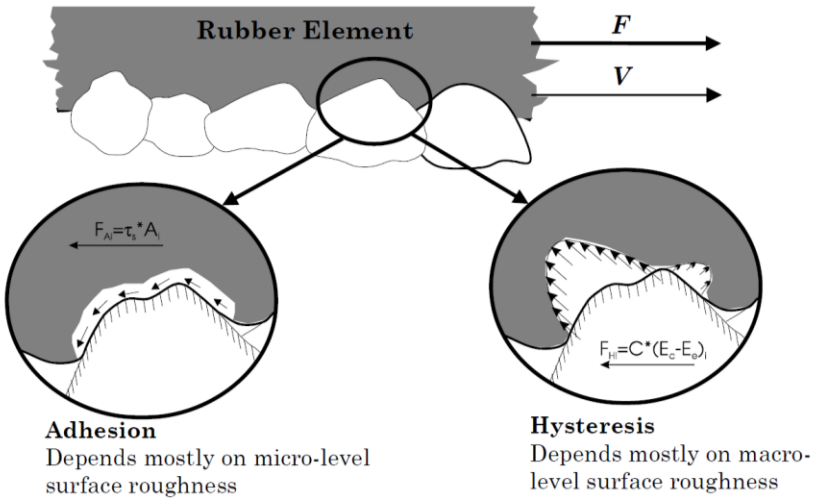

Figure 2.8 Key Mechanisms of Pavement-Tire Friction (Hall et al., 2009)

Because adhesion force is developed at the pavement–tire interface, it is most responsive to the micro-level asperities (micro-texture) of the aggregate particles contained in the pavement surface. In contrast, the hysteresis force developed within the tire is most responsive to the macro-level asperities (macro-texture) formed in the surface via mix design and/or construction techniques. As a result of this phenomenon, adhesion governs the overall friction on smooth-textured and dry pavements, while hysteresis is the dominant component on wet and rough-textured pavements. Labbate (2001) considered pavement surface condition (including asphalt type, nominal aggregate size, and texture depth) and contact area (considering tire loading, inflation pressure and type of tire) simultaneously to investigate the pavement skid resistance performance. The result implied dynamic trend of skid resistance development: an initial loss in early life followed by an increase and thereafter a reduction to equilibrium conditions.

Hall et al. (2009) grouped four categories factors that influencing pavement friction force: pavement surface characteristics, vehicle operational parameters, tire properties, and environmental factors. Pavement surface texture is characterized by the asperities present in a pavement surface. Such asperities may range from the micro-level roughness contained in individual aggregate particles to a span of unevenness stretching several feet in length.

The influence of asphalt mixture type and Portland cement concrete surface textures on pavement friction performance had been widely studied (Asi, 2007; Ahammed & Tighe, 2008). Studies also found that air temperature and pavement temperature could affect pavement friction performance in short- and long-term, and at low testing speed, friction tended to decrease with increasing of pavement temperature while vice versa for high testing speed (Luo, 2003; Fuents, 2009; Jahromi et al., 2011). Roe et al. (1998) claimed that friction decreased with the increase of testing speed and reached the minimum level by about 100 km/h for smooth tire, the level of high-speed friction depended on a large extent on the low-speed friction, and friction on surfaces with low texture depth fell more rapidly with speed increasing than for coarse textured surfaces. Wilson (2006) identified up to 30% variation of friction performance over short period and seasonal variation of friction coefficient was not obvious nor predictable sinusoidal shape. Kotek and Florkova (2014) did long time friction monitoring on various pavements and derived that friction coefficient were affected by characteristics such as age of wearing course, traffic intensity, and climate conditions of pavement, and there was no definite dependency of friction on traffic intensity. Dan et al. (2015) measured friction coefficient on pavement specimen with different age, water, snow, ice, and temperature condition, the result implied that new pavement exhibited higher sensitivity to temperature variation in friction performance than other factors, and the friction evaluation models and friction levels for different pavement conditions were proposed.

2.2.2 Skid Resistance Measurement

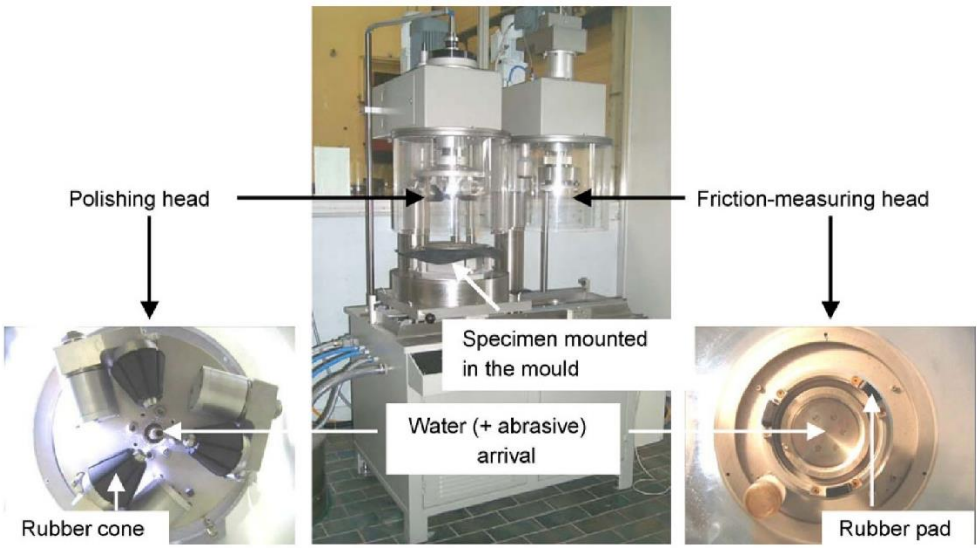

Figure 2.9 Machine Wehner/Schulze (Do et al., 2007)

Wehner-Schulze machine was developed in Germany and widely used in polishing and measuring skid resistance and macro- or micro-texture profile of aggregate or pavement mix specimen (Figure 2.9). Kane et al. (2010) utilized Wehner-Schulze-machine to simulate the polishing process and measure friction on pavement specimen in lab, and developed a model to predict texture or friction evaluation due to traffic polish. Ueckermann et al. (2015) employed Wehner/Schulze machine in lab and ViaFriction in field to collect friction data and validate the proposed rubber friction model which can calculate skid resistance based on the measured texture. Do et al. (2007) applied Webner/Schulze machine to collect skid resistance as well as texture profiles of asphalt mix under different traffic polishing levels, and compared the result with field test of friction performance. The result demonstrated that once the asphalt binder was removed, the pavement friction performance was controlled mainly by the micro-texture of aggregate. Studies using Wehner-Schulze machine to predict pavement or aggregate skid resistance can be found in other references (Do et al., 2009; Arampamoorthy & Patrick, 2011; Chen & Wang, 2011; Dunford et al., 2012; Dunford, 2013; Friel et al., 2013,).

Figure 2.10 British Pendulum Tester

The British Pendulum Tester (BPT) is a dynamic pendulum impact-type tester used to measure the energy loss when a rubber slider edge is propelled over a test surface (Figure 2.10). ASTM E0303-93R13 illustrates the procedure for measuring surface friction properties using the BPT. A drag pointer indicates the BPT Number: the greater the friction between the slider and the test surface, the more the swing is retarded, and the larger the BPN reading. Steven (2009) established a temperature correction equation for the BPT and evaluated the influence of different operators, instruments, levels of slider pad wear and temperature. Asi (2007) applied BPT to evaluate skid resistance performance of different pavement mixes considering different binder contents, different aggregates along with different mixture design procedures.

Figure 2.11 Dynamic Friction Tester

ASTM E1911-09a provides specification on measuring paved surface frictional properties using the Dynamic Friction Tester (DFT) (Figure 2.11). The DFT consists of a horizontal spinning disk fitted with three spring loaded rubber sliders. The water is sprayed in front of the sliders and a constant load is applied to the slider as the disk rotates on the test surface. The torque is monitored continuously as the disk rotational velocity reduces due to the friction between the sliders and the test surface, and then used to calculate the friction coefficient at 20, 40, 60, and 80 km/h.

Figure 2.12 Locked-Wheel Skid Trailer

The Locked-Wheel Skid Trailer (ASTM E274-06) measures the steady-state friction force on a locked test wheel as it is dragged under constant load and at constant speed (typically at 64 km/h [40 mph]) over a wet pavement surface (Figure 2.12). In this test, water is sprayed on the pavement surface in front of the test tire when the tire reaches test speed in order to simulate wet conditions. Friction of the pavement surface is determined from the resulting force or torque and is reported as skid number (SN). A higher SN indicates greater frictional resistance. Friction measured from this device is related to braking without antilock brakes. The Locked-Wheel Skid Trailer operates with a slip ratio of unity. Both rib and smooth tires can be used in the test, as standardized by ASTM E501-94 and ASTM E524-88, respectively. Kotek and Kovac (2015) measured pavement skid resistance by different tires, and inferred that micro-texture had more influence on friction coefficient tested by tread tire because the grooves in the tire tread provide channels much larger than the macro-texture of pavement surfaces, while macro-texture contributed more variation to friction performance measured with smooth tire.

Figure 2.13 Mu-Meter

Another method testing side force friction on paved surface is pulling the Mu-Meter (Figure 2.13) over a pavement surface at a constant speed while the test wheels are under a constant static load.

(ASTM E670-09). This method provides data of the side force friction (and other data) along the whole length of the test surface being tested which is applied to a variety of computerized algorithms enabling the production of results including (but not limited to) rolling averages, numeric and graphical representations, friction mapping and reports formatted in the layout approved by a wide variety of national airport regulators.

Figure 2.14 Grip Tester

Grip Tester (Figure 2.14) has been used in recent years by FHWA on many demonstration projects in the United State. It is designed to continuously measure the longitudinal friction along the wheel path operating around the critical slip of an ABS at highway speed across the entire stretch of a road with much lower water consumption, which can provide greater detail about spatial variability and be an ideal option for project and network level friction management. The device has the capability to test at highway speeds (50 mph/80 km/h) as well as low speeds (20 mph/32 km/h) using a constant water film thickness. The collected data are recorded in 3-ft (0.9 m) intervals by default and can be adjusted by the user. It also follows ASTM E274 - 11 "Standard Test Method for Skid Resistance of Paved Surfaces Using a Full-Scale Tire".

ASTM E1960 (2015) introduced the calculation procedure to produce the International Friction Index (IFI) from pavement macro-texture and wet pavement friction by different devices using smooth tread test tire. Yager (2013) also covered other pavement friction and texture measuring devices used in airport runway survey worldwide and provided friction rating based on friction readings of different equipment. Detailed requirement, maintenance procedure and relevant measuring equipment for airport pavement skid resistance management were documented in FAA AC 150/5320-12C (FAA, 1997).

2.3 Relationship between Pavement Texture and Skid Resistance

Various researches were conducted in past decades to explore the relationship between pavement texture and skid resistance performance. Gardiner et al. (2004) measured friction on sites with Superpave and Marshall Mix designs, the result revealed that friction related more to the nominal maximum size of aggregate, which is the key factor in change in pavement surface macrotexture, rather than mix design practices. Li et al. (2007) evaluated the influence of the aggregates characteristics on pavement friction performance considering different mixture designs and texture properties, and concluded coarse aggregate pavement generated more consistent friction performance than other regular mixes. Asi (2007) did friction test over different pavement mixes, the result implied that harder aggregate induced higher friction value while vice versa for asphalt content. Kumar and Wilson (2010) demonstrated more than 24% improvement in skid resistance performance when Grade 6 was used comparing with Grade 4 for two geologically similar sourced aggregate chips.

Dr. Masad and his team did a lot of research on aggregate texture and its relationship to HMA pavement surface skid resistance. Masad (2007) measured the skid resistance of pavements constructed using three different aggregate sources and three different aggregate gradations. The skid resistance was found to be related not only to average aggregate texture, but also to the texture distribution within an aggregate sample. The developed method can be used in models for

predicting the change in asphalt pavement skid resistance as a function of aggregate texture, mixture properties, and environmental conditions. Masad et al (2009) and Rezaei et al. (2009) developed a model to determine the skid resistance (IFI) of an asphalt mixture based on aggregate characteristics and gradation. The parameters of this model were determined as functions of initial and terminal aggregate texture, rate of change in aggregate texture after different polishing intervals, and the Weibull distribution parameters describing aggregate gradation. A lot aggregate properties measurement in surface mixes and conducted field pavement friction and texture measurements on selected sections were finished. Consequently, a method and software were developed for predicting asphalt pavement skid resistance incorporating aggregate resistance to polishing, mixture gradation, and traffic (Masad et al., 2010; Masad et al., 2011; Rezaei & Masad, 2013).

Do et al. (2009) proposed a predictive model of the skid resistance incorporating the polishing, the binder removal and the ageing effect, and the predictions exhibited similar trend as the field observations. Goodman (2009) did friction and texture measurement on pavement with different asphalt mixtures at various levels of polishing in lab and field, and developed series of models introducing friction and texture at the mix design stage. Kassem et al. (2013) conducted a series of lab test with the objective to develop a predictive model for friction loss on pavement surface. Tests demonstrates aggregate with higher hardness has higher abrasive resistance. Coarse aggregate gradation shows bigger MPD value than fine mixture, while micro-texture decreases with increasing of polishing number and decreasing of aggregate hardness. Finally, the international friction index (IFI) predictive model was built considering texture, aggregate angularity, and aggregate gradation. Arambula et al. (2013) concluded aggregate with higher soundness value and polishing resistance such as (SAC-A) exhibited higher friction number than SAC-B. Ahammed and Tighe (2012) summarized an equation to predict skid number considering MTD, vehicle speed along and aggregate type with a fair correlation. Researchers employed CT

meter and DF Tester to obtain pavement texture and friction data, and decomposed texture by 'Hilbert-Huang transform' into 'base intrinsic mode functions' to predict friction (Rado & Kane, 2014; Kane et al., 2015).

Other researchers try to predict pavement skid resistance by incorporating pavement micro-texture. Ergun et al. (2004) measured friction and macro-texture of pavement on road sections with different surface characteristics in Belgian. Micro-texture measurement of pavement core sample token at same sections were conducted in lab. Finally, after statistically analyzing on micro- and macro-texture, a new model is founded to predict road surface friction. Results show that at any speed there are strong effects from both macro- and micro-texture on road surface frictions. Serigos (2013) collected pavement micro-texture by AMES Laser Texture Scanner (LTS) which can collect 1 point every 0.015 mm. After analyzing the accurate texture profile, the research realized skid resistance at low speeds of the wet pavement surfaces was significantly affected by both the micro-and the macro-texture of the pavement surface. Incorporating the characterization of the surface micro-texture to the macro-texture significantly improved the prediction of the pavement skid resistance. In another research, micro-texture was measured by a laser scanner with 0.015mm resolution, Slop Variance (SV) and Root Mean Square (RMS) were calculated based on micro-texture profile and researcher stated pavement friction number increases as micro-texture SV and RMS values increase (Li et al, 2015). Ueckermann et al. (2015) measured pavement macro- and micro-texture by optical testing system and proposed a rubber friction model to predict surface skid resistance, and concluded non-contact skid resistance measurement was possible in the future.

2.4 Summary

In a summary, there are tremendous researches on pavement texture and surface skid resistance properties. However, the relationship between pavement texture and friction is not fully understood yet. For one reason, these two have been recognized as individual aspects of

pavement surface characteristics for a long time. The data collection and data analysis of pavement friction is different from that for pavement texture. For another reason, pavement texture is just one of factors affecting pavement friction measurement result. Parameters such as pavement temperature, testing speed, testing tire slip ratio, and so on, also bring influence to the collected friction data.

Secondly, although there are studies trying to relate pavement texture and friction data, the results are limited to small number of pavement types or finite accuracy performance. Research focus on the contribution of pavement micro-texture to friction is limited in the field. A friction prediction model with consistently high accuracy for various roads is not available yet. Finally, with the development of survey technology and computing power of computers, it is possible to provide in-depth understanding of the relationship between texture and friction for the purpose of developing friction prediction model with consistently high accuracy to replace existing friction measurement methodologies. Therefore, the object of this study is to exploring pavement 2D/3D texture data and surface skid resistance using soft computing techniques to perform non-contact pavement friction evaluation.

CHAPTER III NOVEL MACRO- AND MICRO-TEXTURE INDICATORS FOR PAVEMENT FRICTION USING HIGH-RESOLUTION 3D SURFACE DATA

3.1 3D Areal Texture Parameters

After a thorough literature review, there are five different categories of 3D areal parameters used in various areas: height parameters, volume parameters, hybrid parameters, spatial parameters, and feature parameters, all of which are calculated and used to relate pavement texture characteristics to friction performance in this study. The first four categories of parameters are generally classified as field parameters which are calculated using all the data point measured in a 3D surface. The last category is calculated based upon the features which play specific role in a particular function on a 3D image. For each category, several different texture parameters are used for various purposes. The definitions of the 3D areal parameters and their calculations for each category are provided in the following sections.

3.1.1 Height Parameters

The arithmetic mean height (Sa), the root mean square height (Sq), the skewness (Ssk), the Kurtosis (Sku), the maximum height of the surface (Sp, Sv, and Sz), and the traditional MPD are typical height texture parameters. The definitions of Sa, Sq, Ssk, and Sku are shown in Equation 1 individually

$$S_a = \frac{1}{A}\iint_A z(x,y)\,dx\,dy$$

$$S_q = \sqrt{\frac{1}{A}\iint_A z^2(x,y)\,dx\,dy}$$

$$S_{sk} = \frac{1}{{S_q}^3}\frac{1}{A}\iint_A z^3(x,y)\,dx\,dy$$

$$Sk_u = \frac{1}{{S_q}^4}\frac{1}{A}\iint_A z^4(x,y)\,dx\,dy \quad (3.1)$$

Where z(x, y) is the height of pixel in mm at location (x, y) within the 3D image (Leach, 2012).

Sp is the maximum peak height, Sv is the maximum pit height, and Sz is the maximum height of the surface (Leach, 2012). The calculation of MPD is defined in ASTM standard (ASTM E1845-15), which only considers the average height of the two highest peaks of two 50 mm profile segments. Sa is generally used to capture the roughness variation of road surfaces under traffic wear in laboratory (Dunford, 2012). Sa and Sq are insensitive in differentiating peaks, valleys and the spacing of the various texture features, thus pavement surfaces with same Sa or Sq may function quite differently (Michigan Metrology, 2014).

3.1.2 Volume Parameters

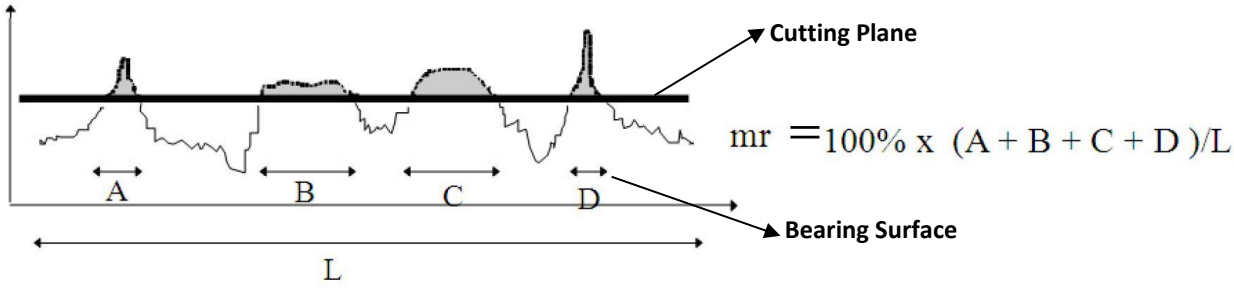

(a) Definition of Material Ratio (*27*)

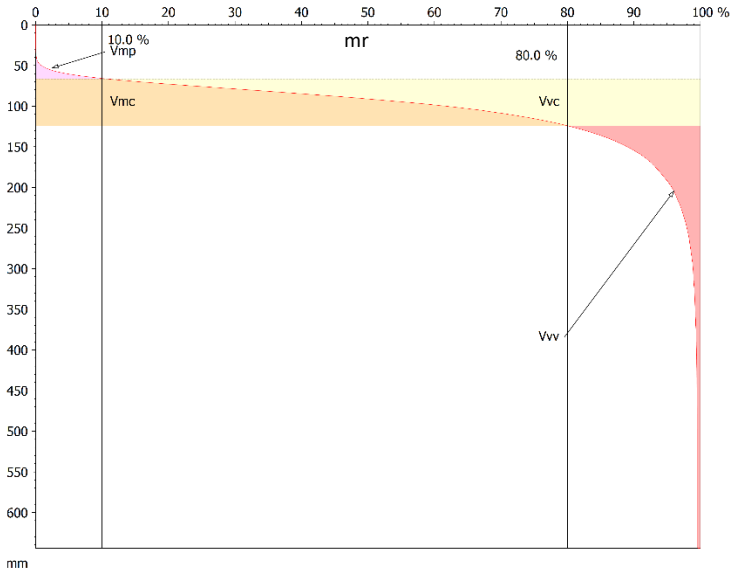

(b) Areal Material Ratio Curve

Figure 15 Calculation of Volume Parameters

The volume parameters, including the void volume (Vv), the material volume (Vm), the peak material volume (Vmp), the core material volume (Vmc), the core void volume (Vvc) and the dales void volume (Vvv), are function related parameters (Leach, 2012;Michigan Metrology, 2014). The material ratio (mr), defined in Figure 3.1(a), is the ratio in percentage of the length of bearing surface at any specified depth in a profile (Michigan Metrology, 2014). mr simulates surface wear of a 3D pavement surface which provides a bearing surface for vehicle tires. As the cutting plane moves down from the highest peak to the lowest valley of a profile, mr will increase along with the bearing surface and range up to 100%. The areal material ratio curve (the dashed line as shown in Figure 3.1(b)) is the cumulative curve of mr from the highest peak to the lowest valley (Michigan Metrology, 2014).

Vv (Vm) for a material ratio mr is calculated by integrating the volume enclosed above (below) the 3D texture image and below (above) the horizontal cutting plane at the height corresponding to mr (Leach, 2012). Vvc (Vmc) is defined as the difference between two void (material) volume

values calculated at different heights corresponding to mr1 and mr2, while Vvv (Vmp) is defined as the void (material) volume calculated at the height corresponding to mr2 (mr1)

$$V_{vc} = V_v(mr1) - V_v(mr2)$$

$$V_{mc} = V_m(mr2) - V_m(mr1)$$

$$V_{vv} = V_v(mr2)$$

$$V_{mp} = V_m(mr1) \quad (3.2)$$

Where mr1 = 10%, mr2 = 80%, and the unit of volume parameters is mm3/mm2 herein (Leach, 2012). In Figure 3.5(b), Vvc (Vmc) is the area enclosed above (below) the areal material ratio curve and between the heights corresponding to mr1 and mr2, and Vvv (Vmp) is the area enclosed above (below) the areal material ratio curve and between the height corresponding to mr2 (mr1). The volume parameters can characterize wear and rolling properties during a running-in procedure (Deltombe et al., 2011; Adelle, 2006). Vmc is useful to understand how much material is available for load support once the top levels of a surfaces are worn away (Michigan Metrology, 2014).

3.1.3 Hybrid Parameters

The hybrid parameters are useful to consider both the height and spacing information of a 3D image simultaneously to evaluate texture characteristic (Li et al., 2016). The root mean square gradient (Sdq) and developed interfacial area ratio (Sdr) are defined as Equation 3.3 and considered herein to differentiate the surface with similar degree of roughness (Leach, 2012; Michigan Metrology, 2014). Sdq and Sdr are affected both by texture amplitude and spacing: a surface with same roughness and wider spaced texture may induce a lower value of Sdq or Sdr (Michigan Metrology, 2014).

$$S_{dq} = \sqrt{\frac{1}{A}\iint \left(\frac{\partial z^2}{\partial x} + \frac{\partial z^2}{\partial y}\right) dxdy}$$

$$S_{dr} = \frac{(Texture\_Surface\_Area) - (Cross\_Sectional\_Area)}{Cross\_Sectional\_Area} \quad (3.3)$$

3.1.4 Spatial Parameters

The calculation of spatial parameters involves the understanding of the autocorrelation function (ACF) which evaluates the correlation of the original surface and the duplicated surface with a relatively shift (Dx, Dy) (Leach, 2012; Michigan Metrology, 2014). The autocorrelation length (Sal) defines the distance over the surface such that the new location will have minimal correlation with the original location, and the texture aspect ratio (Str) is the division of the Sal and the length of slowest decay ACF in any direction (Michigan Metrology, 2014). The texture direction (Std), with values between 0º and 180º, is also included to identify the angular direction of the dominant lay comprising a surface (Leach, 2012; Michigan Metrology, 2014). Str can be applied to evaluate surface texture isotropy, and Sal may find application related to the interaction of electromagnetic radiation with the surface and also tribological characteristics such as friction and wear (Leach, 2012; Michigan Metrology, 2014).

3.1.5 Feature Parameters

The feature parameters herein consider the peak density (Spd), the peak curvature (Spc), and the significant height (S5p, S5v, and S10z). A surface point higher than its surrounding area is called a peak, and the significant peaks on a surface are segmented by inverting the surface and applying the watershed segmentation algorithm and the pruning of the change tree by a specified pruning factor (Leach, 2012). Spd and Spc are defined in Equation 3.4 with unites of $1/mm^2$ and 1/mm respectively (Leach, 2012; Michigan Metrology, 2014). S5p (S5v) is the arithmetic mean height of the five highest (lowest) significant peaks (pits), and S10z is simply the sum of S5p and S5v with unit of mm (Leach, 2012).

Spd can be used in applications where contact is involved along with other parameters, and the peak density can be used to quantify aggregate micro-texture with respect to wear in laboratory (Nataadmadja et al., 2012; Leach, 2012). Spc is useful in predicting the degree of elastic and plastic deformation of a surface under different loading conditions and thus may be used in predicting friction, wear and real area of contact for thermal/electrical applications (Michigan Metrology, 2014). The curvature of a profile was able to quantify aggregate micro-texture with respect to the surface friction under wear condition in laboratory (Nataadmadja et al., 2012).

$$S_{pd} = \frac{Number\ of\ peaks}{Area}$$

$$S_{pc} = \frac{1}{N} \iint_{Peak-Area} \left(\frac{\partial^2 z(x,y)}{\partial x^2}\right) + \left(\frac{\partial^2 z(x,y)}{\partial y^2}\right) dx\, dy \tag{3.4}$$

3.2 Field Data Collection

3.2.1 LTPP SPS-10 Testing Site

The Long Term Pavement Performance (LTPP) recently initiated the Specific Pavement Study 10 (SPS-10) to evaluate the short and long term performance of warm mix asphalt (WMA) mixtures in relative to the conventional hot mix asphalt (HMA). The WMA technology is defined as an asphalt concrete paving material produced and placed at temperatures approximately 50 ºF cooler than those used for conventional HMA (Prowell et al., 2012). The experimental matrix includes, at a minimum, one HMA control section and two WMA test sections using foaming process and chemical additive with 10-25% RAP and RAS content (Puccinelli et al., 2014). Under the SPS-10 experiment initiative, the Oklahoma Department of Transportation (ODOT) constructed six LTPP SPS-10 sections on State Highway 66 (SH-66) in Yukon in November 2015. The annual average daily traffic (AADT) on this road section is 5,900. The average temperature ranges from 35.9 ºF in January to 81.2 ºF in July. This newly constructed site is selected as the testing bed in this study to collect pavement 3D texture and friction data.

(a) Site Location (Google Map)

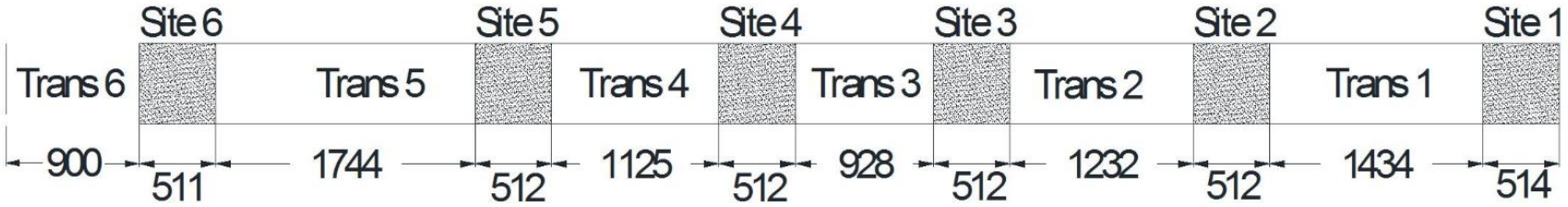

(b) Site Layout (Unit: ft)

Figure 16 LTPP SPS-10 Site in Oklahoma

Table 3.1 lists the experiment design for the SPS-10 sections, and Figure 3.2 shows the site location and the corresponding length for each section. As shown in Table 3.1, Sections 1 to 3 are the required SPS-10 experimental designs, while Sections 4 to 6 are the supplemental sections with mixes chosen by the ODOT Division Office. Sections 1 to 3 are constructed as the conventional HMA control section, WMA using Astec double barrel green (foaming process) and Evotherm M1A (chemical additive) with the same aggregate combination. Sections 4 and 5 are WMA using Evotherm M1A constructed with the same aggregate combination as the first three sites but different binder grades. Section 6 is constructed with stone matrix asphalt (SMA) without fibers (typically used to combat drain down issues) using the same binder grade as those in the first three Sections. The insoluble residue values of the aggregates used in Section 6 and mainline are different from the other sites.

Table 3.1 Experiment Design for LTPP SPS-10 Site in Oklahoma

Section ID	Binder	Comment	Aggregate Combination	Insoluble Residue (%)
1	PG 70-28	HMA with RAP + RAS	1	56.3
2	PG 70-28	WMA Foaming with RAP + RAS	1	56.3
3	PG 70-28	WMA Chemical with RAP + RAS	1	56.3
4	PG 64-22	WMA Chemical with RAP + RAS	1	56.3
5	PG 58-28	WMA Chemical with RAP + RAS	1	56.3
6	PG70-28	WMA Stone mix with mineral filler	2	43.6
Mainline	PG70-28	HMA with RAP	3	60.8

Note:
Aggregate Combination 1 contains 38% 5/8 Chips + 35% Stone Sand + 12% Sand + 12% RAP + 3% RAS;
Aggregate Combination 2 contains 90% 5/8 Chips + 10 Mineral Filler;
Aggregate Combination 3 contains 34% 5/8 Chips + 13% Scrns. + 30% Stone Sand + 13% Sand + 10% RAP.

The gradation curves of the aggregate combinations are shown in Figure 3.3. The gradation of aggregate combination 1 and 3 is close to each other, whereas the aggregate combination 2 for the

SMA MWA is distinctively different. All the gradations of the mixes meet the corresponding specification requirements for ODOT.

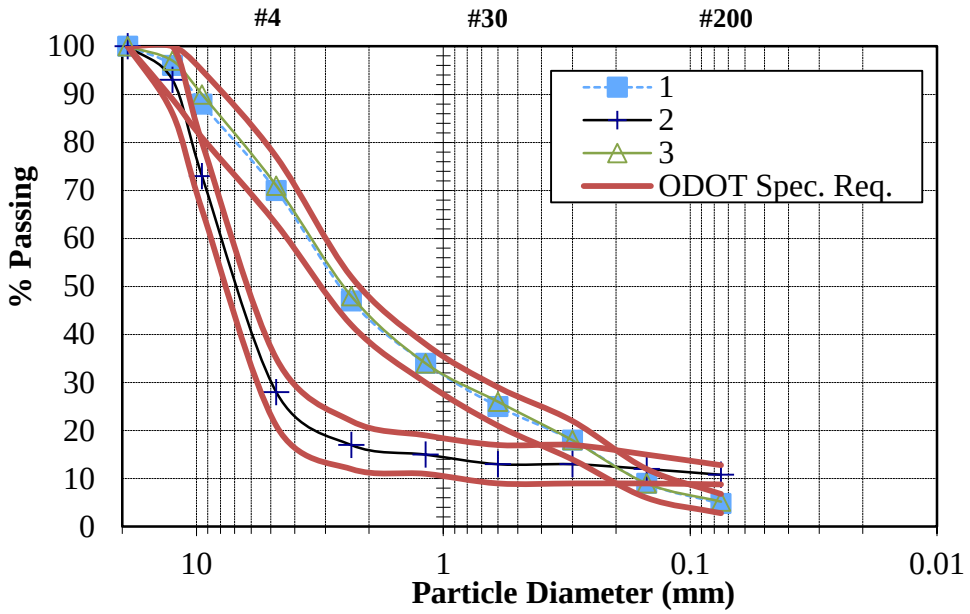

Figure 17 Gradation Curves for Aggregate Combinations

3.2.2 Data Collection Devices

A 3D surface measurement and analysis device, named LS-40 Portable 3D Surface Analyzer (Figure 3.4(a)) (LS-40 for short), scans a 114.3 mm (4.5 in.) by 101.6 mm (4 in.) pavement surface and collects 3D texture data with height resolution (z) at 0.01 mm (0.00039 in.) and lateral resolution (x, y) at 0.05 mm (0.0020 in.). LS-40 provides 3D surface data to calculate MPD by processing thousands of profiles over the entire scanned surface according to ASTM standard (ASTM E1845-15), with optional processing modules of measuring other surface features, such as aggregate form factor, angularity calculation based on multiple contour measurements, and micro-texture indicators, such as Root Mean Square (RMS). LS-40 can not only be used in the laboratory, but also be placed on a localized pavement surface area in the field to collect 2048 by 2448 cloud points for pavement texture characterization. Figures 3.4(c) and 3.4(e) are two example 3D pavement data collected on Section 2 and 6 respectively.

(a) LS-40 Portable 3D Surface Analyzer

(b) Dynamic Friction Tester

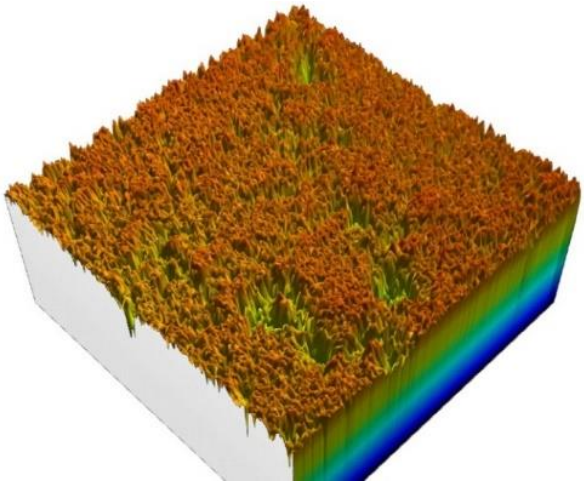

(c) 3D Texture Data (Section 2)

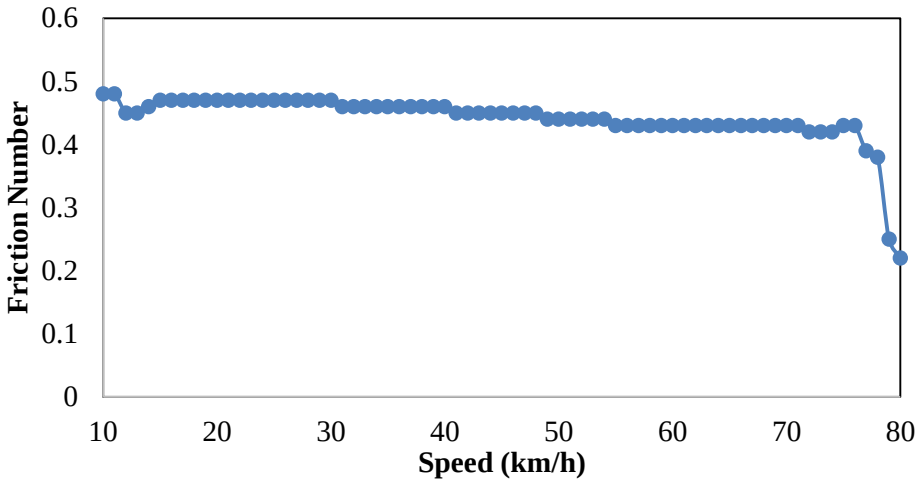

(d) DFT Friction Data (Section 2)

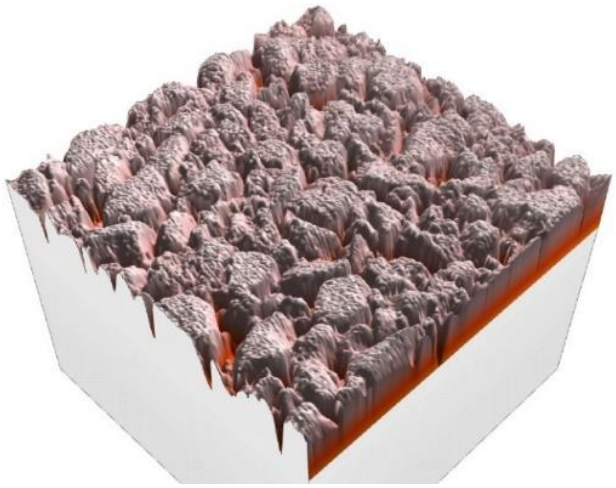

(e) 3D Texture Data (Section 6)

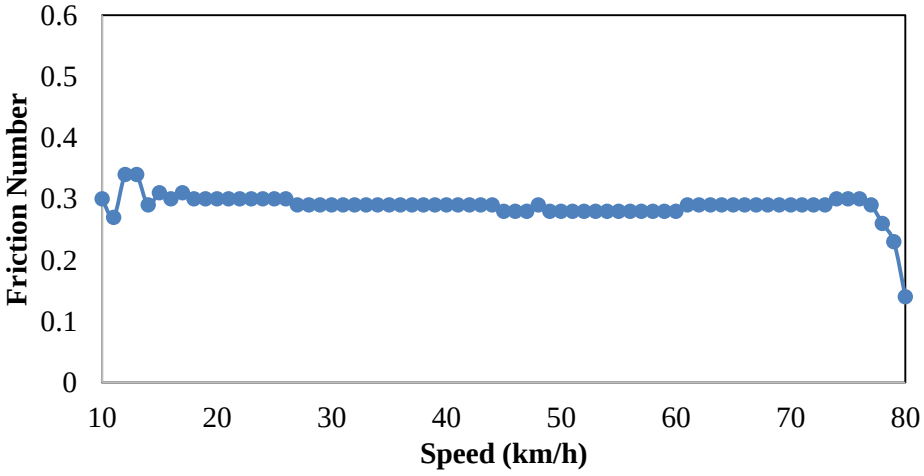

(f) DFT Friction Data (Section 6)

Figure 18 Data Collection Devices and Example Data Sets

ASTM E1911-09a provides specification on measuring paved surface frictional properties using the Dynamic Friction Tester (DFT). A DFT (Figure 3.4(b)) consists of a horizontal spinning disk fitted with three spring loaded rubber sliders. The water is sprayed in front of the sliders and a constant load is applied to the slider as the disk rotating on the test surface. The torque is monitored continuously as the disk rotational velocity reduces due to the friction between the sliders and the test surface, then it is used to calculate the surface friction coefficients. DFT has been widely used in friction measurement under various conditions to explore the speed dependency of pavement friction by measuring friction at various speeds. Figures 3.4(d) and 3.4(f) are two example DFT friction data measured at the same locations where texture data are collected as demonstrated in Figures 3.4(c) and 3.4(e).

3.3 Preliminary Result

The data collection efforts described herein include two data collection activities, the first on November 13th, 2015 immediately after the construction of the testing site and the second on May 25th 2016 when the Sections were approximately 6-month in age, on the six LTPP SPS-10 Sections and the transition sections in-between. LS-40 Portable 3D Surface Analyzer and DFT were used to measure pavement 3D surface data and friction data separately in the right wheel-path (approximately 0.9 m (3 ft.) from the shoulder) in parallel at the same predefined locations. Within each LTPP SPS-10 section, three pairs of LS-40 3D data and DFT friction data were obtained at 30 m (100 ft.) interval starting from the beginning of the section. As the mainline after each LTPP SPS-10 section, another three pairs of pavement texture and friction measurement were conducted at 91 m (300 ft.) interval from the ending of the section. Therefore, thirty-six pairs of pavement 3D texture and friction data measurement were obtained for each data collection. Finally, sixty-nine pairs of pavement texture and friction data are analyzed in this article after three data sets are removed due to the bad data quality.

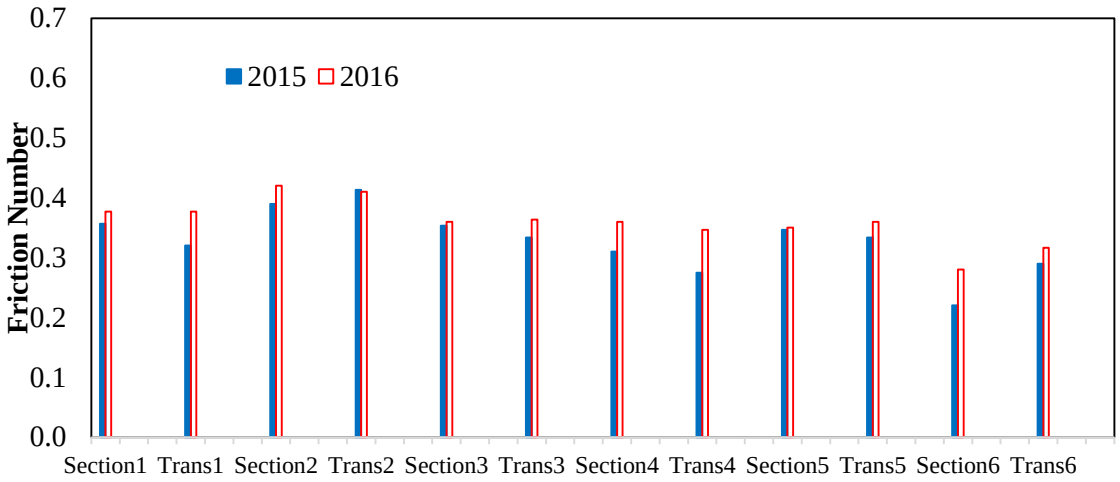

(a) Friction Number at 70 km/h

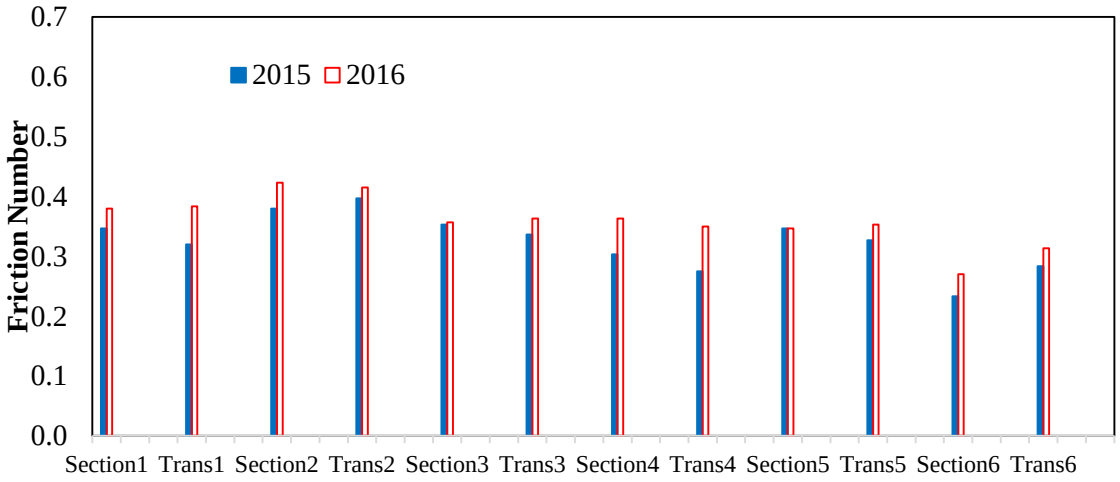

(b) Friction Number at 60 km/h

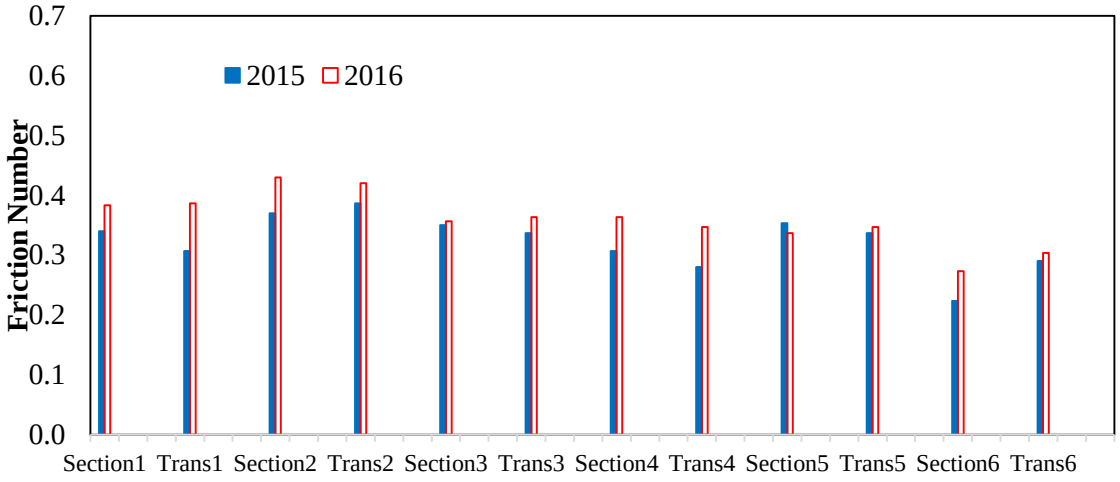

(c) Friction Number at 50 km/h

(d) Friction Number at 40 km/h

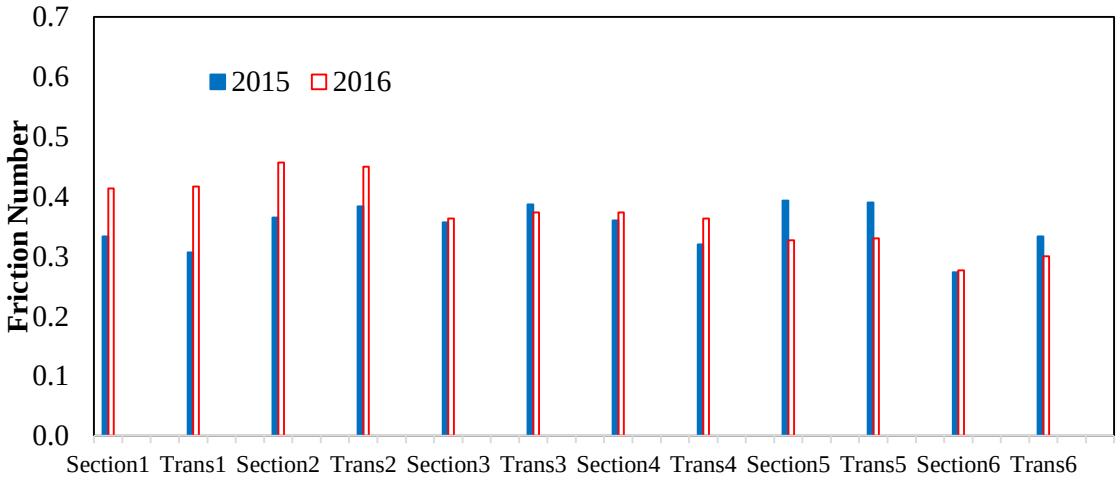

(e) Friction Number at 30 km/h

(f) Friction Number at 25 km/h

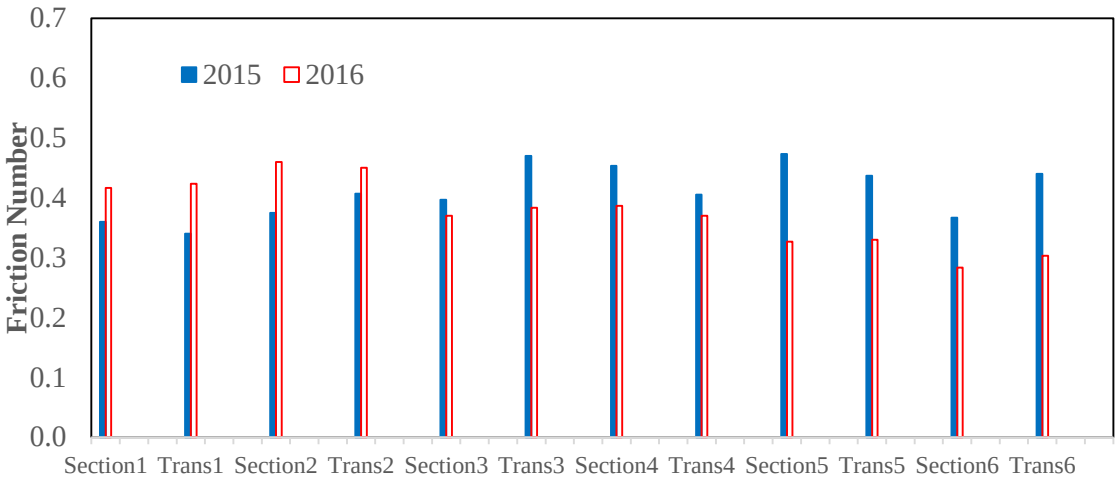

(g) Friction Number at 20 km/h

(h) Friction Number at 15 km/h

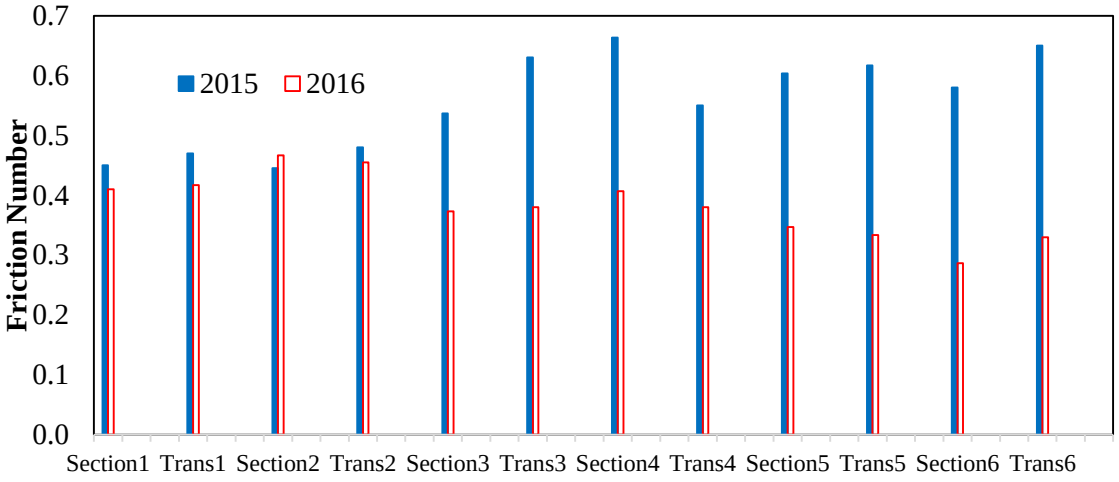

(i) Friction Number at 10 km/h

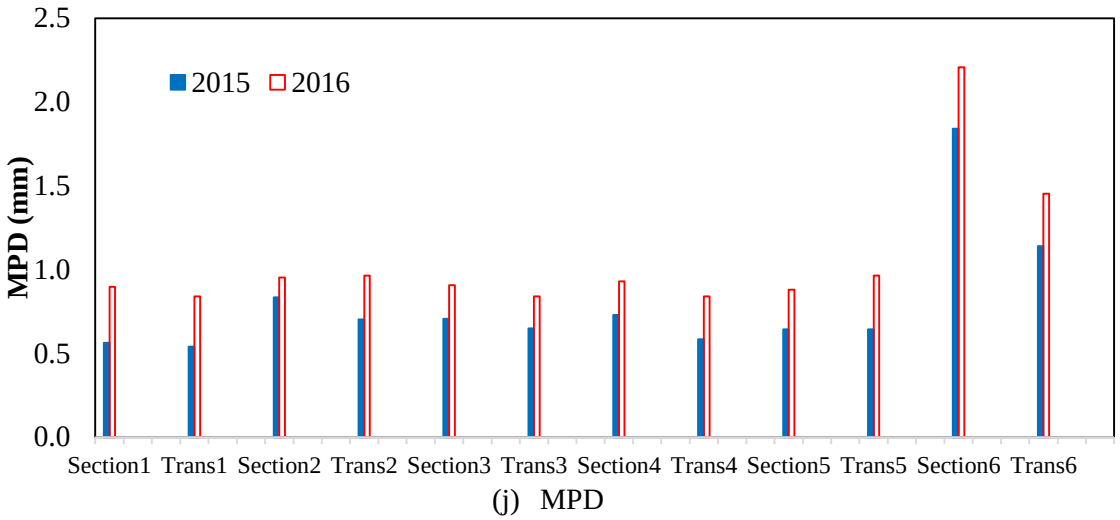

(j) MPD

Figure 19 Average DFT Friction at Various Testing Speeds and MPD Summary

For preliminary analysis, MPD for each 3D measurement is calculated, while pavement DFT friction numbers at various testing speeds from 10 km/h (6 MPH) to 70 km/h (44 MPH) are produced. The average DFT friction numbers at speeds from 10 km/h (6 MPH) to 70 km/h (44 MPH) and the average MPD for each SPS-10 section and transition are plotted in Figure 3.5. It is illustrated that the average friction numbers at speeds over 40 km/h (25 MPH) show an increase tendency between the two data collection events (Figures 3.5(a) through 3.5(d)), whereas the average friction numbers at speeds lower than 20 km/h (12 MPH) exhibit a decrease tendency for most of the locations (Figures 3.5(g) to 3.5(i)). For example, the average friction numbers at 60 km/h (37 MPH) for Sections 1 through 6 are 0.35, 0.38, 0.35, 0.30, 0.35, and 0.23 for the first data collection in 2015, and 0.38, 0.42, 0.36, 0.36, 0.34 and 0.27 for the second collection in 2016. The average friction numbers at 10 km/h for Sections 1 through 6 are 0.45, 0.45, 0.54, 0.66, 0.60, and 0.58 in 2015, while 0.41, 0.47, 0.37, 0.41, 0.35 and 0.29 in 2016. At speeds from 20 km/h to 30 km/h (Figures 3.5(e) to 3.5(g)), no consistent tendency is observed on these sections. On the other hand, the average MPD values for each of the six SPS-10 section and transition section display an increasing tendency, as shown in Figure 3.5(j). The average MPD for Sections 1 through 6 are 0.56 mm (0.022 in.), 0.84 mm (0.033 in.), 0.71 mm (0.028 in.), 0.73 mm (0.029 in.), 0.64 mm (0.025 in.), and 1.84 mm (0.072 in.) in 2015, and 0.90 mm (0.035 in.), 0.95 mm

(0.037 in.), 0.91 mm (0.036 in.), 0.93 mm (0.037 in.), 0.88 mm (0.035 in.), and 2.21 mm (0.087 in.) in 2016.

Generally the evolution of skid resistance with an initial increase in friction coefficient occurs in the following months immediately after the laying of the road surface. Due to the applications of traffic polish, the bitumen film which masks the aggregate is gradually removed and the pavement friction number gradually increases. During the binder removal phase, more aggregate is exposed to the pavement surface. The binder removal period could range from 6 months to 2 years (Do et al. 2007). Since 64 km/h (40 MPH) is the standard testing speed to collect friction number (ASTM E1911-09a), it is logical that the friction numbers have increased over the last 6 month as shown in Figure 3.5(b). In addition, "new" surface texture may be generated under potential "differential" traffic polishing (Nataadmadja et al. 2012), which probably results in the increase of the average MPD values during the last 6-month period.

On the other hand, Section 6 shows distinct higher average MPD values comparing to those on the other sections for both data collections (Figure 3.5(j)), while the average DFT friction numbers on Section 6 are relatively lower for testing speeds over 25 km/h (16 MPH) (Figures 3.5(a) to 3.5(f)). The relatively lower insoluble residue value of the aggregate (Table 3.1) and the observed thick bitumen film after construction are the possible reasons for the lower skid resistance of Section 6. In addition, friction and MPD data on Section 6 show opposite development tendency for both collection events at speeds lower than 20 km/h (12 MPH) (Figures 3.5(g) to 3.5(j)). Since MPD fails to capture the differences and variations in friction performance both at high and low speeds, new texture parameters are needed to be developed to relate pavement texture with friction performance at macro- and micro-level.

3.4 Selection of 3D Texture Parameters

3.4.1 Correlation Analysis

Considering all five categories of 3D areal parameters aforementioned, there are twenty-four different parameters available to represent the 3D texture characteristics of a pavement surface. The calculation of those parameters are calculated via the Mountains® software. The correlation analysis is conducted within each category and among different categories to remove the parameters who exhibit strong correlations and remove their potential multicollinearity for regressional friction model development. Correlation coefficient of 0 means that there is no correlation, -1 denotes a perfect negative correlation, while +1 suggests a perfect positive correlation between the two variables. A correlation greater than 0.8 is generally described as strong, whereas a correlation less than 0.5 is generally described as weak (Correlation Coefficient, 2016).

3.4.2 Correlations within Each Category

The correlation coefficients within each category are summarized in Tables 3.2(a) to 3.2(c).

- Based on Table 3.2(a), Sq and Ssk are kept to represent as the height parameters since their correlation coefficients with other parameters are less than 0.5. The traditional texture indicator MPD is excluded herein because it is highly correlated with many height parameters such as Sq, Sp, Sv, Sz, and Sa.
- Based on Table 3.2(b), only Vmc is kept as the volume parameter, and Sdq is selected as the hybrid parameter to evaluate the friction performance between the vehicle tire and the pavement surface.
- Based on Table 3.2(c), Sal and Str are selected as the spatial parameters while Spd, Spc and S5v are selected as feature parameters due to their lower correlation coefficients with other parameters.

In summary, after the correlation analysis within each texture parameter category, only Sq, Ssk, Vmc, Sdq, Sal, Str, Spd, Spc and S5v are determined as the potential 3D areal parameters, which are not highly correlated within each category, for the development of relationship between pavement texture and friction performance.

3.4.3 Correlations among Categories

Subsequently, correlation analysis among different categories is performed for the previously identified 3D parameters within each category, since correlations may be strong among the parameters within different categories. As shown in Table 3.2(d), Sq, Sdq, Str, Spc, and S5v are excluded because their correlation coefficients with other parameters are larger than 0.5. Correspondingly, Ssk, Vmc, Sal and Spd, which represents the height, volume, spatial and feature attributes of a 3D surface respectively, are selected as the final list of the 3D areal parameters for friction model development. The statistics of the selected 3D areal parameters on each SPS-10 section and transition are plotted in Figure 3.6 to evaluate the variations of these texture indicators between these two data collection events:

- Vmc and Spd demonstrate decreasing tendency with traffic polish for most locations (Figures 3.6(b) and 3.6(c)), while Ssk and Sal exhibit inconsistent tendency (Figures 3.6(a) and 3.6(d)).
- As can be seen in Figure 3.6(c) and Figure 3.4(i), the development of Spd corresponds well to the variation tendency of DFT friction number at the speed of 10 km/h (6 MPH).
- On the other hand, because Vmc represents the part of the surface material which does not interact with another surface in contact (25), the smaller the Vmc value, the more surface materials are involved in the contact process with vehicle tires. Therefore, it is observed from Figure 3.6(b) and Figures 3.5(a) and 3.5(b) that the development of Vmc corresponds well to the variation tendency of friction number at speeds over 60 km/h (37 MPH) for all the sections.

Table 3.2 Correlation Analyses of 3D Areal Texture Parameters

Parameter	**Sq**	**Ssk**	Sku	Sp	Sv	Sz	Sa	MPD
Sq	1.0	-0.2	0.3	0.9	0.9	1.0	1.0	0.9
Ssk	-0.2	1.0	-1.0	-0.3	-0.2	-0.1	-0.1	-0.2
Sku	0.3	-1.0	1.0	0.4	0.3	0.2	0.2	0.3
Sp	0.9	-0.3	0.4	1.0	1.0	0.9	0.9	0.9
Sv	0.9	-0.2	0.3	1.0	1.0	0.9	0.9	0.9
Sz	1.0	-0.1	0.2	0.9	0.9	1.0	1.0	0.9
Sa	1.0	-0.1	0.2	0.9	0.9	1.0	1.0	0.9
MPD	0.9	-0.2	0.3	0.9	0.9	0.9	0.9	1.0

(a) Height Parameters

Parameter	Vm	Vv	Vmp	**Vmc**	Vvc	Vvv	**Sdq**	Sdr
Vm	1.0	0.7	1.0	0.7	0.7	0.6	-	-
Vv	0.7	1.0	0.7	1.0	1.0	1.0	-	-
Vmp	1.0	0.7	1.0	0.7	0.7	0.6	-	-
Vmc	0.7	1.0	0.7	1.0	1.0	0.9	-	-
Vvc	0.7	1.0	0.7	1.0	1.0	0.9	-	-
Vvv	0.6	1.0	0.6	0.9	0.9	1.0	-	-
Sdq	-	-	-	-	-	-	1.0	0.8
Sdr	-	-	-	-	-	-	0.8	1.0

(b) Volume and Hybrid Parameters

Parameter	**Sal**	**Str**	Std	**Spd**	**Spc**	S10z	S5p	**S5v**
Sal	1.0	-0.3	-0.1	-	-	-	-	-
Str	-0.3	1.0	0.5	-	-	-	-	-
Std	-0.1	0.5	1.0	-	-	-	-	-
Spd	-	-	-	1.0	-0.3	-0.3	-0.3	-0.3
Spc	-	-	-	-0.3	1.0	0.9	0.8	0.9
S10z	-	-	-	-0.3	0.9	1.0	0.9	0.9
S5p	-	-	-	-0.3	0.8	0.9	1.0	0.6
S5v	-	-	-	-0.3	0.9	0.9	0.6	1.0

(c) Spatial and Feature Parameters

Parameter	Sq	**Ssk**	**Vmc**	Sdq	**Sal**	Str	**Spd**	Spc	S5v
Sq	1.0	-0.2	1.0	0.7	-0.1	0.6	-0.3	0.8	0.8
Ssk	-0.2	1.0	0.0	0.2	0.2	0.2	0.4	0.1	-0.0
Vmc	1.0	0.0	1.0	0.7	-0.1	0.6	-0.3	0.9	0.9
Sdq	0.7	0.2	0.7	1.0	-0.0	0.4	-0.1	0.8	0.7
Sal	-0.0	0.2	-0.1	-0.0	1.0	-0.3	-0.1	-0.1	-0.1
Str	0.6	0.2	0.6	0.4	-0.3	1.0	-0.1	0.5	0.5
Spd	-0.3	0.4	-0.3	-0.1	-0.1	-0.1	1.0	-0.3	-0.3
Spc	0.8	0.1	0.9	0.8	-0.1	0.5	-0.3	1.0	0.9
S5v	0.8	-0.0	0.9	0.7	-0.1	0.5	-0.3	0.9	1.0

(d) Among Categories

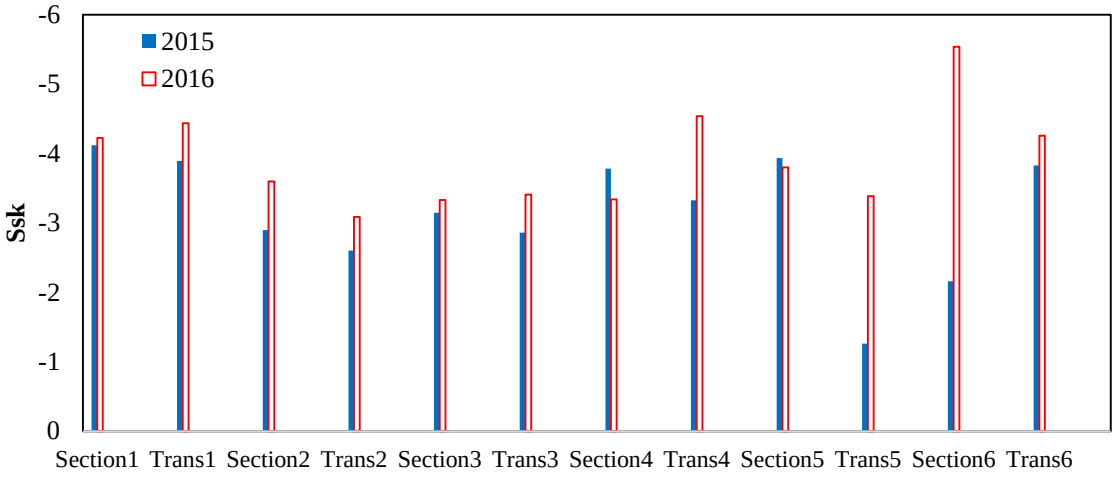

(a) Skewness, Ssk

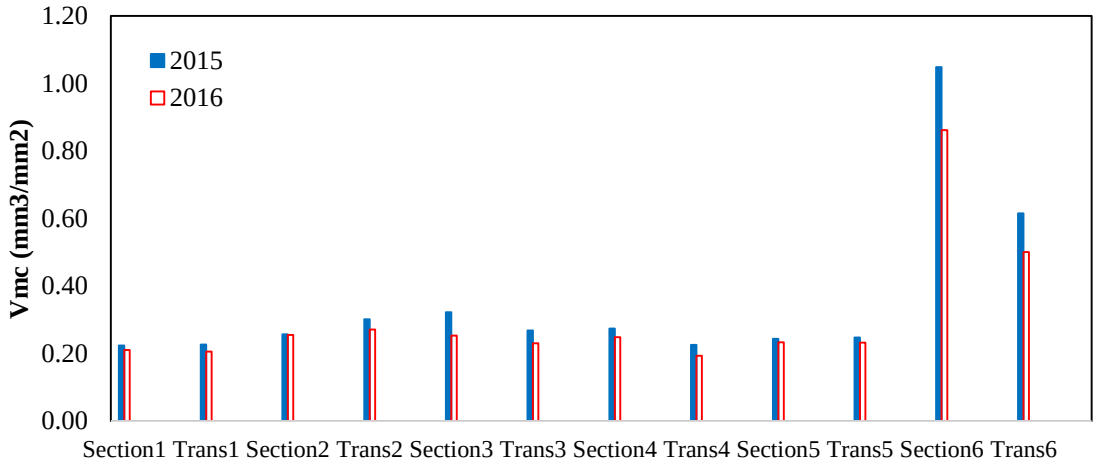

(b) Core Material Volume, Vmc

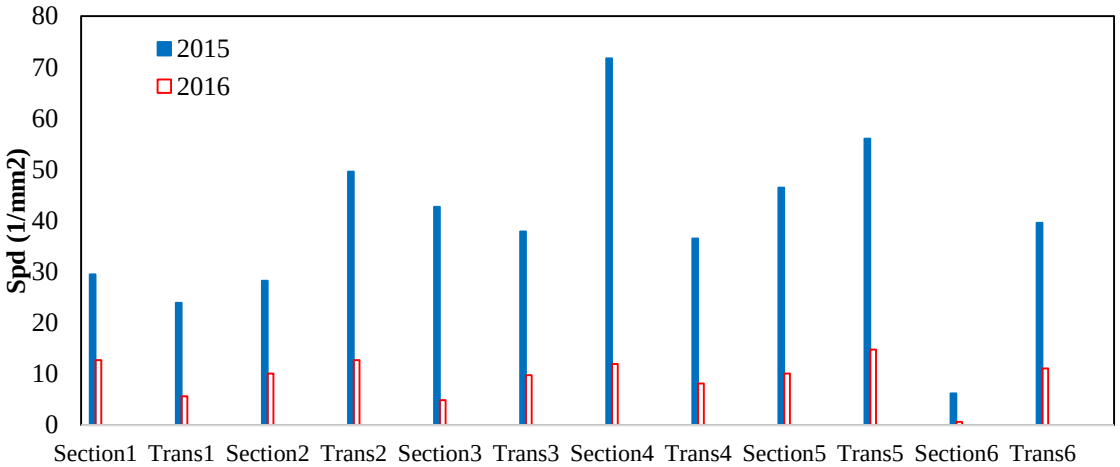

(c) Peak Density, Spd

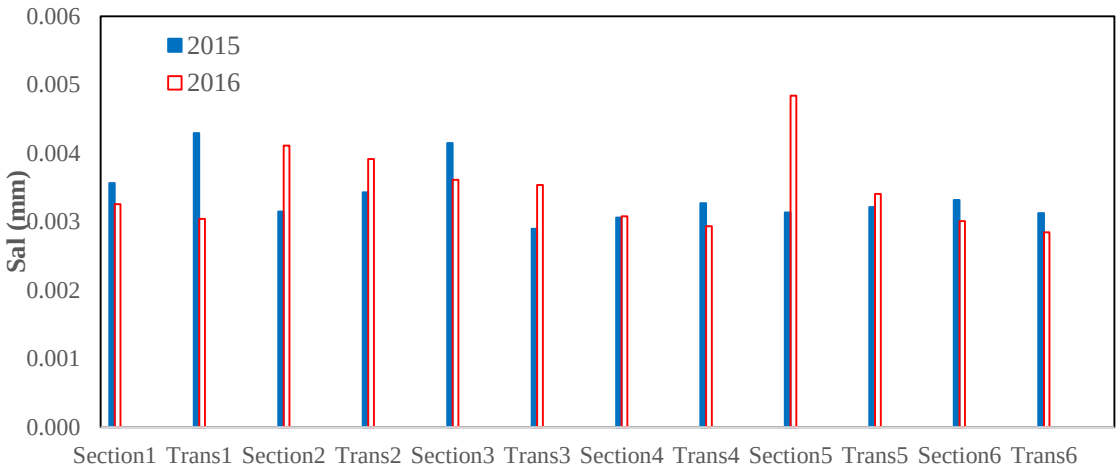

(d) Autocorrelation Length, Sal

Figure 20 Comparisons of Selected 3D Pavement Texture Parameters

3.5 Friction Prediction Models based on Selected 3D Areal Texture Parameters

3.5.1 Model Development

The sixty-nine sets of DFT friction numbers at different speeds along with the selected 3D areal texture parameters, Ssk, Vmc, Sal and Spd, are prepared for model development. Every other data sets are used to develop the friction prediction model at different speeds, while the remaining data sets are reserved for model validation. Multivariate linear regression analysis is conducted to identify the significant confidence level of the selected 3D areal texture parameters on friction number at different speeds, and the results are summarized in Table 3.3:

- Vmc and Spd show consistently significant influence on friction numbers for testing speeds over 25 km/h (16 MPH) and less than 20 km/h (12 MPH), individually.
- Ssk is identified as a significant parameter for DFT friction tested at speed of 10 km/h (6 MPH) only.
- Sal is not a significant factor on friction at any speeds among these selected four parameters.

Table 3.3 Significance of Selected 3D Texture Parameters on DFT Friction at Different Speeds

3D Parameters	Friction Number								
	DFT70	DFT60	DFT50	DFT40	DFT30	DFT25	DFT20	DFT15	DFT10
Ssk	-	-	-	-	-	-	-	*	*
Vmc	**	**	**	**	**	*	-	-	*
Sal	-	-	-	-	-	-	-	-	-
Spd	-	-	-	-	-	-	*	**	***

Note:
DFTxx means the DFT friction number collected at speed xx km/h; Significance codes: '***' $p < 0.001$, '**' $p < 0.01$, '*' $p < 0.05$, '-' $p > 0.05$. For example '*' indicates the P-value is less than 0.05 and the parameter is significant to the friction number; '-' means the P-value is larger than 0.05 and the parameter is not significant to the friction number.

Subsequently, friction prediction models are developed based on only the significant 3D areal parameters at different speeds. The estimated regression coefficients and P-values of friction prediction models are summarized in Table 3.4. All the P-values for the 3D areal texture parameter herein are smaller than 0.05 in the proposed model, indicating their significance to pavement friction. Therefore the friction number at different speeds are valid and can be calculated based on the selected 3D areal parameters as Equation 3.5,

$$Friction\ Number = a + \sum_1^3 \mathrm{T}_i * b_i \tag{3.5}$$

Where a is the estimated coefficient for intercept, T_i represents the Vmc, Ssk and Spd of a 3D pavement surface, and b_i is the estimated coefficient for the corresponding 3D areal parameter at different speeds.

Table 3.4 Statistic Results of Friction Prediction Models

Friction	Estimated Coefficients and P-value			Validation Result		
	Item	Coefficient	P-value	R^2	SSE	# Samples
Models based on Selected 3D Areal Texture Parameters						
70 km/h	Intercept	0.395	6.36E-26	0.58	0.031	34
	Vmc	-0.138	8.07E-05			
60 km/h	Intercept	0.394	7.58E-26	0.57	0.034	
	Vmc	-0.144	4.54E-05			
50 km/h	Intercept	0.391	4.38E-26	0.54	0.038	
	Vmc	-0.136	7.63E-05			
40 km/h	Intercept	0.394	3.83E-26	0.48	0.044	
	Vmc	-0.127	0.00018			
30 km/h	Intercept	0.399	2.74E-25	0.37	0.057	
	Vmc	-0.110	0.001804			
25 km/h	Intercept	0.405	1.16E-24	0.29	0.066	
	Vmc	-0.091	0.012268			
20 km/h	Intercept	0.362	2.81E-23	0.33	0.089	
	Spd	0.001	0.003921			
15 km/h	Intercept	0.368	5.68E-21	0.38	0.131	
	Spd	0.002	8.28E-05			
10 km/h	Intercept	0.414	1.63E-07	0.54	0.209	
	Ssk	0.027	0.043722			
	Vmc	0.181	0.002568			
	Spd	0.004	3.21E-06			
Models based on MPD						
70 km/h	Intercept	0.401	2.44E-20	0.30	0.051	34
	MPD	-0.055	5.52E-03			
60 km/h	Intercept	0.399	4.80E-20	0.29	0.055	
	MPD	-0.056	5.15E-03			
50 km/h	Intercept	0.397	1.91E-20	0.26	0.060	
	MPD	-0.054	5.76E-03			
40 km/h	Intercept	0.399	1.09E-20	0.25	0.063	
	MPD	-0.050	0.00832			
30 km/h	Intercept	0.407	1.06E-20	0.26	0.067	
	MPD	-0.048	0.01288			
25 km/h	Intercept	0.420	5.22E-21	0.26	0.069	
	MPD	-0.048	0.01302			
20 km/h	Intercept	0.441	5.12E-20	0.21	0.097	
	MPD	-0.048	0.02860			
15 km/h	Intercept	0.473	1.29E-16	0.10	0.192	
	MPD	-0.048	0.10751			
10 km/h	Intercept	0.531	6.87E-13	0.16	0.373	
	MPD	-0.061	0.18092			

3.5.2 Model Verification

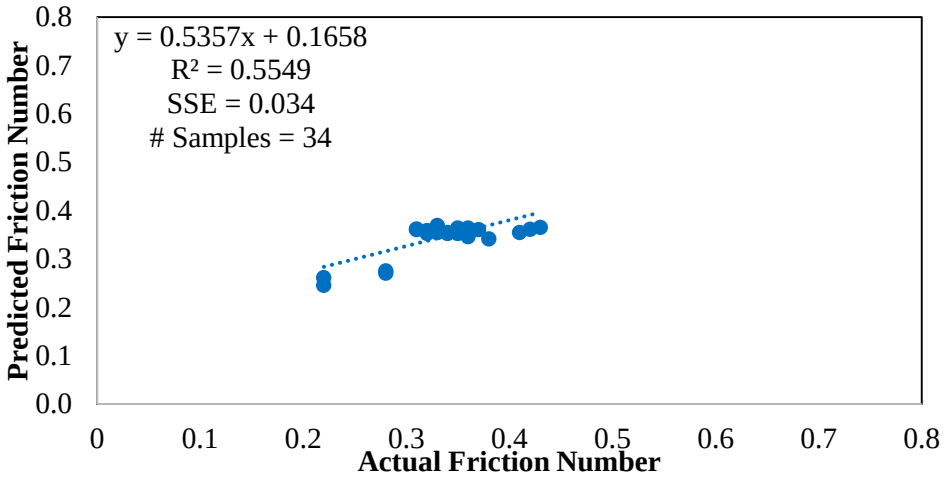

(a) Proposed Model (60 km/h)

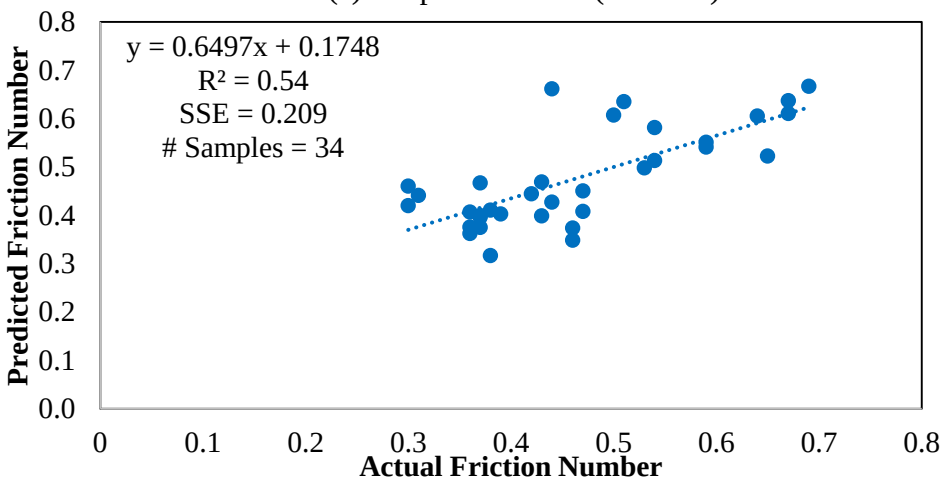

(b) Proposed Model (10 km/h)

Figure 21 Validation Result of Proposed Model

Based on Equation 3.5, the predicted friction numbers of the validation data sets are calculated and compared with the actual friction numbers to validate the proposed models. The validation results of the developed friction prediction model at different speeds are also summarized in Table 3.4. The R-squared values are 0.54 to 0.58 between the predicted and the actual DFT friction numbers at speeds from 10 km/h (6 MPH) to 70 km/h (44 MPH), respectively. Generally speaking, the friction prediction models at higher testing speeds have better performance than those at lower speeds. The sum of squared error (SSE) for the proposed models at speed 70 km/h

(44 MPH) to 10 km/h (6 MPH) increases from 0.031 to 0.209. Example of the actual and the predicted friction numbers at high and low speeds are compared in Figure 3.7.

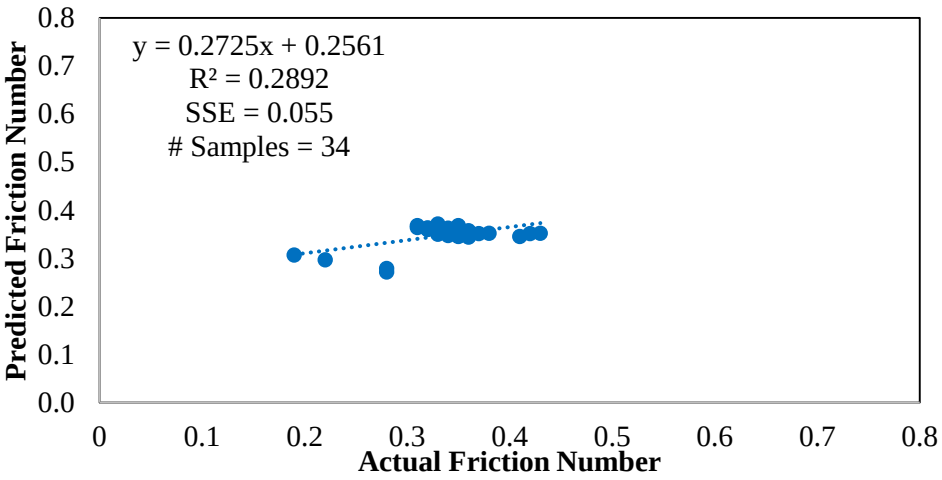

(a) Friction Model via MPD (60 km/h)

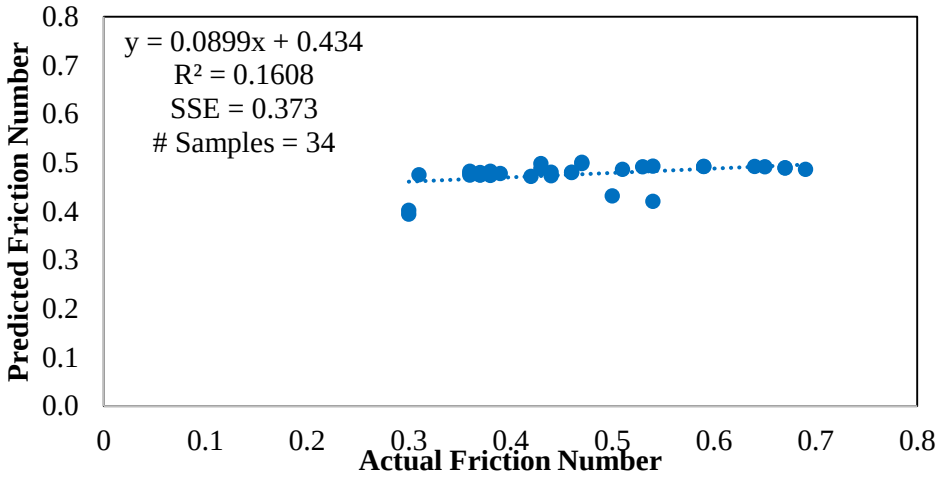

(b) Friction Model via MPD (10 km/h)

Figure 22 Validation Result of Model via MPD

To demonstrate the advantages of the proposed parameters, linear regression friction prediction models at different testing speeds are also developed considering MPD as the influencing texture parameter. The estimated regression coefficients and P-values are also provided in Table 3.4. The P-values for the MPD based models are smaller than 0.05 for testing speeds over 20 km/h (12 MPH), indicating the significance of MPD to pavement friction at high speed. However, the P-values are greater than 0.05 for models at the testing speeds of 15 km/h (9 MPH) and 10 km/h (6 MPH), indicating the insignificance of MPD to pavement friction at low speed. The R-squared

values of the MPD based models range from 0.1 to 0.3 between the predicted and actual DFT friction numbers, which are much lower than those for the proposed models based on the 3D texture indicators. In addition, the sum of squared errors of prediction (SSE) in the MPD based model are consistently higher than those in the models from this paper, proving that the DFT friction models based on the selected 3D areal texture parameters are more robust. Examples of the actual and the predicted friction numbers at high and low speeds are compared in Figure 3.8.

Based on Tables 3.3 and 3.4, Vmc is the only significant parameter on friction number for the models at speeds over 20 km/h (12 MPH), whereas the Spd is the only significant parameter on friction number for the models at speeds 20 km/h (12 MPH) and 15 km/h (9 MPH). Even though there are three significant parameters in the model at 10 km/h, Spd is the dominate parameter over the other two based on their P-values. Therefore, it can be concluded that Vmc and Spd are the 3D areal parameters corresponding to macro- and micro-texture for friction prediction at high (over 40 km/h (25 MPH)) and low speeds (lower than 15 km/h (9 MPH)).

3.6 Summary

The objective of this chapter is to identify suitable pavement texture parameters under 3D to characterize pavement surface texture and friction performance. The LS-40 Portable 3D Surface Analyzer and the Dynamic Friction Tester with necessary software tools are used to perform pavement texture and friction data collection and subsequent calculation of 3D areal parameters and friction numbers at different testing speeds. The 3D surface range data with the resolution of 0.01 mm (0.00039 in.) and 0.05 mm (0.0020 in.) in vertical and lateral direction are collected on the newly constructed LTPP SPS-10 site in Oklahoma with 6 WMA sections. Twenty-four 3D areal texture parameters from five categories, including height parameter, volume parameters, hybrid parameters, spatial parameters and feature parameters, are explored in the study and calculated for each 3D surface data collection to comprehensively evaluate the pavement surface texture characteristics.

Correlation analysis is performed within each texture indicator category and among the categories to select the most relevant and representative 3D areal parameters for friction model development. The results show that Vmc (a volume parameter) and Spd (a feature parameter) can relate the pavement texture at macro- and micro-level for friction in wet conditions at high and low speeds respectively. Multivariate linear regression pavement friction prediction models are developed based on the selected 3D areal texture parameters at different speeds. The validation results demonstrate that the developed friction prediction models produce fairly accurate friction predictions. The selected 3D texture parameters provide better alternative to characterize texture attributes with respect to pavement friction performance, and have the potential to replace the existing contact-based friction measurement methodologies which require consuming water and testing tires with non-contact high-resolution 3D laser-imaging based techniques.

However, the novel 3D texture parameter analysis in this dissertation is limited in this chapter only because of two reasons. Firstly, it requires traffic control to perform static testing using LS-40 and DFT to collect high resolution 3D texture data and corresponding friction data. It's difficult for the research team to gather more high resolution 3D texture data on different pavement types. Secondly, 2D macro-texture data is extensively collected at highway speed by DOTs. With the application of High Speed Profiler, it's easier for the research team to perform 2D macro-texture profile data collection on different pavement surfaces without traffic control. Therefore, following chapters will apply other computing techniques to analyze 2D macro-texture profile for friction prediction.

CHAPTER IV WAVELET BASED MACRO-TEXTURE ANALYSIS FOR PAVEMENT FRICTION PREDICTION

4.1 Wavelet Methodology

Wavelet is an irregular and asymmetric waveform within limited duration that has an average value of zero, and it can be stretched or compressed to match signal at different locations and scales and therefore represent signal in frequency and time domain simultaneously (Misiti et al., 2000). Wavelet transform has been widely used in many civil engineering applications, such as damage detection (Hester & Gonzalez, 2012), corrosion detection (Abbasnia & Farsaei, 2013), crack detection (Wang et al., 2007), effectiveness evaluation of pavement maintenance treatments (Wei et al., 2005; Alhasan et al., 2016; Hassan, 2015), pavement macro-texture profile analysis (Zelelew et al., 2013; Zelelew et al., 2014). Discrete wavelet transform is applied herein to decompose pavement macro-texture profiles into multi-level decompositions in the form of approximation signal and detailed signals. The macro-texture profile can be represented as a series of profiles corresponding to distinct wavelength sub-bands (Zelelew et al., 2014)

$$s(t) = a_L(t) + \sum_{j=1}^{L} d_j(t) \tag{4.1}$$

where $a_L(t)$ is the approximation signal corresponding to the longer wavelength, $d_j(t)$ is the detail components relating to the shorter wavelength at level j, and L is the number of sub-bands or decomposition levels.

After profile decomposition, the energy of each decomposition level can be applied to interpret pavement macro-texture profile at various scales (Wei et al., 2005; Zelelew et al., 2014). The energy content for a particular decomposed sub-band is obtained as below (Zelelew et al., 2014)

$$E_j^d = \sum_{i=1}^{N} \left| d_j(x) \right|^2 \tag{4.2}$$

where E_j^d and $d_j(x)$ are the wavelet energy indicator and detail coefficients for the *j*th decomposition level of a macro-texture profile, and N is the number of data points in the decomposed macro-texture profile. Specifically, the total energy (TE) of given macro-texture profile is the summation of E_j^d from the first to the Lth sub-band and can be calculated as (Zelelew et al., 2014):

$$TE = \sum_{j=1}^{L} E_j^d \tag{4.3}$$

The relative energy (RE) is the percentage of the energy at the *j*th decomposed sub-band as compared to the total energy (Zelelew et al., 2014):

$$RE_j = \frac{E_j^d}{TE} \times 100\% \tag{4.4}$$

The REs at various sub-bands constitute the energy distribution of a given macro-texture profile at different wavelengths.

4.2 Data Collection and Preliminary Result

4.2.1 Data Collection

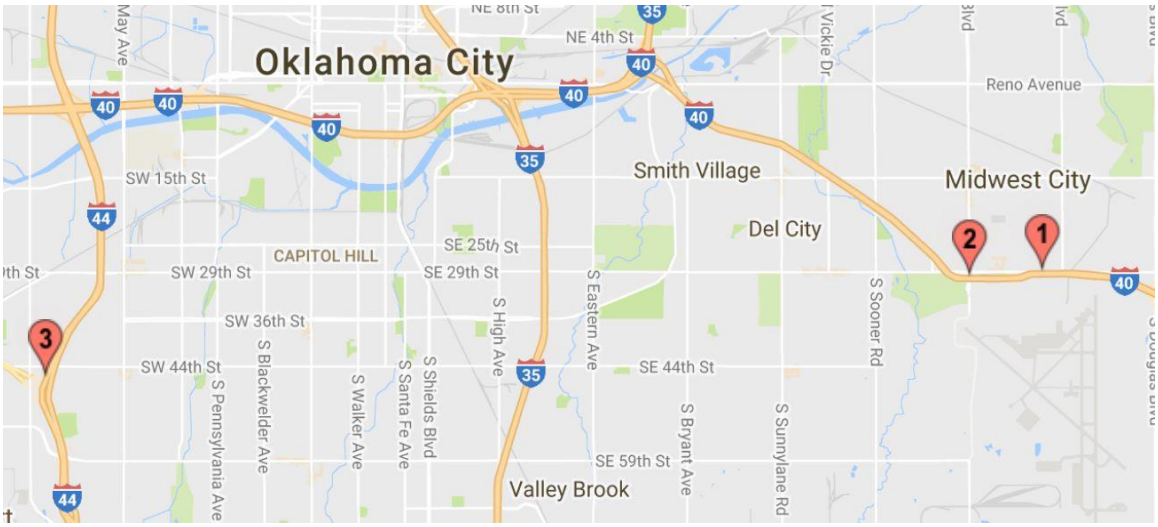

(a) Oklahoma City (Urban Interstate Highways)

(b) Salina (Rural State Highway)

Figure 23 HFST Sites in Oklahoma

High Friction Surface Treatment (HFST) has gained its popularity in recent years in the United States with proved capability in improving pavement friction and thus roadway safety particularly

at horizontal curves (ATSSA, 2013; Merritt, 2014). The data collection in this paper includes macro-texture and friction testing of two HFST sites on Interstate 40 (I-40), one HFST site on Interstate 44 (I-44) and three HFST sites on State Highway 20 (SH-20) in Oklahoma. The locations of the six HFST sites are shown in Figure 4.1. Sites 1-3 were built at three locations in the Oklahoma City metropolitan area, while Sites 4-6 located on curvy two-lane rural highway with various longitudinal grades without shoulder. The existing pavements on I-40, I-44, and SH-20 were constructed with stone matrix asphalt (SMA), Portland cement concrete (PCC), and conventional hot mix asphalt (HMA) respectively. HFST were installed on all the three traffic lanes in the east bound of I-40 and the west bound of I-44, while one lane for both directions on SH-20. Considering different traffic directions and number of lanes of these sites, 15 data collections were conducted in November 2015 and the detailed information for each site is summarized in Table 4.1.

Table 4.1 Information of HFST Sites

Data Collection ID	Lane /Direction	Site ID	Site Location	Abutting Pavement	AADT	Functional Class	Radius (M)	Grade (%)
1	Right	Site 1	I-40	SMA	64678	Interstate	2000	-2.5
2	Middle							
3	Left							
4	Right	Site 2					2000	-1.5
5	Middle							
6	Left							
7	Right	Site 3	I-44	Concrete	129000	Interstate	2000	-2
8	Middle							
9	Left							
10	North	Site 4	SH-20	HMA	390	Minor Arterial	400	3.5
11	South							
12	North	Site 5					500	3
13	South							
14	North	Site 6					200	-3.5
15	South							

Note: AADT is annual average daily traffic.

4.2.2 Data Collection Devices

The AMES Model 8300 Survey Pro High Speed Profiler (Figure 4.2(a)) is used to collect surface macro-texture data at 0.0005 m (0.020 in) sampling interval at highway speeds. Mean Profile Depth (MPD) is calculated as the pavement texture index based on the ASTM E1845-15 standard. Grip Tester (Figure 4.2(b)), designed following the ASTM E2340/E2340M-11R15 standard, can continuously measure pavement longitudinal friction operating around the critical slip of an anti-lock braking system (ABS). Comparing to the traditional locked-wheel friction testing method, Grip Tester can provide greater details of skid resistance with spatial variability for project and network level friction management. The device can operate at highway speed of 80 km/h (50 MPH) as well as low speed of 32 km/h (20 MPH) using the desired water film thickness sprayed in front of the testing tire during data collection.

The friction numbers were reported for each data collection to represent the pavement surface skid resistance conditions. To determine the effectiveness of HFST in improving surface properties, all the data sets are collected beginning 100 m (328 ft.) to 150 m (492 ft.) before and through 100 m (328 ft.) to 150 m (492 ft.) after each HFST section.

(a) High Speed Profiler

(b) Grip Tester

Figure 24 Field Data Collection Devices

4.2.3 Preliminary Results

Friction numbers and MPD values were obtained at 1 meter interval for the HFST sites. Examples of pavement friction number and MPD data are shown in Figures 4.3 and 4.4 to demonstrate pavement friction and macro-texture conditions for these sites.

All sites show clear improvement of skid resistance and differentiation of the HFST section from the abutting pavements for all the data collections (Figures 4.3(a) and 4.4(a)). The average friction number on HFST sections is 1.00, while the friction number of abutting pavement surfaces without HFST has an average of 0.50. The differences of MPD between the HFST sections and adjacent pavements vary among these data sets. For example, MPD values of collection #7 are much higher on HFST section in contrast to those on the abutting concrete pavement (Figure 4.3(b)), whereas MPDs of collection #1 don't show noticeable difference between the HFST section and its adjacent pavement (Figure 4.4(b)). On average, the mean value of MPD on the 6 HFST sites is 1.70 mm (0.067 in.), while the MPDs of the regular pavement surfaces has an average of 1.34 mm (0.053 in.).

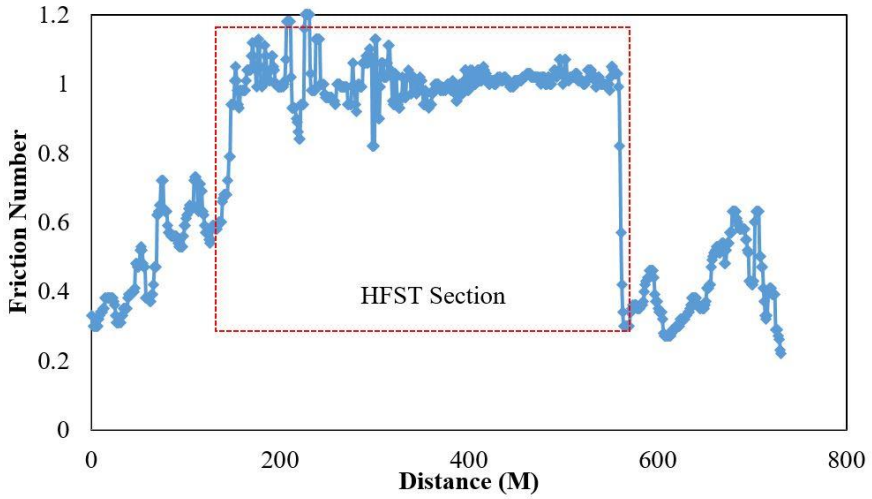

(a) Friction

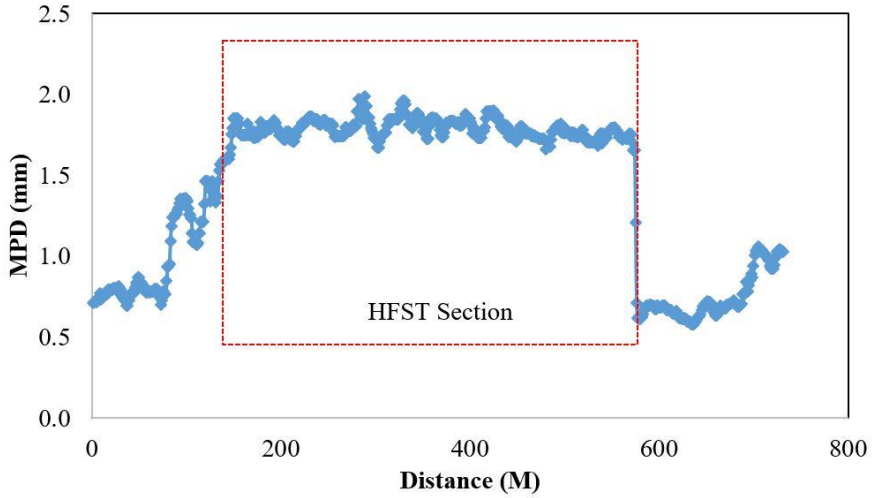

(b) MPD

Figure 25 Distinct Friction and MPD Difference (Data Collection #7)

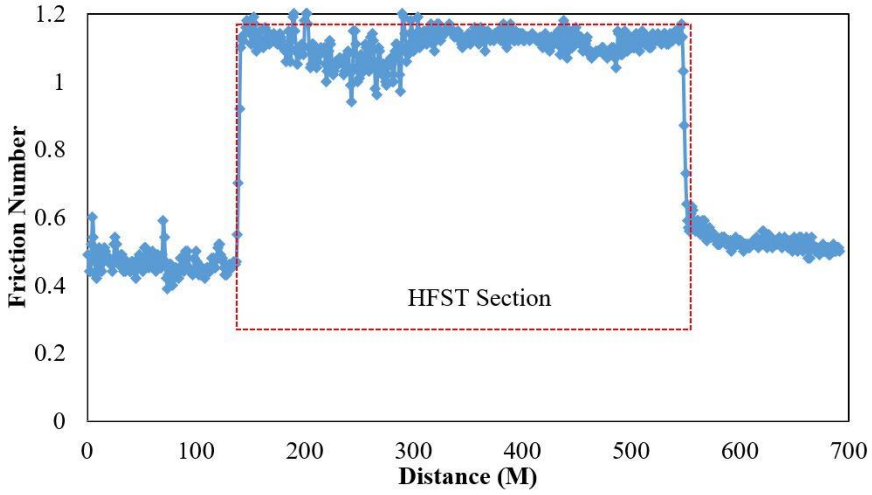

(a) Friction

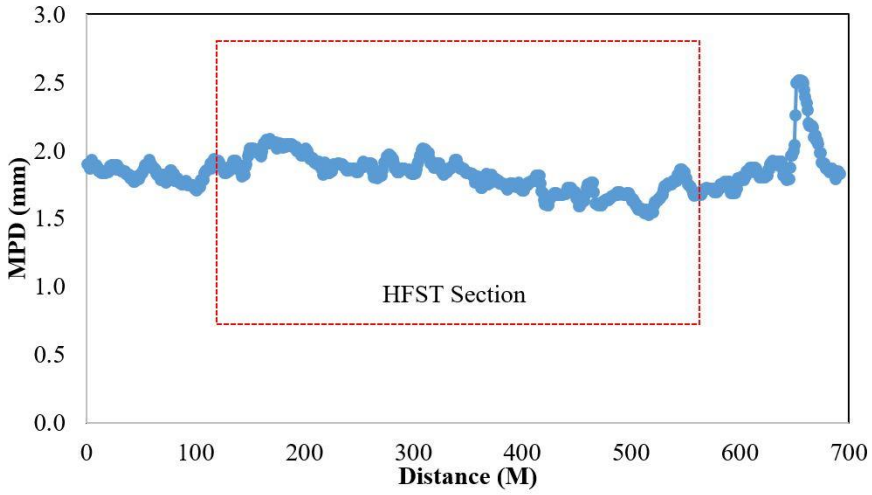

(b) MPD

Figure 26 Distinct Friction Difference Only (Data Collection #1)

The scatter plot between friction numbers and the corresponding MPDs of collection #1 are demonstrated in Figure 4.5. For the 691 pairs of friction number and MPD values, the R-squared value of the regression is close to 0. It means no direct relationships can be developed between pavement friction number and MPDs.

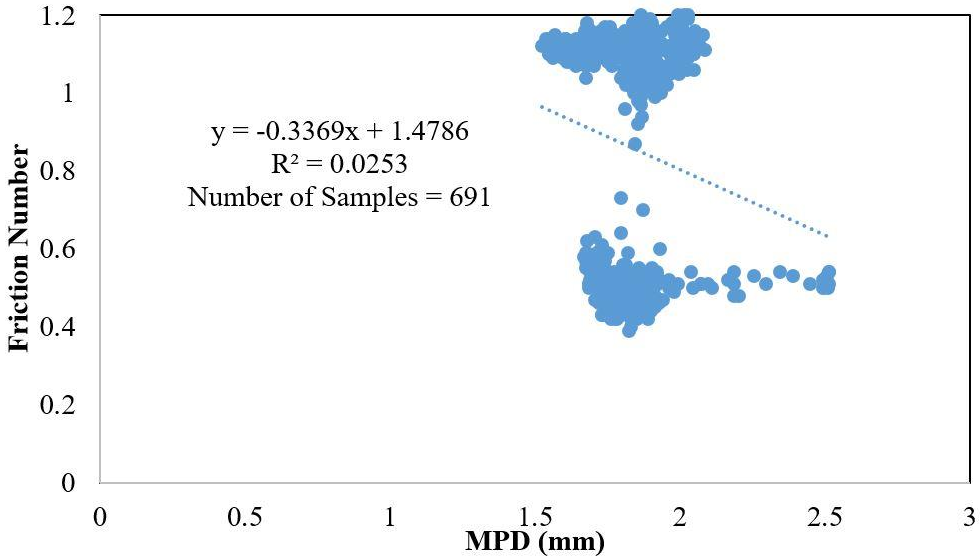

Figure 27 Scatter Plot of Friction Number and MPD (Data Collection #1)

A paired t-test with equal variance was performed for each HFST site. Since the length of HFST application and non-HFST surfaces (lead-in and lead-out) may not be the same, the sample sizes for the t-tests are not equal and the missing value codes (NA) for these sections with fewer observations are added in the test data. The P-value is used to determine whether the difference between the mean of two groups is likely to be due to chance. The t-test results for friction number and MPD for data collection are summarized in Table 4.2. There is strong evidence that the HFST surfaces have significantly different friction number and surface texture MPD values than the abutting pavement (with an average of P value = 0 for all the HFST sites).

Table 4.2 T-Test Results for Friction Number and MPD

Data Collection ID	Friction Number				MPD (mm)			
	Mean - HFST	Mean - Non HFST	P value	Sig. Diff?	Mean - HFST	Mean - Non HFST	P value	Sig. Diff?
1	1.10	0.50	0.00	Yes	1.85	1.66	0.00	Yes
2	1.03	0.47	0.00	Yes	1.80	1.69	0.00	Yes
3	1.02	0.42	0.00	Yes	1.82	1.77	0.00	Yes
4	1.08	0.59	0.00	Yes	1.82	1.60	0.00	Yes
5	1.00	0.44	0.00	Yes	1.78	1.51	0.00	Yes
6	1.05	0.58	0.00	Yes	1.82	1.54	0.00	Yes
7	1.00	0.47	0.00	Yes	1.77	0.92	0.00	Yes
8	1.01	0.41	0.00	Yes	1.83	0.70	0.00	Yes
9	1.02	0.33	0.00	Yes	1.71	0.72	0.00	Yes
10	0.86	0.59	0.00	Yes	1.85	1.40	0.00	Yes
11	0.87	0.45	0.00	Yes	1.84	1.20	0.00	Yes
12	1.03	0.62	0.00	Yes	1.28	1.03	0.00	Yes
13	0.99	0.48	0.00	Yes	1.37	1.31	0.00	Yes
14	1.04	0.67	0.00	Yes	1.37	1.26	0.00	Yes
15	0.93	0.54	0.00	Yes	1.49	1.42	0.00	Yes

4.3 Wavelet Analysis of Macro-texture Profiles

A Daubechies wavelet of order 3 (db3) is selected as the mother wavelet and the wavelet analysis is carried out using the MATLAB Wavelet Toolbox to decompose the collected macro-texture profiles. Subsequently, TE and RE are calculated every 1 meter and compared among the four pavement types to reveal the distinct characteristics of macro-texture composition.

With the sample interval of 0.483 mm for the obtained macro-texture profiles, there are 2072 data points for every 1 meter of macro-texture profile, which requires a total of 11 decomposition levels for wavelet analysis ($2^{11} = 2048$). However it is widely accepted that the upper bound of macro-texture wavelength is 50 mm, and therefore only 7 decomposition levels, denoted as Level 1 (D1) through Level 7 (D7), are considered in this paper to calculate TE and RE at 1 meter interval for the macro-texture profiles.

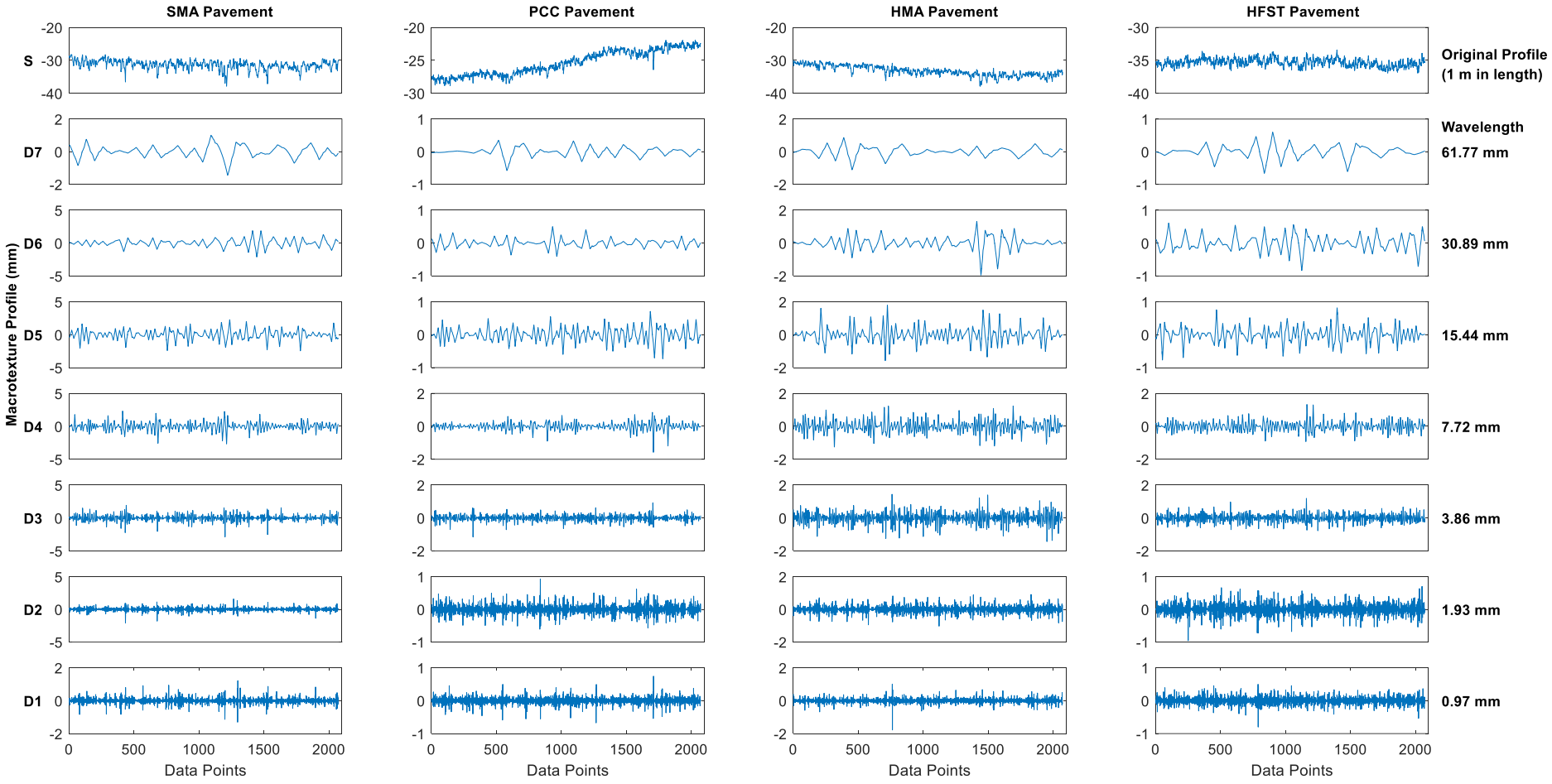

Figure 28 Wavelet Decompositions of Macro-texture Profiles

4.3.1 Total Energy Analysis

The original macro-texture profiles and the decomposed macro-texture profiles for the seven decomposition levels are shown in Figure 4.6. In total there are four kinds of pavement surfaces in the data collection, including the three existing surfaces (hot mix asphalt – HMA on SH20, stone-matrix asphalt – SMA on I40, Portland cement concrete –PCC on I44) and the HFST. For the *j*th decomposition results, the horizontal axis shows the number of data points and the vertical axis represents the amplitude of pavement macro-texture profiles. The equivalent wavelengths for each decomposition level are provided on the right margin of the figure.

The total energies of the macro-texture profiles for the four pavement surface types are calculated and provided in Figure 4.7 for each decomposition level. The overall total energies on SMA, HMA, HFST, and PCC pavement are 2,254, 1,532, 1,401, and 337 mm^2 respectively. The sequence of the overall TE among the pavement categories agrees well with the coarseness level of pavement macro-texture profiles observed from Figure 4.6. For friction, the average friction numbers are 0.50, 0.56, 1.0, and 0.40 for the SMA, HMA, HFST, and PCC pavements. Therefore, a pavement section with coarser macro-texture doesn't guarantee a higher pavement friction number. For example, the total energy of the HFST sections is 1401 mm^2, which is not the maximum among the four pavement surfaces, while it has the highest friction number.

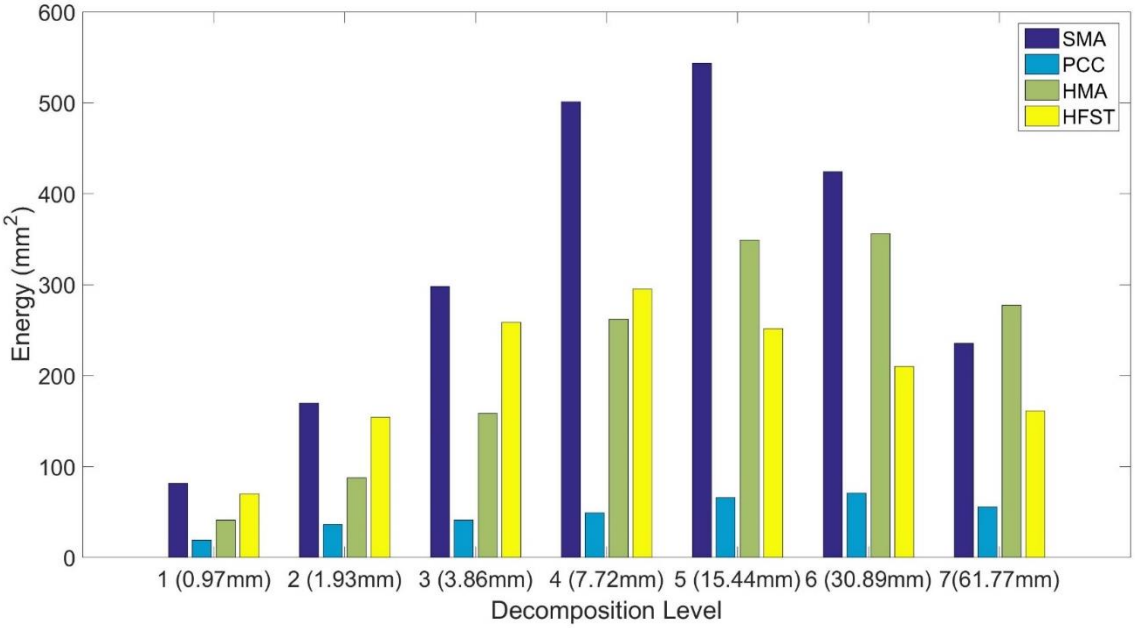

Note: The number in the bracket is the corresponding wavelength of each decomposition level.

Figure 29 Total Energy Distribution

4.3.2 Relative Energy Analysis

Considering the wide range of wavelength (0.5~50 mm) for macro-texture, pavement macro-textures at various wavelengths may have different contributions to pavement friction performance. Therefore, it's necessary to investigate the relative energy distribution of macro-texture profiles at each decomposition level and how it impacts the friction performance for different pavement surface types. The cumulative RE distribution at each decomposition level is shown in Figure 4.8.

It is noticed that (1) more than 50% of energy of macro-texture on HFST sections stores within the first four decomposition levels, which correspond to wavelengths ranging from 0.97 mm to 7.72 mm; (2) while more than half of the energy of the macro-textures for the other three pavement types distributes within the last three decomposition levels, which correspond to wavelengths from 15.44 mm to 61.77 mm.

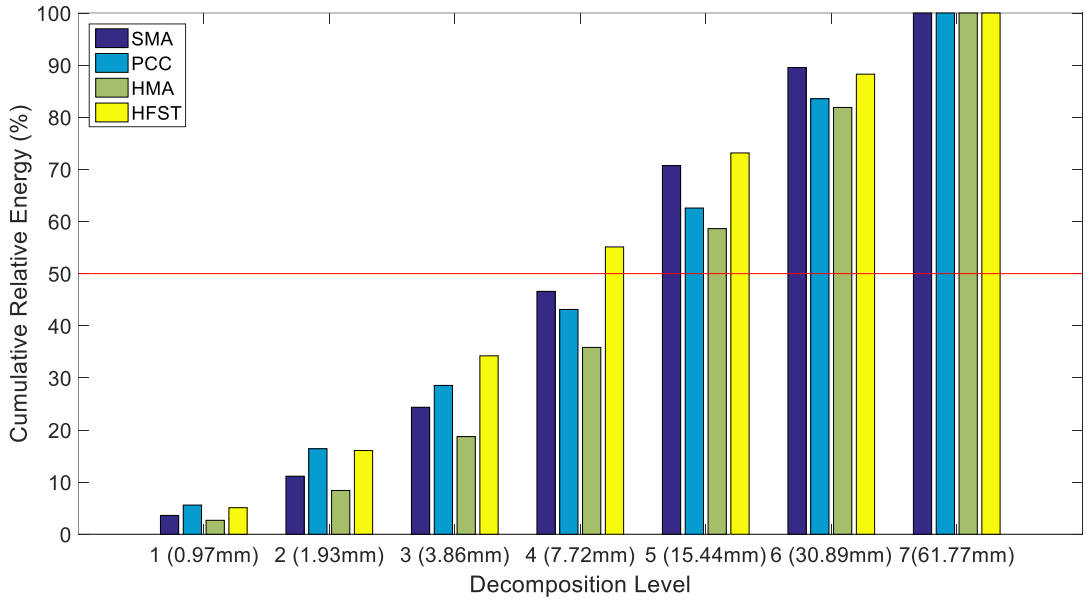

Note: The number in the bracket is the corresponding wavelength of each decomposition level.

Figure 30 Cumulative Relative Energy Distribution

Table 4.3 Correlation Coefficients between RE and Friction Number

Site ID	Correlation Coefficients						
	D1	D2	D3	D4	D5	D6	D7
1	0.93	0.95	0.94	-0.21	-0.86	-0.74	-0.02
2	0.06	0.35	0.76	0.58	-0.34	-0.33	-0.37
3	-0.39	0.12	0.79	0.86	0.26	-0.57	-0.45
4	0.29	0.52	0.83	0.79	-0.39	-0.77	-0.55
5	0.58	0.68	0.76	0.50	-0.65	-0.63	-0.47
6	0.81	0.84	0.73	-0.19	-0.75	-0.62	-0.05

Subsequently, correlation analysis between relative energy of macro-texture at various decomposition levels and friction number is performed. The correlation coefficients are summarized in Table 4.3 for each site. Correlation coefficient of 0 means that there is no correlation, -1 denotes a perfect negative correlation, while +1 suggests a perfect positive correlation between the two variables. For these six sites, the correlation coefficients between REs and friction number are negative from the 5th to the 7th composition levels (D5 to D7) (except D5 at Site 3), and positive from the 1st to the 3rd composition levels (D1 to D3) (except

D1 at Site 3). In other words, the pavement friction performance improves with macro-texture at wavelength from 0.97 mm to 3.86 mm while decreases with macro-texture at wavelength from 15.44 mm to 61.77 mm. The correlation coefficient between the relative energy at the 4th composition level (D4) and friction number varies among the sites, which indicates that the contribution of pavement macro-texture at the wavelengths between 3.86 mm and 7.72 mm to pavement friction is inconsistent and depending on the pavement surface type.

4.4 Friction Prediction Model

Table 4.4 Estimated Coefficients and P-value for Friction Prediction Model

Item	Intercept	*TE*	RE_1	RE_2	RE_3	RE_4	RE_5	RE_6	RE_7
Coefficient	0.142	6.34E-05	0.092	-0.113	0.1	0.004	-0.039	0.01	0.016
P-value	0.042	6.03E-06	0.007	0.006	0.003	0.003	0.002	0.001	0.001

The collected macro-texture profiles and friction data of collection #1, #7, and #12 are combined by pavement types (SMA, HMA, PCC and HFST) as regression data set for friction prediction model development. Multivariate linear regression is performed to predict friction number based on the TE and RE of pavement macro-texture profiles:

$$Friction\ Number = a + TE * b + \sum_{j=1}^{7} RE_j * c_j \quad (4.5)$$

where a, b, and c_j are the estimated coefficients for intercept, TE and RE_j separately. The estimated regression coefficients and corresponding P-values of the multivariate model are summarized in Table 4.4. All P-values of TE and RE_j herein are smaller than 0.05, indicating their significance to pavement friction.

Based on the generated coefficients, all the collected macro-texture profiles and friction data for the 15 data collections are used to validate the proposed model. The validation result of the developed friction prediction model is summarized in Table 4.5. The number of friction data

samples ranges from 358 to 1184 for each data collection. R-squared values range from 0.42 to 0.93, with the highest R squares for I-40 sections, followed by I-44 and SH-20.

Table 4.5 Validation Result of Friction Prediction Model

Site Location	Site ID	Data Collection ID	R^2	SSE	No. of Points
I-40	Site 1	1	0.93	2	654
		2	0.90	4	628
		3	0.83	4	750
	Site 2	4	0.85	3	584
		5	0.84	4	597
		6	0.79	6	607
I-44	Site 3	7	0.79	7	621
		8	0.62	13	618
		9	0.78	11	610
SH-20	Site 4	10	0.71	10	358
		11	0.79	5	402
	Site 5	12	0.53	5	361
		13	0.78	3	510
	Site 6	14	0.67	9	1184
		15	0.42	8	700

Examples of validation with the highest (Collection #1 of Site #1 on I-40) and the lowest (Collection #15 of Site #6 on SH-20) R-squared values are shown in Figure 4.9. Site 1 locates on I-40 with moderate horizontal curve, minimum longitudinal grade, and minor distress on the existing surface, while Site 6 locates on SH-20 with sharp horizontal reverse curves, steep longitudinal grades, and significant amount of defects on the existing pavement. For data collections on sharp curves with the existence of lateral gravity forces, centrifugal forces, and possible consistent acceleration/deceleration of the data collection vehicle, the friction and macro-texture data collected generally show significant higher variabilities, resulting in the low R-squared values in the models.

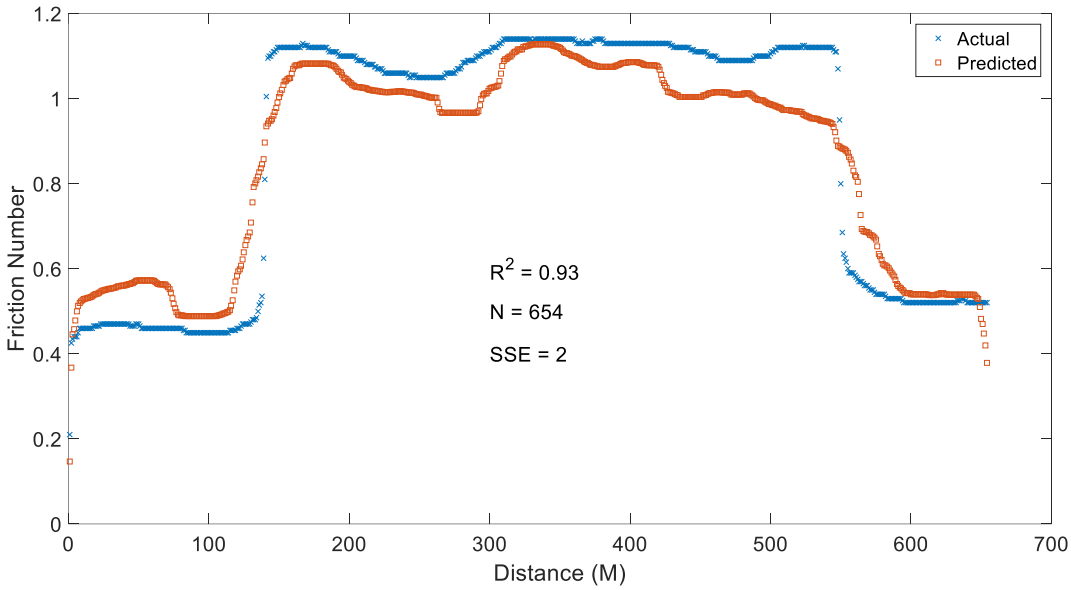

(a) Prediction with the Highest R-squared Value (Collection #1)

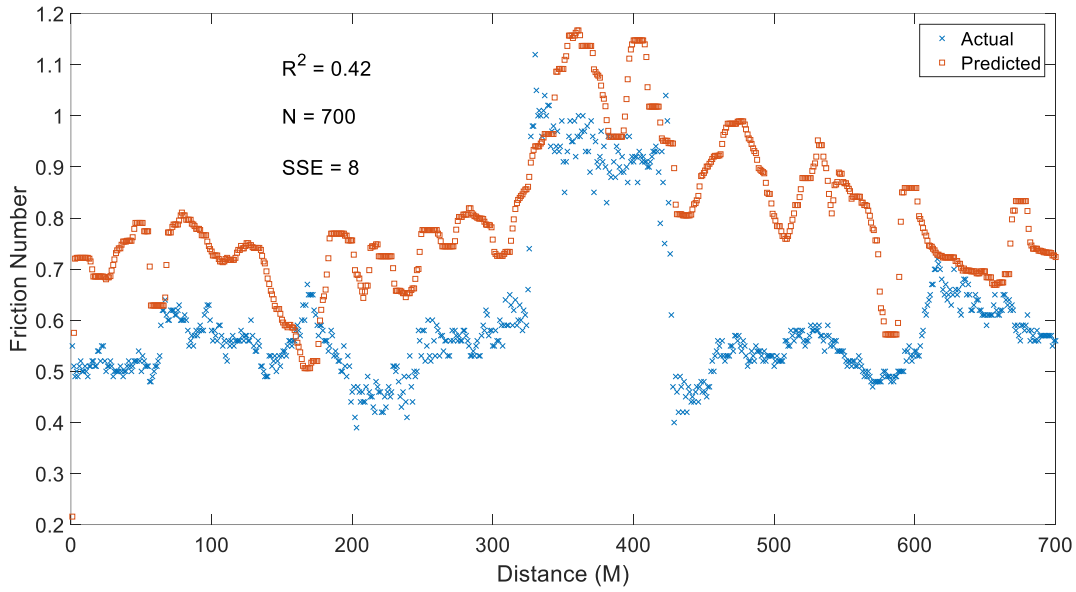

(b) Prediction with the Lowest R-squared Value (Collection #15)

Figure 31 Example of Pavement Friction Prediction Result

It should be emphasized that the quality of texture and friction data is critical for a robust model development. HFST Site #1 was installed on moderate curves on asphalt pavement surface, and the adjacent pavement had minor pavement surface distress. The data collected on Site #1

exhibits high repeatability and consistency among the data collection on the multiple lanes. Therefore, the regression friction models have high R-squared values on Site #1. HFST Sites 2 and 3 were installed on bridge decks with existing asphalt and concrete surfaces on slightly curved highways. Even though minor distress were observed before installation, faulting along the slab joints on the deck are noticeable. As a result, the macro-texture and friction data contain significant amount of data points with abnormal measurement values especially along the joints. The vehicle excitation also happens when vehicle moving on the transition section between pavement and bridge deck. Due to the vehicle excitation, the repeatability and consistency of friction and macro-texture data collection on Site #2 and Site 3 are not as good as those collected on Site #1. Accordingly, the regression models have lower R-squared values as compared to those for Site #1.

Sites #4 to #6 are located on SH-20 on a low volume roadway but with many sharp horizontal curves and longitudinal grades. In addition, the existing pavements had experienced extensive crack sealing and rutting on the surface. The data sets collected on these sites have the lowest repeatability and consistency, leading to the low levels of R-squared values.

4.5 Summary

In this chapter, discrete wavelet transform is implemented to decompose pavement surface 2D macro-texture data into multi-scales to extract more information from 2D macro-texture profile. Pavement 2D macro-texture and friction data on six HFST sites that were installed on existing SMA, PCC, and HMA pavement surfaces are analyzed. 15 pairs of pavement 2D macro-texture and friction data were collected with length ranging from 358 m (1174 ft.) to 1184 m (3885 ft.) considering the number of lanes and traffic directions of the sites. Total energy and the relative energy distributions are calculated for the decomposed 2D macro-texture profiles from wavelet transform, and the relationship between the energy indicators and pavement friction performance

is studied. Pavement friction prediction model is developed based on multivariate linear regression method incorporating energy indicators of pavement macro-texture.

The average MPD and friction numbers on HFST sections are 1.70 mm (0.067 in.) and 1.00 respectively, while the MPD and friction numbers of non-HFST surfaces have the average of 1.34 mm (0.053 in.) and 0.50. For Site #1 and #2, the friction data is significantly higher on HFST sections than those on adjacent SMA pavements, whereas the MPD values exhibit minor difference between HFST and existing pavement surface. Even though it is widely accepted that pavement skid resistance is tied to surface macro-texture, MPD alone is not adequate for the pavement friction prediction.

The energy distributions for macro-texture on the different pavement surfaces could vary significantly. On HFST sections, more than 50% of the energy is distributed within the 1st to the 4th decompositions levels (D1 to D4), with the wavelengths ranging from 0.97 mm to 7.72 mm. While for the other three pavement surface types, including SMA, PCC, and tradition HMA, more than 50% of the energy of macro-texture profiles is distributed within the 5st to the 7th decomposition levels (D5 to D7) with longer wavelengths ranging from 15.44 mm to 61.77 mm.

Seven decomposition levels are considered in this paper for macro-texture analysis. All the energy indicators for the seven levels show significant contributions to the pavement friction performance and are used as the independent variables for friction model development. The energies at wavelengths from 0.97 mm to 3.86 mm contributes positively to pavement friction while those at wavelengths from 15.44 mm to 61.77 mm demonstrates negative impacts.

It is worth mentioning that the pavement types and collected 2D texture data are limited in this chapter because only 6 HFST sites are tested. With the idea of improving the pavement categories and the size of collected texture data for the non-contact friction model development, more powerful computing techniques, such as machine learning, should be implemented.

CHAPTER V CONVOLUTIONAL NEURAL NETWORK BASED FRICTION PREDICTION MODEL USING PAVEMENT MACRO-TEXTURE DATA

5.1 Deep Learning

Substantial effort has been put into studies in the non-contact prediction of pavement friction. Experiment-based and model-based friction estimation methods have shown their advantage with reasonable accuracy and repeatability using data collected in vehicle or tire via optical sensor, acoustic sensor, tire tread sensor, or camera (Khaleghian et al., 2017). “Hilbert-Huang transform”, fractal analysis, power spectral analysis, wavelet analysis, or other novel methods have been applied with the purpose to explore unconventional parameters characterizing texture properties and reveal the linkage of pavement texture with pavement friction prediction (Kane et al., 2015; Villani et al., 2014; Hartikainen et al., 2014; Yang et al., 2017; Li et al., 2017). However, no consistent relationships between pavement texture and friction have been developed so far. This study attempts to use a new analysis technique to understand if a consistent relationship on a quantitative scale exists.

Artificial Neural Network (ANN) is defined as “a computing system made up of a number of simple, highly interconnected processing elements which process information by their dynamic state response to external inputs” (Caudill, 1987). ANN typically contains input layer, hidden layer, and output layer which are connected via numerous interconnected “nodes” containing “activation function”. ANN can extract patterns and detect trends in complicated data sets which

are too complex to be analyzed by either humans or other traditional computing techniques (Stergious & Siganos, 2017). Traditional ANN has been around for decades, and applications of traditional ANN in transportation engineering include simulating pavement structural condition (Plati et al., 2016), predicting the rate of vehicle crashes (Najafi et al., 2016), and estimation of tire/road fiction force (Matuško et al., 2008; Luque, 2013). Nevertheless, traditional ANN is limited to shallow layers of neurons due to restriction of training speed.

With vast improvement in computing and processing power of computers in the last two decades, deep learning (or deep neural network) with millions to billions of artificial neurons and modified network structures has recently become an extreme powerful methodology with exceptional performance in addressing difficult problems such as object detection and classification in image processing, speech recognition and text classification in natural language processing (Längkvist et al., 2014; Sutskever et al., 2014; LeCun et al., 2015; Schmidhuber, 2015). Convolutional Neural Network (CNN), one of the most popular methodologies in deep learning, has demonstrated many research and commercial successes (Krizhevsky et al., 2012; Wang et al., 2012; Abdel-Hamid, 2014). CNN has also been successfully applied in solving challenges in transportation industry, such as traffic sign classification and pavement crack detection (Cireşan et al., 2011; Zhang et al., 2016; Zhang et al., 2017).

5.2 Field Data Collection

5.2.1 Data Collection Sites

The data collection effort described herein covers 49 HFST sites in 12 states for a research project sponsored by the Federal Highway Administration (FHWA). HFST, as one of the innovations in Every Day Counts program of FHWA, has been installed at numerous horizontal curves throughout the U.S. with demonstrated effectiveness in improving skid resistance and reducing crashes (Izeppi et al., 2010; Sprinkel et al., 2015; Li et al., 2016). The locations of the data collection sites are shown in Figure 5.1. Pavement macro-texture with AMES profiler and friction

data with Grip Tester are collected at traffic speed. 50 data collections are conducted herein considering the directions and number of lanes for each site. The length of data collection ranges from 374 m (1227 ft.) to 5,342 m (17527 ft.).

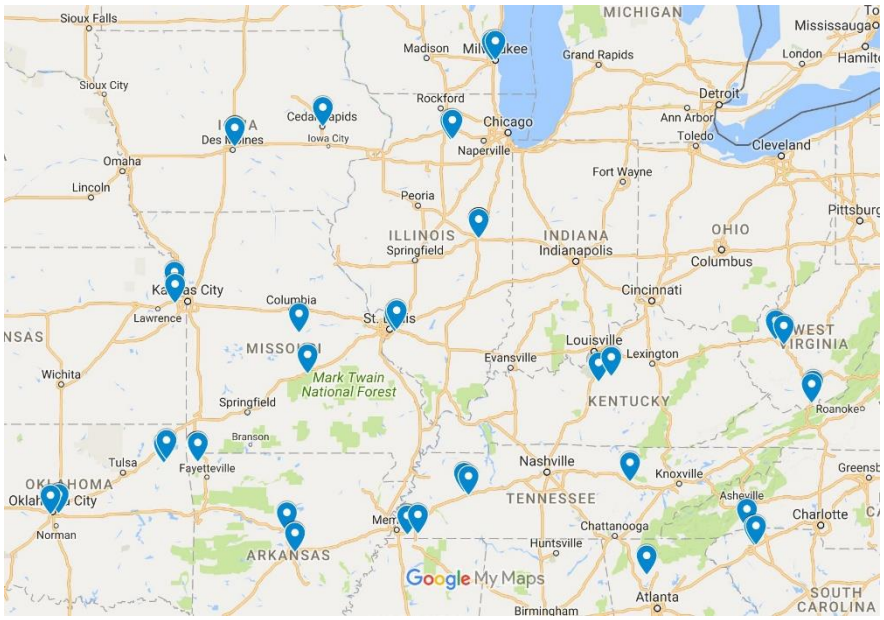

Figure 32 Data Collection Sites

Besides HFST sections, the adjacent untreated lead-in and lead-out sections, including flexible pavements, rigid pavements, and bridge decks with or without grooving, are also included in the data collection for a wide variety of pavement texture profiles and friction characteristics ranging from the highest value (1.0) to the lowest value (0.2). Example pavement sections and corresponding route names are displayed in Figure 5.2.

(a) HFST Pavement (GA-140)

(b) Flexible Pavement (TN-298)

(c) Rigid Pavement (OK-I44)

(d) Bridge Deck (WV-I64)

(e) Grooved Flexible Pavement (MO-I44)

(f) Grooved Rigid Pavement (WI-I94)

Figure 33 Examples of Collected Pavement Categories

5.2.2 Preliminary Result

Texture data was collected at the speed of 80 km/h (50 MPH) when possible, or the allowable driving speed limits on sharp curves or ramps. Similarly, friction data was collected at the standard designated testing speed of 64 km/h (40 MPH) when possible, or the allowable driving speed.

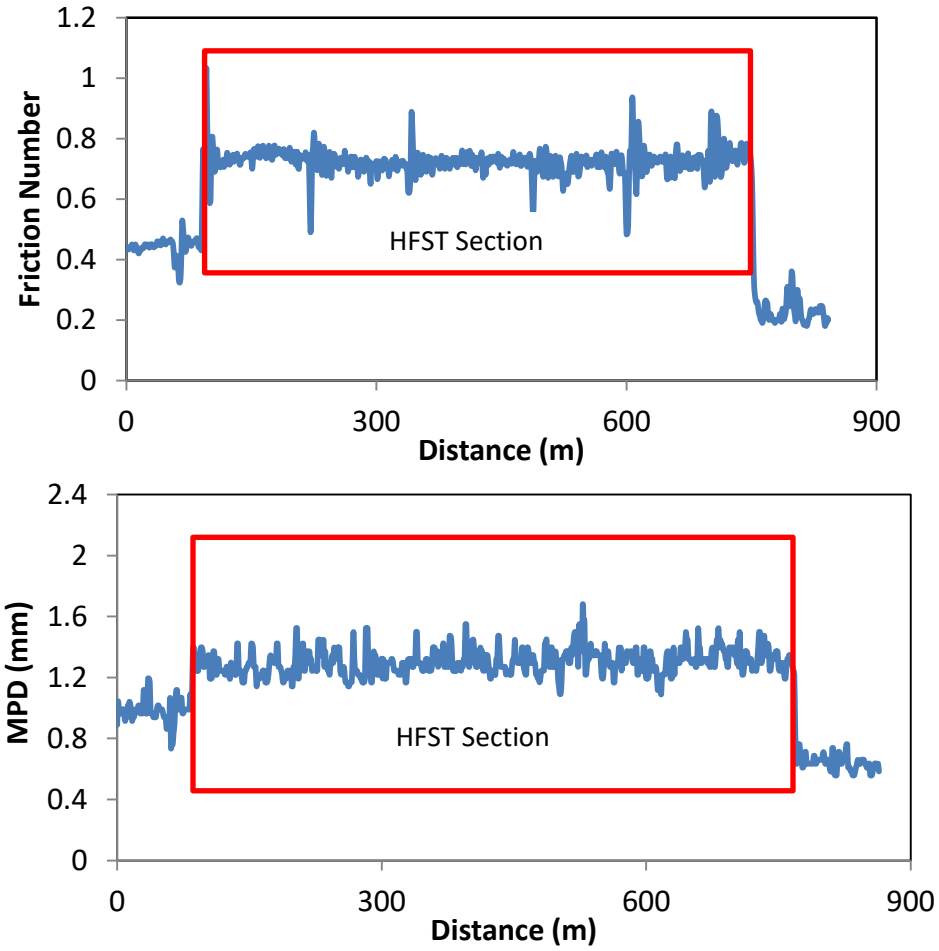

(a) Apparent Friction and MPD Improvement (Site A: IA-I380)

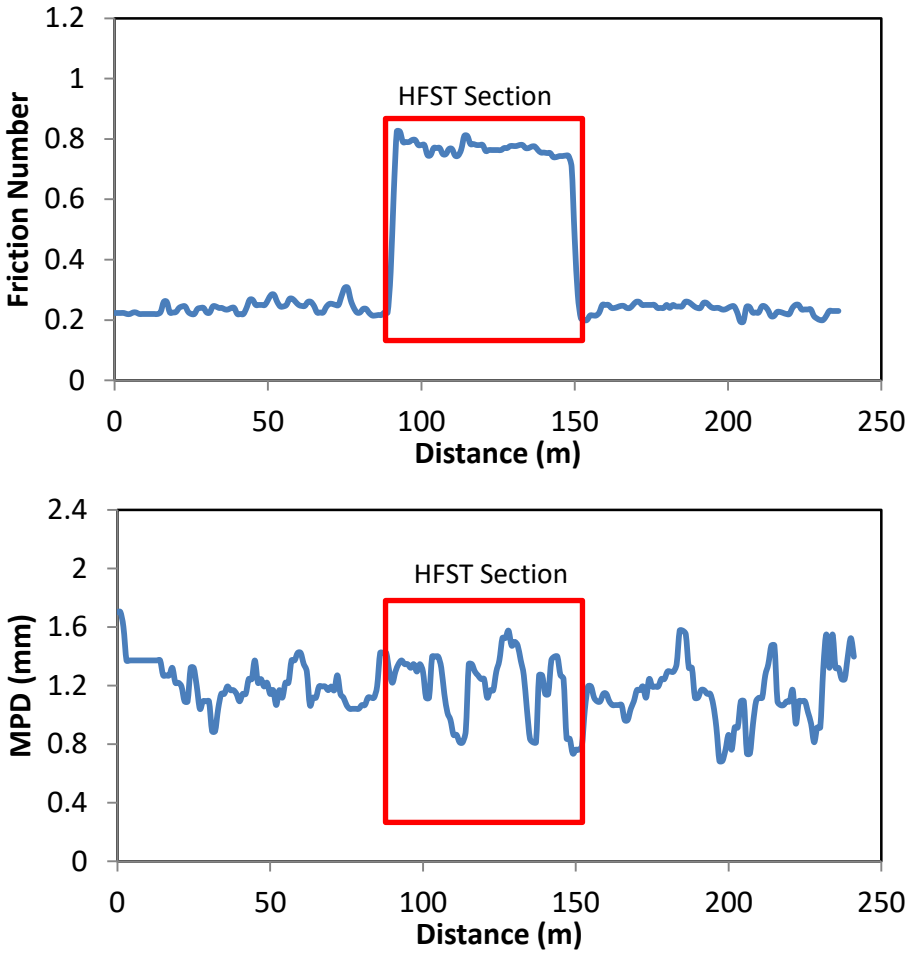

(b) Apparent Friction but Minor MPD Improvement (Site B: OK-SH20)

Figure 34 Examples of Preliminary Result

Firstly, MPD is calculated and friction number is recorded at every 1 m (3.28 ft.) to represent pavement texture and skid resistance characteristic. Pavement friction and MPD on two example sites are displayed in Figure 5.3. For both sites, the HFST sections provide distinct higher friction number as compared to adjacent untreated lead-in and lead-out sections. The average friction numbers on HFST sections are 0.72 and 0.77, while the friction of abutting untreated pavement surfaces have an average of 0.34 and 0.25. For the first site (Figure 5.3(a)), HFST generates noticeable higher MPD value than the neighboring regular sections: the mean MPDs are 1.30 mm (0.0511 in.) on HFST and 0.82 mm (0.0323 in.) on abutting pavement. However, for the second site (Figure 5.3(b)), the untreated pavements next to the HFST produce similar MPD value as the

HFST section: the average MPDs are 1.21 mm (0.0476 in.) on HFST and 1.18 mm (0.0465 in.) on untreated pavements. This example indicates that pavement section with higher friction number doesn't necessarily show higher MPD.

Furthermore, the scatterplot of MPD and friction number can assist exploring the relationship between pavement skid resistance and traditional texture indicator MPD. As shown in Figure 5.4(a), a fairly good linear relationship is obtained for Site A, with the coefficient of determination of 0.6881. However, for Site B, since the HFST section maintains significantly higher skid resistance but similar MPD as compared to the untreated abutting pavement sections (Figure 5.3(b)). The coefficient of determination is only 0.0194 for Site B, which is displayed in Figure 5.4(b). This inconsistent relationship is actually not uncommon per the research team's experience and prior studies by others. As a result, the conventional pavement texture indicator MPD is inadequate to predict pavement friction number consistently for diversified pavement surfaces.

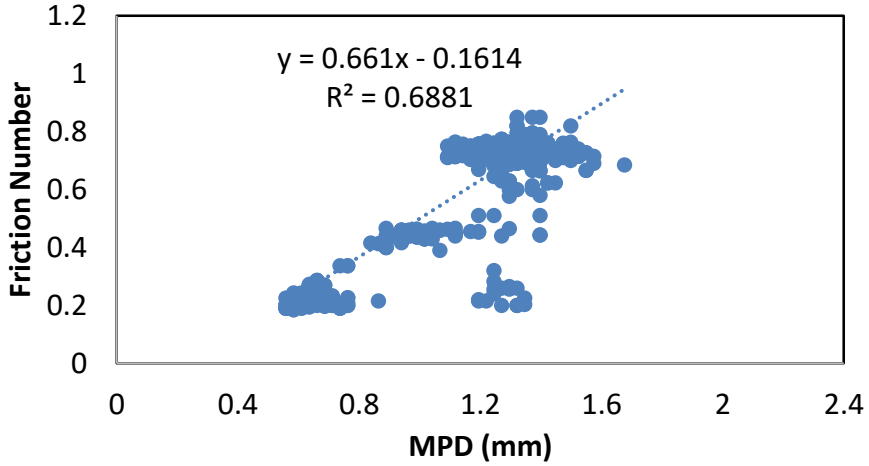

(a) Site A: IA-I380

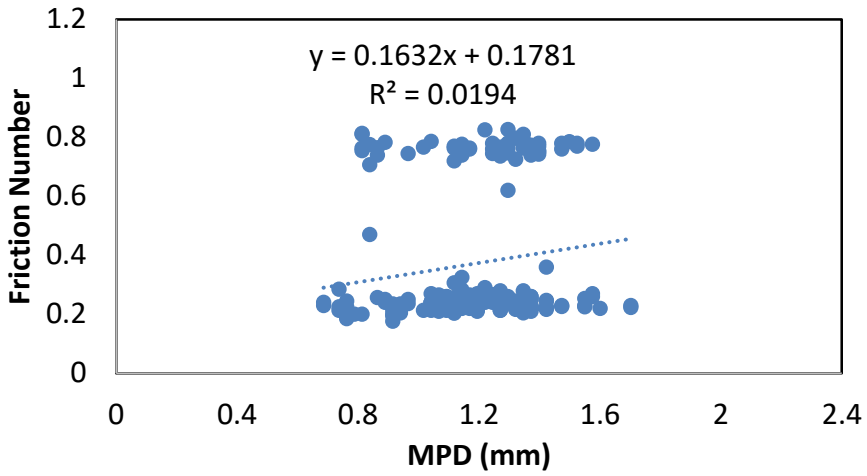

(b) Site B: OK-SH20

Figure 35 Relationship of Friction Number and MPD

5.3 Methodology

This chapter proposes FrictionNet to predict pavement friction number via macro-texture data as the only input. Rather than calculating MPD or applying traditional signal analysis techniques to represent texture characteristic with respect to friction performance, FrictionNet implements a Convolutional Neural Network (CNN) based architecture to explore one-to-one correspondence between pavement texture and friction data. With a given texture profile, FrictionNet is designed to predict the corresponding friction number ranging from 0.2 to 1.0 by simulating testing with a Grip Tester.

5.3.1 Data Preparation

All pavement macro-texture and friction data used in this article are collected by the High Speed Profiler and Grip Tester as introduced in Chapter 4.2. For each data collection, measured macro-texture profile and friction number are paired every 1 meter for the following training process. Instead of using raw macro-texture profile, spectrogram of macro-texture profile is computed and passed to the CNN network as the training input. Every 1 meter long raw macro-texture profile contains 2,000 points, and it is represented via a spectrogram with dimension of 50 × 38. This preprocessing method of raw texture profile can be found in other studies of natural language

processing which also deals with one-dimensional (1D) signal in CNN network training for information retrieval (Dieleman and Schrauwen 2014, and Huang et al. 2015). Figure 5.5 shows a spectrogram example which represents the time and frequency decomposition of macro-texture profile. As the collected friction numbers, they are rounded to the nearest 0.1 with a range from 0.2 to 1.0 which represents the most likely friction number for diversified pavement surface categories.

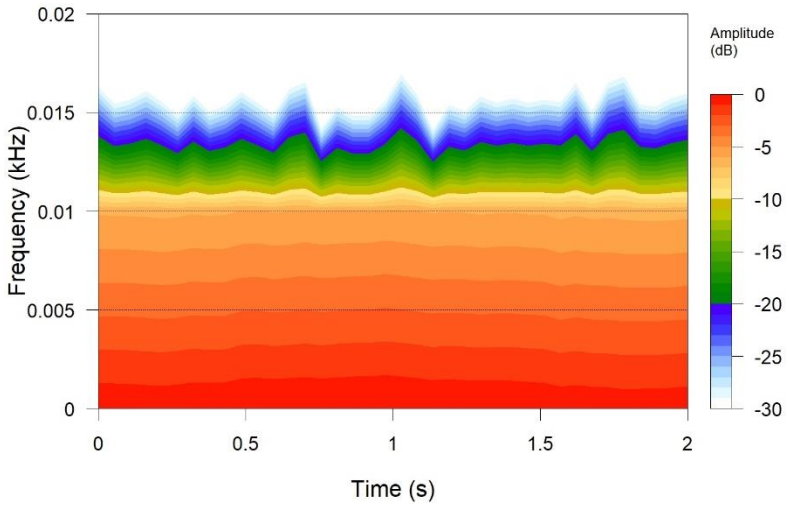

Figure 36 Example Spectrogram of Texture Profile

In total, there are 50 data collections accomplished on those field sites with a total length of 63,648 m (208,818.9 ft.). It is worth mentioning that these collected data is highly imbalanced over different classes. In other words, the obtained texture and friction data has an imbalanced distribution between the different classes. For example, there are 15,319 friction value equal to 0.8 whereas only 2,328 of them are 1.0. However, this imbalanced data will underperform CNN since CNN assumes a balanced distribution of classes in the training data. Therefore, sampling method, as introduced in other studies (Chen et al., 2004; He & Garcia, 2009), is adopted herein to generate a balanced distribution of classes in the prepared dataset and to improve the performance of proposed model. Finally, 63,000 pairs of macro-texture and friction data with balanced distribution of classes are prepared by the research team for the development of

FrictionNet. 80%, 10%, and 10% of the prepared data are randomly selected with the purpose for training, validation, and testing, respectively.

5.3.2 Architecture

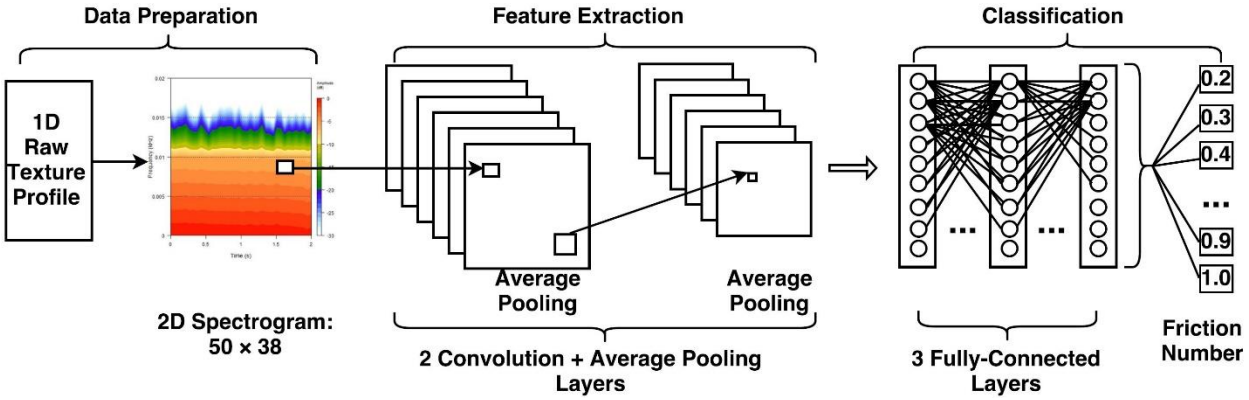

Figure 37 FrictionNet Architecture

As depicted in Figure 5.6, the proposed FrictionNet is constituted by six layers: two convolution layers, three fully-connected layers, and one output layer. The input of the proposed FrictionNet is spectrogram of raw texture profile with size of 50 × 38. The output layer produces the probability distribution of predicted friction level over the 9 class friction numbers via softmax function. There are 64 and 96 kernels with size 3 × 3 for the first and second convolutional layers. 64, 96, and 32 neurons are contained in each fully-connected layer from the left to the right as shown in Figure 5.6. Average pooling of size 2 × 2 without overlapping is followed after each convolutional layer. The activation function herein for convolutional and fully-connected layers is the hyperbolic tangent function which is commonly used as the activation function in artificial neural networks (Ciresan et al., 2012).

The tuned parameters with a total number of 606,409 in FrictionNet are summarized in Table 5.1 for each layer. The network is trained with 350 iterations through the training data set with 50,400 pairs of pavement texture spectrogram and friction data. With one NVIDIA GeForce GTX TITAN Black graphics processing unit (GPU) card, the training process takes 2.73 hours and reaches a high training and validation accuracy. The library MXNet

(https://mxnet.incubator.apache.org/) in R is implemented herein for the development of FrictionNet.

Table 5.1 Parameters for FrictionNet

Layer	Number of Parameters
Layer 1: Convolution	640
Layer 2: Convolution	55,392
Layer 3: Fully Connected	540,736
Layer 4: Fully Connected	6,240
Layer 5: Fully Connected	3,104
Layer 6: Output	297
Total	606,409

5.4 Training Techniques

5.4.1 Learning Method

Stochastic gradient descent is adopted in this CNN model as learning method with a batch size of 30 examples, momentum of 0.9, and weight decay of 0.0005. A small weight decay is important to tune the CNN model, and the update of weight is defined as

$$\begin{cases} v_{i+1} = 0.9 * v_i - 0.0005 * \epsilon * w_i - \epsilon * \langle \frac{\vartheta L}{\vartheta w} | w_i \rangle_{D_i} \\ w_{i+1} = w_i + v_{i+1} \end{cases} \quad (5.1)$$

where i is the iteration index, v is the momentum variable, ϵ is the learning rate, and $\langle \frac{\vartheta L}{\vartheta w} | w_i \rangle_{D_i}$ is the average over the ith batch D_i of the deviative of the objective with respect to w, evaluated at w_i (Krizhevsky et al., 2012).

5.4.2 Weight Initialization

Right weight initialization can insure the network converging with reasonable training time and the loss function not going anywhere. The weights in each layer of proposed network is initialized via the Xavier initialization which is designed to keep the scale of gradients roughly the same in all layers. This initializer fills the weights with random numbers in the range of [-c, c], where $c =$

$\sqrt{\frac{2.34}{n_i}}$ in this model and n_i is the number of neurons feeding into weights (Glorot & Bengio, 2010).

5.4.3 Combat Overfitting

Overfitting refers to a model that models the training data too well that the noise or random fluctuations in the training data is picked up and learned as concepts by the model (Brownlee, 2016). Overfitting can occur during tuning those 606,409 parameters in the FrictionNet model. Regularization methods including L2 regularization and dropout layers are applied to combat overfitting and make the network better at generalizing beyond the training data. L2 regularization, also known as weight decay, modifies the cost function by adding an extra term which is the sum of the squares of all the weights in the network. The extra term can be expressed as

$$L2\ Regularization\ Term = \frac{\lambda}{2n}\sum_{\omega}\omega^2 \tag{5.2}$$

where $\lambda > 0$ is known as the regularization parameter, and n is the size of the training set (Nielsen, 2017).

Dropout layer is another efficient technique to reduce overfitting and gives major improvements over other regularization methods (Krizhevsky et al., 2012; Srivastava et al., 2014). Two dropout layers are utilized herein after the first and the second fully-connected layers with probability of 0.25. With this dropout layer, 25% of the hidden neurons in the first two fully-connected layers will be randomly deleted during training. This significantly increases the robustness of model with different random subsets of the neurons, and therefore reduce test errors and overfitting (Krizhevsky et al., 2012).

5.4.4 Cost Function

Cross Entropy is employed in FrictionNet as cost function to address the learning slowdown issue and measure how close the actual output to the desired output (Nielsen, 2017). Since the

prediction of friction number via FrictionNet is a discrete multi-class classification problem, the Cross Entropy in this article can be defined as

$$H(p,q) = -\sum_x p(x) log q(x) \tag{5.3}$$

where p and q are the actual and predicted friction number at *x*th training individually. Cross Entropy can improve the learning speed and learn at a rate controlled by the similarity between the actual and predicted friction number (Zhang et al., 2017).

5.4.5 Softmax Function

Softmax function is popular as the final layer of a neural network which yields the predicted probability scores for the class label to deal with multi-class classification challenges (Glorot & Bengio, 2010; Krizhevsky et al., 2012; Abdel-Hamid et al., 2014; Nielsen, 2017). The calculated probabilities range from 0 to 1 for each class, while the sum of all probabilities will be 1. The target class will have the highest probability score among all the classes. The softmax function can be explained as

$$P\left(y = j \middle| z^{(i)}\right) = \emptyset_{softmax}\left(z^{(i)}\right) = \frac{e^{z^{(i)}}}{\sum_{j=0}^{k} e^{z_k^{(i)}}} \tag{5.4}$$

where the net input z is defined as $z = w_0 x_0 + w_1 x_1 + \cdots + w_m x_m = \sum_{l=0}^{m} w_l w_l$ (w is the weight vector, x is the feature vector of a training sample, and w_0 is the bias unit) (Raschka, 2015). It computes the probability that this training sample *x*(i) belongs to class j given the weight and net input *z*(i). Accordingly, softmax function is applied in the output layer herein so that the FrictionNet can predict friction number over 9 classes ranging from 0.2 to 1.0 with 0.1 as interval.

5.4 Results

In this multi-class classification problem, the performance of FrictionNet is evaluated via classification accuracy score which is defined as the number of correct predictions made divided

by the total number of predictions made by the model, multiplied by 100 to turn it into a percentage. The classification accuracy score can be expressed as

$$accuracy(y, \hat{y}) = \frac{1}{n}\sum_{i=0}^{n-1} 1(\hat{y}_i == y_i) * 100 \tag{5.5}$$

where $\hat{y}$ and y are the predicted and actual friction number.

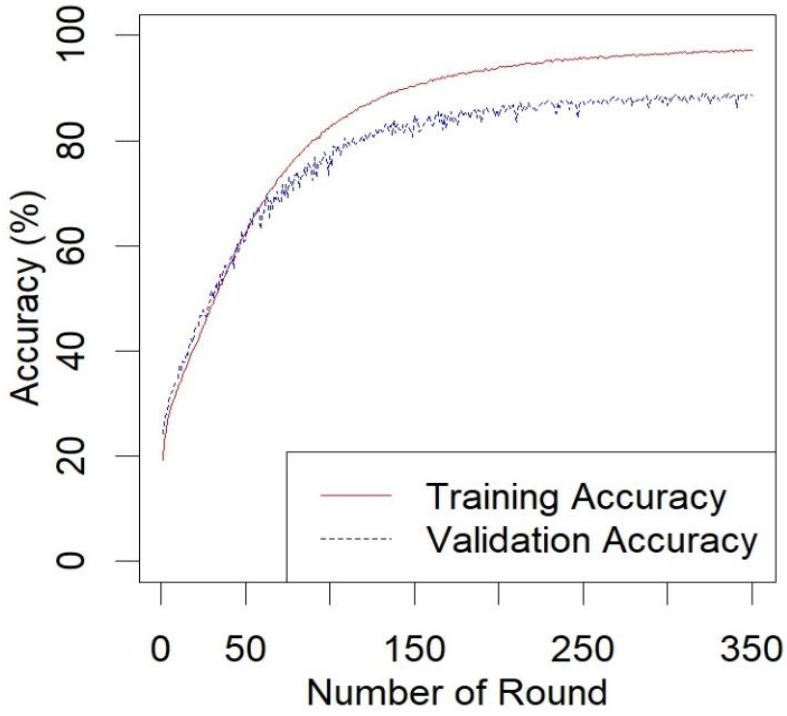

Figure 38 Classification Accuracy Summary

50,400 and 6,300 pairs of pavement texture spectrogram and friction data are involved in the training and validation of FrictionNet. The classification accuracies for training and validation data are displayed in Figure 5.7. The training only takes 350 iterations and 2.73 hours before reaching satisfactory accuracy. With the L2 regularization and dropout layers, the validation classification accuracy stays close to that of training data during training, which indicates no overfitting problem happens in this model. Particularly, the highest classification accuracy 96.85% for FrictionNet is observed at the 314th iteration. Therefore, the parameters saved at the

314th iteration are considered as optimal. Using the optimal parameters, the classification accuracy on training data arrives at 96.85% while it attains 88.92% for validation data.

In addition, the classification accuracy for testing data with another 6,300 samples is 88.37% using the optimal parameters. The detailed predicted and actual friction numbers for testing data are summarized in Table 5.2. The numbers located along the diagonal represent the correct predictions, while the numbers site below or above the diagonal denote the wrong predictions. As shown in Table 5.2, few predictions generate result away from the diagonal, which demonstrates that FrictionNet can predict correct friction number with adequate accuracy. To better visualize the performance of FrictionNet, the actual and predicted friction number of 50 randomly selected samples from the testing data are plotted in Figure 5.8. Only 3 false predictions appear in this random sample. Once again, the proposed network can predict pavement friction number with high accuracy using texture data as input.

Table 5.2 Summary of Testing Accuracy

Testing Accuracy		**Predicted Friction Number**								
		0.2	**0.3**	**0.4**	**0.5**	**0.6**	**0.7**	**0.8**	**0.9**	**1**
Actual Friction Number	**0.2**	**687**	17	12	12	8	5	4	0	4
	0.3	20	**577**	34	12	12	3	10	5	2
	0.4	24	54	**557**	18	16	6	9	7	6
	0.5	16	28	16	**618**	12	3	8	3	2
	0.6	9	18	5	4	**638**	7	8	3	3
	0.7	4	11	5	2	2	**659**	9	2	3
	0.8	10	34	11	11	18	28	**562**	39	13
	0.9	9	8	7	6	4	11	28	**616**	7
	1	0	1	2	0	0	1	2	0	**653**

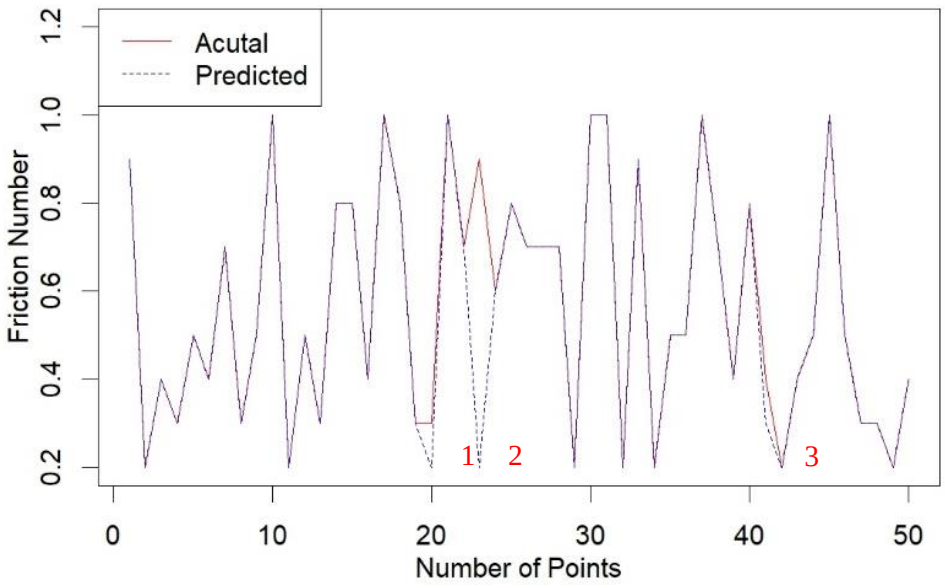

Figure 39 Testing Result Demonstration

5.5 Summary

Different from applying wavelet methodology to decompose 2D macro-texture profiles in Chapter 4, a Convolutional Neural Network (CNN) based efficient network architecture christened as FrictionNet is developed using 2D macro-texture data as a whole for pavement friction prediction with more data sets gathered on more pavement types. Data collections are accomplished via AMES High Speed Profiler for 2D macro-texture profile and Grip Tester for friction data on 49 field sites in 12 states. Diversified pavement types are included in the study, such as HFST, flexible pavement, rigid pavement, bridge deck, and grooved pavement.

Using 504,000 pairs of pavement texture and friction data prepared by the research team, FrictionNet is trained on one GPU device recursively with 350 iterations. The input to FrictionNet is spectrogram of pavement texture profile, and the corresponding output is the predicted friction levels from 0.2 to 1.0 in 0.1 interval. FrictionNet encloses 606,409 parameters to train with an architecture of two convolution layer, three fully-connected layers, and one output layer. The training of FrictionNet is successfully completed with various efficient training

techniques, including stochastic gradient descent, Xavier initialization, L2 regularization and dropout layers, Cross Entropy, and softmax function. Then another two disparate datasets with 6,300 samples are processed by the trained FrictionNet with the purpose for validation and testing. The overall accuracy of FrictionNet on the training, validation, and testing datasets are 96.85%, 88.92%, and 88.37%, respectively. The result demonstrates the proposed algorithm consistently previses the friction number for various field sites with pavement macro-texture data as the only input. This research demonstrates the potential of using highway speed non-contact texture measurements for pavement friction evaluation with applications of deep-learning techniques.

CHAPTER VI CONCLUSIONS AND FUTURE WORK

6.1 Conclusions

This research investigates the possibility of using non-contact pavement texture measurements for pavement friction evaluation based on three different soft computing methodologies. Ultra-high resolution 3D surface image and 2D texture profile are collected by LS-40 Portable 3D Surface Analyzer and AMES High Speed Profiler, while a Dynamic Friction Tester and Grip Tester are applied to measure the corresponding friction data. Novel 3D macro- and micro-texture parameters are calculated for the high-resolution 3D texture data, while discrete wavelet analysis and CNN based model are applied to better utilize the high speed texture profile data for pavement friction prediction.

Chapter 3 explores five categories of 3D areal texture parameters to characterize pavement texture attributes and develop friction prediction models with the most influencing 3D texture parameters. The newly constructed LTPP SPS-10 site in Oklahoma is selected as the testing bed. Twenty-four 3D texture parameters are calculated for the high-resolution 3D texture data. Correlation analyses is conducted to exclude those who exhibit strong correlations and remove the potential multicollinearity for regressional friction model development. The core material volume and the peak density are identified as the most influential macro- and micro-texture parameters which exhibit good correlation with friction data at high- and low-speed

in wet conditions. The results indicate the identified 3D texture parameters provide better alternatives to characterize pavement surface texture attributes with respect to the pavement friction performance. The pavement friction model is therefore developed based on the selected 3D texture parameters.

Chapter 4 implements discrete wavelet transform to decompose pavement 2D macro-texture profile data into multi-scale characteristics and investigate their suitability for pavement friction prediction. Pavement 2D macro-texture and friction data were collected within the left wheel-path from six HFST sites in Oklahoma. The collected macro-texture profiles are decomposed into multiple wavelengths, and the Total Energy (TE) and Relative Energy (RE) are calculated as indicators to represent macro-texture characteristics at various wavelengths. Correlation analysis is performed to examine the contribution of the energy indicators on pavement friction. The macro-texture energy within wavelengths from 0.97 mm to 3.86 mm contributes positively to pavement friction performance while the energy within wavelengths from 15.44 mm to 61.77 mm shows negative contributions. Subsequently, pavement friction prediction model is developed incorporating the macro-texture energy indicators.

Chapter 5 implements deep learning, the fastest-growing technique in machine learning, to investigate the application of pavement texture profile data for pavement skid resistance analysis. 49 HFST sites distributed in 12 states are tested including various types of lead-in and lead-out pavement sections. FrictionNet, a Convolutional Neural Network (CNN) based DL architecture, is developed to predict pavement friction levels using texture profile as a whole. This architecture is composed of six layers including two convolution layers, three fully-connected layers, and one output layer, with 606,409 tuned hyper-parameters. 50,400 pairs of texture and friction data sets are employed for training, while another 12,600 pairs for validation and testing. The input data of the FrictionNet is the spectrogram of the original texture profile at every meter, and the output of FrictionNet is the friction levels ranging from 0.2 to 1.0 in 0.1 intervals. The FrictionNet achieves

96.85% accuracy for training, 88.92% for validation, and 88.37% for testing. The result demonstrates the potential of using highway speed non-contact texture measurements for pavement friction evaluation.

6.2 Future Work

In Chapter 3, only sixty-nine pairs of data sets are collected in this study for the selection of 3D pavement texture parameters and the development of friction prediction models. Additional 3D data sets should be collected on various pavement categories in the future to validate the applicability of the identified 3D texture parameters and optimize the performance of proposed friction prediction models. In addition, additional 3D texture parameters should be explored to better capture the pavement texture and characterize friction simultaneously.

In Chapter 4, it is recognized that pavement surface conditions and the geometric characteristics of the roadway could significantly impact the repeatability and the accuracy of 2D macro-texture and friction data collection using High Speed Profiler and Grip Tester. For example, the Sites #4 to #6 locate on a low volume road with sharp horizontal curves, and steep longitudinal grades and extensive cracking and defects on the existing surfaces. The 2D macro-texture and friction data collected on these sites show extensive variations with many abnormal data points, therefore the proposed friction prediction model on these sites are less robust comparing to the result on the other sections. In future, perform pavement texture and friction data collection simultaneously to reduce the side effect of vehicle wondering during data collection.

In Chapter 5, a CNN based model is utilized to train FrictionNet with macro-texture profile data as the inputs. Many other deep learning methodologies, such as VGG and recurrent neural network (RNN) should be tested in the future to further improve the accuracy of FrictionNet. Besides, time series texture data measured over time should be added in the future to explore the capability of FrictionNet for pavement friction deterioration.

ACKNOWLEDGEMENTS

This dissertation was prepared under research projects, “Long Term Performance Monitoring of High Friction Surfacing Treatment (HFST) Sites” sponsored by the Federal Highway Administration (FHWA), and “Aggregate Characteristics-Based Preventive Maintenance Treatments for Optimized Skid Resistance of Pavements” sponsored by the Oklahoma Department of Transportation (ODOT). The opinions expressed in the paper are those of the authors, who are responsible for the accuracy of the facts and data herein, and do not necessarily reflect the official policies of the sponsoring agency. This article does not constitute a standard, regulation, or specification.

REFERENCES

Abbasnia R. and Farsaei A. 2013. Corrosion Detection of Reinforced Concrete Beams with Wavelet Analysis. International Journal of Civil Engineering, Transaction A: Civil Engineering, Vol. 11, No. 3, 160-169.

Abdel-Hamid O. et al. 2014. Convolutional Neural Networks for Speech Recognition. IEEE/ACM Transactions on Audio, Speech, and Language Processing, 22(10), pp. 1533-1545.

Adelle W. 2006. Quantitative characterisation of surface finishes on stainless steel sheet using 3D surface topography analysis. Doctoral thesis, University of Huddersfield.

Ahammed M.A. and Tighe S.L. 2008. Concrete Pavement Surface Textures and Multivariables Frictional Performance Analysis: a North American Case Study. Canadian Journal of Civil Engineering, Vol. 35, No. 7, 727-738.

Ahammed M.A. and Tighe S.L. 2010. Pavement surface friction and noise: integration into the pavement management system. Canadian Journal of Civil Engineering, Vol. 37, 1331-1340.

Ahammed M.A. and Tighe S.L. 2012. Asphalt Pavements Surface Texture and Skid Resistance – Exploring the Reality. Canadian Journal of Civil Engineering, Vol. 39, 1-9.

Alhasan A., White D.J. and Brabanterb K.D. 2016. Continuous Wavelet Analysis of Pavement Profiles. Automation in Construction, Vol. 63, 134-143.

American Association of State Highway and Transportation Officials (AASHTO). 2008. Guide for Pavement Friction, 1st Edition. AASHTO. Washington D.C.

American Traffic Safety Services Association (ATSSA). 2013. Safety Opportunities in High Friction Surfacing. Accessed 14 Mar. 2016, from http://www.dbiservices.com/sites/default/files/resources/ATSSA-HFST-LoRes.pdf.

Arambula E. et al. 2013. Performance and Cost Effectiveness of Permeable Friction Course (PFC) Pavements. FHWA/TX-12/0-5836-2. FHWA, U.S. Department of Transportation.

Arampamoorthy H. and Patrick J. 2011. Potential of the Wehner-Schulze Test to Predict the On-Road Friction Performance of Aggregate. NZ Transport Agency Research Report 443. NZ Transport Agency, Wellington, New Zealand.

Asi I.M. 2007. Evaluating Skid Resistance of Different Asphalt Concrete Mixes. Building and Environment, Vol. 42, 325-329.

ASTM Standard E1859/E1859M-11R15, 2015. Standard Test Method for Friction Coefficient Measurements between Tire and Pavement Using a Variable Slip Technique. ASTM International, West Conshohocken, PA, 2015, DOI: 10.1520/ E1859/E1859M-11R15.

ASTM Standard E1911-09a, 2009. Standard Test Method for Measuring Paved Surface Frictional Properties Using the Dynamic Friction Tester. ASTM International, West Conshohocken, PA, 2009, DOI: 10.1520/E1911-09AE01.

ASTM Standard E1960-07, 2015. Standard Practice for Calculating International Friction Index of a Pavement Surface. ASTM International, West Conshohocken, PA, 2015, DOI: 10.1520/E1960-07R15.

ASTM Standard E2157-15, 2015. Standard Test Method for Measuring Pavement Macro-texture Properties Using the Circular Track Meter. ASTM International, West Conshohocken, PA, 2015, DOI: 10.1520/E2157-15.

ASTM Standard E2340/E2340M-11R15, 2015. Standard Test Method for Measuring the Skid Resistance of Pavements and Other Trafficked Surfaces Using a Continuous Reading, Fixed-Slip Technique. ASTM International, West Conshohocken, PA, 2015, DOI: 10.1520/E2340_E2340-11R15.

ASTM Standard E0303-93R13, 2013. Standard Test Method for Measuring Surface Friction Properties Using the British Pendulum Tester. ASTM International, West Conshohocken, PA, 2013, DOI: 10.1520/E0303-93R13.

ASTM Standard E501-08, 2008. Standard Specification for Standard Rib Tire for Pavement Skid-Resistance Tests. ASTM International, West Conshohocken, PA, 2008, DOI: 10.1520/E501-08.

ASTM Standard E524-08, 2008. Standard Specification for Standard Smooth Tire for Pavement Skid-Resistance Tests. ASTM International, West Conshohocken, PA, 2008, DOI: 10.1520/E0524-08.

ASTM Standard E965-15, 2015. Standard Test Method for Measuring Pavement Macro-texture Using a Volumetric Technique. ASTM International, West Conshohocken, PA, 2015, DOI: 10.1520/E0965-15.

ASTM Standard E274/E274M-11, 2011. Standard Test Method for Skid Resistance of Paved Surfaces Using a Full-Scale Tire. ASTM International, West Conshohocken, PA, 2008, DOI: 10.1520/E0274_E0274M-11.

ASTM Standard E670-09, 2009. Standard Test Method for Testing Side Force Friction on Paved Surfaces Using the Mu-Meter. ASTM International, West Conshohocken, PA, 2008, DOI: 10.1520/E0670- 09.

ASTM Standard E1845-15, 2015. Standard Practice for Calculating Pavement Macro-texture Mean Profile Depth. ASTM International, West Conshohocken, PA, 2009, DOI: 10.1520/E1845-15.

ASTM Standard E2380/E2380M-15, 2015. Standard Test Method for Measuring Pavement Texture Drainage Using an Outflow Meter. ASTM International, West Conshohocken, PA, 2015, DOI: 10.1520/E2380_E2380M-15.

Bijsterveld W. and Val M. 2016. Towards Quantification of Seasonal Variations in Skid Resistance Measurements. Road Materials and Pavement Design, 17:2, pp. 477-486, DOI: 10.1080/14680629.2015.1090909.

Bischoff D. 2008. Investigative Study of the Italgrip TM System. WI-04-08. Wisconsin Department of Transportation, Madison, WI.

Bitelli G. et al. Laser Scanning on Road Pavements: A New Approach for Characterizing Surface Texture. Sensors, Vol. 12, 2012, pp. 9110-9128, DOI: 10.3390/s120709110.

Bledsoe J. 2015. Missouri Demonstration Project: The Use of High-Friction Surface Treatments on Missouri Highways. FHWA, U.S. Department of Transportation.

Brownlee J. 2016. Overfitting and Underfitting With Machine Learning Algorithms. Accessed 14 October. 2017, from https://machinelearningmastery.com/overfitting-and-underfitting-with-machine-learning-algorithms/.

Caudill M. 1987. Neural Network Primer, Part I. AI Expert, pp. 46–52.

Chen C., Liaw A., and Breiman L. 2004. Using Random Forest to Learn Imbalanced Data. University of California, Berkeley, vol. 110.

Chen X.H. and Wang D.W. 2011. Fractal and Spectral Analysis of Aggregate Surface Profile in Polishing Process. Wear, Vol. 271, 2746-2750.

Chen D. et al. 2015. Exploring the Feasibility of Evaluating Asphalt Pavement Surface Macro-texture Using Image-based Texture Analysis Method. Road Materials and Pavement Design, 16:2, 405-420, DOI:10.1080/14680629.2015.1016547.

Cireşan D., Meier U., Masci J. and Schmidhuber J. 2011. A Committee of Neural Networks for Traffic Sign Classification. The 2011 International Joint Conference on Neural Networks, San Jose, CA, pp. 1918-1921.

Cireşan D., Meier U., Masci J. and Schmidhuber J. 2012. Multi-column Deep Neural Networks for Image Classification. 2012 IEEE Conference on Computer Vision and Pattern Recognition, Providence, RI, pp. 3642-3649.

Corley-Lay J.B. 1998. Friction and Surface Texture Characterization of 14 Pavement Test Sections in Greenville, North Carolina. In Transportation Research Record: Journal of the Transportation Research Board, N0. 1639, Transportation Research Board of the National Academies, Washington, D.C., 155-161.

Correlation Coefficient. MathBits.com Accessed 9 July, 2016 from http://mathbits.com/MathBits/TISection/Statistics2/correlation.htm.

Dan H. et al. 2015. Experimental Investigation on Skid Resistance of Asphalt Pavement under Various Slippery Conditions. International Journal of Pavement Engineering, DOI: 10.1080/10298436.2015.1095901.

Deltombe R., Kubiak K.J., Bigerelle M. 2011. How to select the most relevant 3D roughness parameters of a surface. Scanning, Vol. 36, No. 1, pp. 150-160, DOI: 10.1002/sca.21113.

Dieleman S. and Schrauwen B. 2014. End-to-End Learning for Music Audio. 2014 IEEE International Conference on Acoustics, Speech and Signal Processing (ICASSP), pp. 6964-6968.

Do M. et al. 2007. Pavement Polishing-Development of a Dedicated Laboratory Test and its Correlation with Road Results. Wear, Vol. 263, 36-42.

Do M. et al. 2009. Evolution of Road-Surface Skid-Resistance and Texture Due to Polishing. Wear, Vol. 266, 574-577.

Do M. et al. 2009. Physical Model for the Prediction of Pavement Polishing. Wear, Vol. 267, 81-85.

Doty R.N. 1974. A Study of the Sand Patch and Outflow Meter Method of Pavement Surface Texture Measurement. Symposium on Surface Texture and Standard Surfaces. Washington, D.C.

Dunford A.M. et al. 2012. Three-Dimensional Characterization of Surface Texture for Road Stones Undergoing Simulated Traffic Wear. Wear, Vol. 292-293, 188-196.

Dunford A. 2013. Friction and the Texture of Aggregate Particles Used in the Road Surface Course. Ph.D. Dissertation, University of Nottingham, United Kingdom.

Dupont P., and Bauduin A. 2005. Pavement skid resistance: French national policy towards promoting road projects. Bulletin Des Laboratories Des Ponts Et Chaussees: Managing Road Pavement Skid Resistance, Ref. 4521, France, 159–168.

Ergun M., Iyinam S., and Iyinam A.F. 2005. Prediction of Road Surface Friction Coefficient Using Only Macro- and Micro-texture Measurements. Journal of Transportation Engineering, Vol. 131, 311-319.

Federal Aviation Administration (FAA). 1997. Measurement, Construction and Maintenance of Skid-resistant Airport Pavement Surfaces (Advisory Circular AC 150/5320-12C). Office of Airport Safety and Standards, FAA, Washington D.C.

Flintsch G.W., Leon E.D., McGhee K.K., and Al-Qadi I.L. 2003. Pavement Surface Macro-texture Measurement and Application. In Transportation Research Board Annual Meeting CD-ROM, Transportation Research Board of the National Academies, Washington, D.C.

Flintsch, G.W. and McGhee, K. K. 2009. NCHRP Synthesis 401: Quality management of Pavement Condition Data Collection, Transportation Research Board, National Research Council, Washington, D.C.

Flintsch G.W. et al. 2012. The Little Book of Tire Pavement Friction. Pavement Surface Properties Consortium. Accessed 1 May 2015, from https://secure.hosting.vt.edu/www.apps.vtti.vt.edu/1-pagers/CSTI_Flintsch/The%20Little%20Book%20of%20Tire%20Pavement%20Friction.pdf

Friel S. et al. 2013. Use of Wehner Schulze to Predict Skid Resistance of Irish Surfacing Materials. Airfield and Highway Pavement, France, 12 p.

Fuents L.G. 2009. Investigation of the Factors Influencing Skid Resistance and the International Friction Index. Ph.D. Dissertation, University of South Florida, Tampa, FL.

Gardiner M.S. et al. 2004. Influence of Hot Mix Asphalt Macro-texture on Skid Resistance. Journal of Testing and Evaluation, Vol. 32, No. 1, pp. 7-16.

Glorot X. and Bengio Y. 2010. Understanding the Difficulty of Training Deep Feedforward Neural Networks. Proceedings of the Thirteenth International Conference on Artificial Intelligence and Statistics, in PMLR 9, pp. 249-256.

Goodman, S.N. 2009. Quantification of Pavement Textural and Frictional Characteristics Using Digital Image. Ph.D. Dissertation, Carleton University, Ottawa, Canada.

Hall J.W. et al. 2009. NCHRP Web Document 108: Guide for Pavement Friction. Transportation Research Board, National Research Council, Washington, D.C.

Hartikainen L., Petry F. and Westermann S. 2014. Frequency-wise Correlation of the Power Spectral Density of Asphalt Surface Roughness and Tire Wet Friction. Wear, Vol. 317, pp. 111-119.

Hassan R. 2015. Two Applications of Wavelet Analysis for Project Level Pavement Management. International Journal of Sustainable Development and Planning, 10(2), 217-228.

Hayes G.G., Ivey D.L., and Gallaway B.M. 1983. “Hydroplaning, Hydrodynamic Drag, and Vehicle Stability”. Special Technical Publication 793, American Society for Testing and Materials (ASTM), Philadelphia, Pennsylvania.

He H. and Garcia E.A. 2009. Learning from Imbalanced Data. IEEE Transactions on Knowledge and Data Engineering, 21(9), pp.1263–1284.

Henry, J.J. 2000. NCHRP Synthesis 291: Evaluation of Pavement Friction Characteristics. Transportation Research Board, National Research Council, Washington, D.C.

Hester D. and Gonzàlez A. 2012. A Wavelet-based Damage Detection Algorithm based on Bridge Acceleration Response to A Vehicle. Mechanical Systems and Signal Processing, 28, 145-166.

Horne W.B. and Buhlmann F. 1983. “A Method for Rating the Skid Resistance and Micro/Macro-texture Characteristics of Wet Pavements”. ASTM International STP No. 793, Philadelphia, Pennsylvania.

Huang J.T., Li J., and Gong Y. 2015. An Analysis of Convolutional Neural Networks for Speech Recognition. 2015 IEEE International Conference on Acoustics, Speech and Signal Processing (ICASSP), pp. 4989-4993.

International Slurry Surfacing Association. High Performance Slurry Systems. Accessed 25 Jan 2016, from https://www.mdt.mt.gov/publications/docs/brochures/research/toolbox/ISSA/highperf.pdf.

Izeppi E., Flintsch G. and McGhee K. 2010. Field Performance of High Friction Surfaces. Publication FHWA/VTRC 10-CR6. FHWA, U.S. Department of Transportation.

Jahromi S.G. et al. 2011. Evaluation of Pavement Temperature on Skid Frictional of Asphalt Concrete Surface. International Journal of Pavement Engineering, 12:1, 47-58, DOI: 10.1080/10298436.2010.501864.

Jayawickrama P.W. and Thomas B. 1998. Correction of Field Skid Measurements for Seasonal Variations in Texas. Transportation Research Record: Journal of the Transportation Research Board, No. 1639, pp. 147–154.

Kanafi M.M. et al. 2015. Macro- and Micro-Texture Evolution of Road Pavements and Correlation with Friction. International Journal of Pavement Engineering, 16:2, 168-179, DOI: 10.1080/10298436.2014.937715.

Kane M., Do M.T. and Piau J.M. 2010. On the Study of Polishing of Road Surface under Traffic Load. Journal of Transportation Engineering, Vol. 136, No. 1, 45-51.

Kane M., Rado Z. and Timmons A. 2015. Exploring the Texture-Friction Relationship: from Texture Empirical Decomposition to Pavement Friction. International Journal of Pavement Engineering, 16:10, 919-918, DOI:10.1080/10298436.2014.972956.

Kassem Emad, Awed Ahmed, Masad E.A., and Little D.N. 2013. Development of Predictive Model for Skid Loss of Asphalt Pavements. In Transportation Research Record: Journal of the Transportation Research Board, N0. 2372, Transportation Research Board of the National Academies, Washington, D.C., 83-96.

Khaleghian S., Emami A., and Taheri S. 2017. A Technical Survey on Tire-Road Friction Estimation. Friction, 5: 123. https://doi.org/10.1007/s40544-017-0151-0.

Kotek P. and Florkova Z. 2014. Comparison of the Skid Resistance at Different Asphalt Pavement Surfaces over Time. Procedia Engineering, Vol. 91, 459-463.

Kotek P. and Kovac M. 2015. Comparison of valuation of Skid Resistance of Pavements by Two Device with Standard Methods. Procedia Engineering, Vol. 111, 436-443.

Kowalski K.J. et al. 2009. Long-Term Monitoring of Noise and Frictional Properties of Three Pavements: Dense-Graded Asphalt, Stone Matrix Asphalt, and Porous Friction Course. In Transportation Research Record: Journal of the Transportation Research Board, N0. 2127, Transportation Research Board of the National Academies, Washington, D.C., 12-19.

Krizhevsky A., Sutskever I., and Hinton G. E. 2012. Imagenet Classification with Deep Convolutional Neural Networks. Advances in Neural Information Processing Systems 25, pp.1106–1114.

Kuemmel, D.A., J.R. Jaeckel, and A. Satanovsky. 2000. Investigative Study of the Italgrip System: Noise Analysis, Report No. WI/SPR-02-00, Wisconsin Department of Transportation, Madison, Wisconsin.

Kumar B. and Wilson D.J. 2010. Prediction of Pavement Surface Skid Resistance and the Effect of Smaller Chip Size. Accessed 17 Feb 2016, from http://www.transportationgroup.nz/papers/2010/07_Wilson__Doug.pdf.

Labbate A. et al. 2001. A Classification of Asphalt Surfacing Textures Based on 3D Imagery. Master Dissertation, University of Bologna, Italy.

Längkvist M., Karlsson L., and Loutfi A. 2014. A Review of Unsupervised Feature Learning and Deep Learning for Time-Series Modeling. Pattern Recognition Letters, 42, pp. 11–24.

Larson R.M. et al. 2004. Pavement surface functional characteristics. In Proceedings of the Fifth International Symposium on Pavement Surface Characteristics — SURF 2004. World Road Association (PIARC), Toronto, Ont. [CD-ROM].

Leach R. 2012. Characterisation of Areal Surface Texture. Springer-Verlag Berlin Heidelberg, DOI: 10.1007/978-3-642-36458-7.

LeCun Y., Bengio Y., and Hinton G. 2015. Deep Learning. Nature, 521, pp. 436–444.

Li L., Wang K.C.P., and Li Q.J. 2016. Geometric Texture Indicators for Safety on AC Pavements with 1 mm 3D Laser Texture Data. International Journal of Pavement Research and Technology, Vol. 9, pp. 49-62.

Li Q. et al. 2016. Effectiveness and Performance of High Friction Surface Treatments at A National Scale. Can. J. Civ. Eng., 43, pp. 812–821, dx.doi.org/10.1139/cjce-2016-0132.

Li Q., Yang G., Zhan Y., Wang K., and Wang C. 2017. Novel Macro- and Micro-texture Indicators for Pavement Friction by Using High-Resolution Three-Dimensional Surface Data. Transportation Research Record: Journal of the Transportation Research Board, No. 2641, pp. 164–176.

Li S. et al. Pavement Surface Micro-texture: Testing, Characterization and Frictional Interpretation. Pavement Performance. Current Trends, Advances, and Challenges, STP 1555, 2012, DOI:10.1520/STP104426.

Li S. et al. 2011. Evaluation of Pavement Surface Friction Treatments. FHWA/IN/JTRP-2012/04. FHWA, U.S. Department of Transportation.

Li S., Zhu K. and Noureldin S. 2007. Evaluation of Friction Performance of Coarse Aggregates and Hot-Mix Asphalt Pavements. Journal of Testing and Evaluation, Vol. 35, No. 6, 1-7.

Liu Q. and Shalaby A. 2015. Relating Concrete Pavement Noise and Friction to Three-Dimensional Texture Parameters. International Journal of Pavement Engineering, DOI: 10.1080/10298436.2015.1095897.

Lu Q. and Steven B. 2006. Friction Testing of Pavement Preservation Treatments: Literature Review. UCPRC-TM-2006-10.

Luo Y. 2003. Effect of Pavement Temperature on Frictional Properties of Hot-Mix-Asphalt Pavement Surfaces at the Virginia Smart Road. Master Dissertation, Virginia Polytechnic Institute and State University, Blacksburg, Va.

Luque P. et al. 2013. Tyre–Road Grip Coefficient Assessment – Part II: Online Estimation Using Instrumented Vehicle, Extended Kalman Filter, and Neural Network. Vehicle System Dynamics, 51:12, pp. 1872-1893, DOI: 10.1080/00423114.2013.841963.

Mahmoud E. and Masad E. 2007. Experimental Methods for the Evaluation of Aggregate Resistance to Polishing, Abrasion, and Breakage. Journal of Materials in Civil Engineering, Vol. 19, No. 11, 977-985.

Masad E., Al-Rousan T., Button J. and Little D. 2007. NCHRP Report 555: Test Methods for Characterizing Aggregate Shape, Texture, and Angularity. Transportation Research Board, National Research Council, Washington, D.C.

Masad E. 2007. Relationship of Aggregate Texture to Asphalt Pavement Skid Resistance Using Image Analysis of Aggregate Shape. Final Report for Highway IDEA Project 114.

Masad E., Rezaei A., Chowdhury A. and Harris P. 2009. Predicting Asphalt Mixture Skid Resistance Based on Aggregate Characteristics. FHWA/TX-09/0-5627-1.

Masad E., Rezaei A., Chowdhury A. and Chowdhury A. 2010. Field Evaluation of Asphalt Mixture Skid Resistance and Its Relationship to Aggregate Characteristics. FHWA/TX-10/0-5627-2.

Masad E., Rezaei A. and Chowdhury A. 2011. Field Evaluation of Asphalt Mixture Skid Resistance and Its Relationship to Aggregate Characteristics. FHWA/TX-11/0-5627-3.

Matuško J., Petrović I., Perić N. 2008. Neural Network based Tire/Road Friction Force Estimation. Engineering Applications of Artificial Intelligence, 21:3, pp. 442–456.

McGhee K.K. and Flintsch G.W. 2003. High-Speed Texture Measurement of Pavements. VTRC 03-R9. Charlottesville, Virginia.

McGovern C., Rusch P. and Noyce D.A. 2011. State Practices to Reduce Wet Weather Skidding Crashes. FHWA-SA-11-21. FHWA, U.S. Department of Transportation.

Merritt D. and Moravec M. 2014. An Update on HFST for Horizontal Curves. Proceeding of Pavement Evaluation 2014, Blacksburg, Virginia. Accessed 14 Mar., 2016 from https://vtechworks.lib.vt.edu/bitstream/handle/10919/54619/Merritt_2.pdf?sequence=1&isAllowed=y.

Michigan Metrology. 2014. Michigan Metrology Surface Texture Parameters Glossary. Michigan Metrology, LLC, MI.

Millar P. et al. 2009. Use of Close Range Terrestrial Photogrammetry to Assess Accelerated Wear of Asphalt Concrete Surface Course Mixes. In: Sixth International Conference on Maintenance and Rehabilitation of Pavements and Technological Control, Politechnico di Torino, Italy. Politechnico di Torino. Vol 27 pp.

Miller et al. 2012. Characterization of Asphalt Pavement Surface Texture. In Transportation Research Record: Journal of the Transportation Research Board, N0. 2295, Transportation Research Board of the National Academies, Washington, D.C., 19-26.

Misiti M., Oppenheim G. and Poggi J. 2000. Wavelet Toolbox for Use with MATLAB: User's Guide. The MathWorks, Inc., Natick, MA.

Moravec M. 2013. High Friction Surface Treatments at High-Crash Horizontal Curves. Arizona Pavements/Materials Conference, Phoenix, AZ.

Najafi S. et al. 2015. Linking Roadway Crashes and Tire-Pavement Friction: A Case Study. International Journal of Pavement Engineering, DOI: 10.1080/10298436.2015.1039005.

Najafi S., Flintsch G.W., and Khaleghian S. 2016. Pavement Friction Management – Artificial Neural Network Approach. International Journal of Pavement Engineering, DOI: 10.1080/10298436.2016.1264221.

Nataadmadja A.D. et al. 2012. Quantifying Aggregate Micro-texture with Respect to Wear-Case of New Zealand Aggregates. Wear, Vol. 332-333, pp. 907-917.

Nielsen M. 2017. Neural Networks and Deep Learning. Online Book. Accessed 19 August. 2017, from http://neuralnetworksanddeeplearning.com/index.html.

Pidwerbesky et al. 2006. Road Surface Texture Measurement Using Digital Image Processing and Information Theory. Land Transport New Zealand Research Report 290. 65pp.

Plati C., Georgiou P., and Papavasiliou V. 2016. Simulating Pavement Structural Condition Using Artificial Neural Networks. Structure and Infrastructure Engineering, 12:9, pp. 1127-1136, DOI: 10.1080/15732479.2015.1086384.

Prowell B.D., Hurley G.C., and Frank B. 2012. Warm-Mix Asphalt: Best Practices. 3rd Edition. NAPA – National Asphalt Pavement Association. Lanham, MD.

Prowell B.D. and Hanson D.I. 2005. Evaluation of Circular Texture Meter for Measuring Surface Texture of Pavements. In Transportation Research Record: Journal of the Transportation

Research Board, N0. 1929, Transportation Research Board of the National Academies, Washington, D.C., 88-96.

Puccinelli J. et al. 2014. Long-Term Pavement Performance Warm Mix Asphalt Study. FHWA, VA.

Rado Z. and Kane M. 2014. An Initial Attempt to Develop an Empirical Relation between Texture and Pavement Friction Using the HHT Approach. Wear, Vol. 309, 233-236.

Raschka S. 2015. Python Machine Learning. Birmingham, UK: Packt Publishing.

Rezaei A., Masad E., Chowdhury A. and Harris P. 2009. Predicting Asphalt Mixture Skid Resistance by Aggregate Characteristics and Gradation. In Transportation Research Record: Journal of the Transportation Research Board, No. 2104, Transportation Research Board of the National Academies, Washington, D.C., 24–33.

Rezaei A. and Masad E. 2013. Experimental-based Model for Predicting the Skid Resistance of Asphalt Pavements. International Journal of Pavement Engineering, Vol. 14, No. 1, 24-35.

Roe P.G., Webster D.C. and West G. 1991. The Relation between the Surface Texture of Roads and Accidents. Research Report 296, Transport and Road Research Laboratory, Crowthorne, Berkshire.

Roe P.G., Parry A.R. and Viner H.E. 1998. High and Low Speed Skidding Resistance: The Influence of Texture Depth. TRL Report 367, Transport Research Laboratory, Crowthorne, Berkshire.

Sarsam S.I. and Ali A.M. 2015. Assessing Pavement Surface Macro-texture Using Sand Patch Test and Close Range Photogrammetric Approaches. International Journal of Materials Chemistry and Physics, Vol. 1, No. 2, 124-131.

Sang Y., Dube M., and Grant M. 2008. Dependence of Friction on Roughness, Velocity, and Temperature. Phys Rev E Stat Nonlin Soft Matter Phys.

Schmidhuber J. 2015. Deep Learning in Neural Networks: An Overview. Neural Networks, 61, pp. 85–117.

Serigos P.A. 2013. The Contribution of Micro- and Macro-Texture to the Skid Resistance of Pavements. Accessed 12 May, 2015 from

http://www.ectri.org/YRS13/Documents/Presentations/Session5b-6a/YRS13_Session5b-6a_Serigos_TRB.pdf.

Sprinkel M., McGhee K., and Izeppi E. 2015. Virginia's Experience with High-Friction Surface Treatments. Transportation Research Record: Journal of the Transportation Research Board, No. 2481, Transportation Research Board, Washington, D.C., pp. 100–106. DOI: 10.3141/2481-13.

Srivastava N., Hinton G., Krizhevsky A., Sutskever I., and Salakhutdinov R. 2014. Dropout: A Simple Way to Prevent Neural Networks from Overfitting. Journal of Machine Learning Research, 15, pp. 1929–1958.

State of South Dakota Department of Transportation (SD DOT). 2015. Accelerated Innovation Deployment (AID) Demonstration Project: High Friction Surface Treatment.

Stergious C. and Siganos D. Neural Networks. Accessed 14 August. 2017, from https://www.doc.ic.ac.uk/~nd/surprise_96/journal/vol4/cs11/report.html#Introduction to neural networks.

Steven B.D. 2009. Friction Testing of Pavement Preservation Treatments: Temperature Correlations and Operator/Machine Variability. CA11-1200 C. State of California Department of Transportation.

Sutskever H., Vinyals O., and Le Q. 2014. Sequence to Sequence Learning with Neural Networks. Advances in Neural Information Processing Systems.

Ueckermann et al. 2015. A Contribution to Non-contact Skid Resistance Measurement. International Journal of Pavement Engineering, Vol. 16, No. 7, 646-659.

Ueckermann et al. 2015. Calculation of Skid Resistance from Texture Measurements. Journal of Traffic and Transportation Engineering, Vol. 2, No. 1, 3-16.

Villani M.M. et al. 2014. Application of Fractal Analysis for Measuring the Effects of Rubber Polishing on the Friction of Asphalt Concrete Mixtures. Wear, Vol. 320, pp. 179-188.

Viner H. et al. 2006. Surface Texture Measurement on Local Roads. TRL Limited PPR148.

Wang Kelvin C.P., Li Q. and Gong W. 2007. Wavelet-Based Pavement Distress Image Edge Detection with à Trous Algorithm. In Transportation Research Record: Journal of the

Transportation Research Board, No. 2024, Transportation Research Board of the National Academies, Washington, D.C., 73–81.

Wang T., Wu D. J., Coates, and Ng A. Y. 2012. End-to-End Text Recognition with Convolutional Neural Networks. In Pattern Recognition (ICPR), IEEE, pp. 3304-3308.

Watkins Q.B. et al. 2010. Rubber Tire Buildup Removal at Hartsfield-Jackson Atlanta International Airport. Proceeding of FAA Worldwide Technology Transfer Conference 2010, Atlantic City, New Jersey.

Watson M. et al. 2011. Hot Mixed Asphalt Pavement Surface Characteristics Related to: Ride, Texture, Friction, Noise and Durability. Minnesota Department of Transportation, Maplewood, MN.

Wei L. et al. 2005. Wavelet Analysis and Interpretation of Road Roughness. Journal of Transportation Engineering. 131(2): 120-130.

Wilson D.J. 2006. An Analysis of the Seasonal and Short-Term Variation of Road Pavement Skid Resistance. Ph.D. Dissertation, The University of Auckland, New Zealand.

Yager T.J. 2013. How Best to Determine Runway/Highway Pavement Surface Friction Performance. Tenth ALACPA Airport Pavement Seminar, Mexico City, Mexico. Accessed 12 Jan, 2016 from http://www.icao.int/nacc/documents/meetings/2013/alacpa10/alacpa10-p22.pdf.

Yang G., Li Q., Zhan Y., Wang K., and Wang C. 2017. Wavelet based Macro-texture Analysis for Pavement Friction Prediction. KSCE J Civ Eng, https://doi.org/10.1007/s12205-017-1165-x.

Zelelew H.M. et al. 2013. Pavement Macro-texture Analysis Using Wavelets. International Journal of Pavement Engineering, 14:8, 725-735, DOI: 10.1080/10298436.2012.705004.

Zelelew H.M. et al. 2014. Wavelet-based Characterisation of Asphalt Pavement Surface Macro-texture. Road Materials and Pavement Design, 15:3, 622-641, DOI:10.1080/14680629.2014.908137.

Zhang A. et al. 2017. Automated Pixel-Level Pavement Crack Detection on 3D Asphalt Surfaces Using a Deep-Learning Network. Computer-Aided Civil and Infrastructure Engineering, 32, pp. 805–819.

Zhang L., Yang F., Zhang Y., and Zhu Y. 2016. Road Crack Detection using Deep Convolutional Neural Network. 2016 IEEE International Conference on Image Processing (ICIP), Phoenix, AZ, pp. 3708-3712.

VITA

GUANGWEI YANG

Candidate for the Degree of

Doctor of Philosophy

Thesis: EXPLORING PAVEMENT TEXTURE AND SURFACE SKID RESISTANCE USING SOFT COMPUTING TECHNIQUES

Major Field: Civil Engineering

Biographical:

Education:

Completed the requirements for the Doctor of Philosophy in Civil Engineering at Oklahoma State University, Stillwater, Oklahoma in December, 2017.

Completed the requirements for the Master of Science in Civil Engineering at Southwest Jiaotong University, Chengdu, China in 2011.

Completed the requirements for the Bachelor of Science in Civil Engineering at Zhengzhou University, Zhengzhou, China in 2008.

Experience:
August 2013-present: Research Assistant, Oklahoma State University
August 2015-present: Teaching Assistant, Oklahoma State University

Professional Memberships:
Student Member of American Society of Civil Engineers (ASCE)
Member of Chinese Overseas Transportation Association
Member of International Society for Weight in Motion